Charles University in Prague

Faculty of Science

Study program: Physical chemistry

Ing. Jan Přech

SYNTHESIS AND POST-SYNTHESIS MODIFICATION OF NOVEL 2-DIMENSIONAL ZEOLITES

Dissertation

Supervisor: Prof. Ing. Jiří Čejka, DrSc.

Prague, 2016

Univerzita Karlova v Praze

Přírodovědecká fakulta

Studijní program: Fyzikální chemie

Ing. Jan Přech

SYNTÉZA NOVÝCH DVOJROZMĚRNÝCH ZEOLITŮ A JEJICH POSTSYNTETICKÉ MODIFIKACE

Disertační práce

Školitel: Prof. Ing. Jiří Čejka, DrSc.

Praha, 2016

Prohlášení

Disertační práce byla vypracována v oddělení Syntézy a katalýzy Ústavu fyzikální chemie J. Heyrovského AV ČR v období 1. 10. 2012 – 10. 6. 2016.

Prohlašuji, že jsem disertační práci zpracoval samostatně a že uvádím všechny použité informační zdroje a literaturu. Tato práce ani její podstatná část nebyla předložena k získání jiného nebo stejného akademického titulu.

V Praze, 10. 6. 2016

Acknowledgement

In the first place I would like to thank my supervisor, Prof. Jiří Čejka, for all advices, support and patience during my studies. I highly regard working under his guidance.

I would like to thank all my colleagues (in alphabetical order) Arnošt Zukal, Dana Vitvarová, Lenka Lupínková, Maksym Opanasenko, Mariya Shamzhy, Martin Kubů, Michal Mazur, Naděžda Žilková, Pavla Eliášová, Valeryia Kasneryk, Zuzana Pavlačková and all others for advices, help and support whenever needed and for nice collegial atmosphere in the laboratory. My thank goes also to Dr. Libor Brabec for taking SEM images, Milan Bouša for taking the EDX spectra and Dr. Galina Sádovská for help with collecting of the DR-UV/Vis spectra.

I would like to thank my family and friends for the support during all my Ph.D. studies.

Thank God.

Content

List of abbreviations and designation of new materials

BET area	Surface area according to Brunauer–Emmett–Teller isotherm
BJH	Barrett-Joyner-Halenda method
C_{16}TMA-OH	Cetyltrimethylammonium hydroxide
CBP	Carbon black pearls
D4R	Double-four ring secondary building unit
DBTH	Dibenzothiophene
DBTHSO	Dibenzothiophene sulphoxide
$DBTHSO_2$	Dibenzothiophene sulphone
DR-UV/Vis	Diffuse reflectance ultraviolet/visible spectroscopy
Desil-TS-1	Desilicated titanosilicate 1
E_{H2O2}	Hydrogen peroxide efficiency
EDX	Energy dispersive spectroscopy
GC	Gas chromatography
GC-MS	Gas chromatograph coupled with a mass spectrometer
IEZ	Interlamellar expanded zeolite
IPC-1PITi	Two-dimensional silica-titania pillared material prepared from IPC-1P
IR	Infrared spectroscopy
MAS NMR	Magic angle spinning nuclear magnetic resonance
Meso-TS-1	Mesoporous titanium silicalite-1
MPS	Methylphenyl sulphide
MPSO	Methylphenyl sulphoxide
$MPSO_2$	Methylphenyl sulphone
N-MeSpa-OH	N-methylsparteinium hydroxide
ODS	Oxidative desulphuration
Ph_2S	Diphenyl sulphide
Ph_2SO	Diphenyl sulphoxide
Ph_2SO_2	Diphenyl sulphone
S	Selectivity
S4R	Single-four ring secondary building unit
S/C	Substrate/catalyst mass ratio
SDA	Structure directing agent (= organic template)
SEM	Scanning electron microscopy
S_{ext}	External surface area
Si/Ti	Silicon to titanium molar ratio
T	Tetrahedrally coordinated atom (e.g. Si, Ti, Al, Ge, B, etc.)
TBOTi	Tetrabutyl orthotitanate
TEM	Transmission electron microscopy
TEOS	Tetraethyl orthosilicate
TEOTi	Tetraethyl orthotitanate
Ti-IPC-1P	Two-dimensional lamellar material prepared by hydrolysis from Ti-**UTL**
Ti-IPC-1PISi	Two-dimensional silica pillared material prepared from Ti-IPC-1P

Ti-IPC-1PITi	Two-dimensional silica-titania pillared material prepared from Ti-IPC-1P
Ti-IPC-1-sw	Two-dimensional swollen material prepared from Ti-IPC-1P
Ti-IPC-2	Three-dimensional titanosilicate with 12-10-ring channel system (**OKO** topology)
Ti-IPC-4	Three-dimensional titanosilicate with 10-8-ring channel system (**PCR** topology)
TOF	Turn-over frequency
TON	Turn-over number
TPA-OH	Tetrapropyl ammonium hydroxide
TS-1	Titanium silicalite 1 (also titanosilicate 1)
TS-1-PISi	Silica pillared lamellar TS-1
TS-1-PITi	Silica-titania pillared lamellar TS-1
V_{meso}	Mesopore volume
V_{mic}	Micropore volume
V_{tot}	Total adsorption capacity
X	Conversion
XRD	X-ray diffraction
XRF	X-ray fluorescence spectroscopy
y	Yield

List of publications

The dissertation thesis is based on following publications:

1) **J. Přech,** M. Kubů, J. Čejka; Synthesis and catalytic properties of titanium containing extra-large pore zeolite CIT-5, Catal. Today 227 (2014) 80–86.
2) **J. Přech,** P. Eliášová, D. Aldhayan, M. Kubů, Epoxidation of bulky organic molecules over pillared titanosilicates, Catal. Today 243 (2015) 134-140.
3) **J. Přech,** D. Vitvarová, L. Lupínková, M. Kubů, J. Čejka, Titanium impregnated borosilicate zeolites for epoxidation catalysis, Microporous Mesoporous Mater. 212 **2015**, 28-34.
4) **J. Přech,** J. Čejka, UTL titanosilicate: An extra-large pore epoxidation catalyst with tunable textural properties, Catal. Today (2016), DOI: 10.1016/j.cattod.2015.09.036.
5) **J. Přech,** R.E. Morris, J. Čejka, Selective oxidation of bulky organic sulphides over layered titanosilicate catalysts, Catal. Sci. Technol. 6 (2016) 2775-2786.

Further publications:

1) M. Kubů, W.J. Roth, H.F. Greer, W. Zhou, R.E. Morris**, J. Přech**, J. Čejka, A New Family of Two-Dimensional Zeolites Prepared from Intermediate Layered Precursor IPC-3P Obtained during the Synthesis of TUN Zeolite. Chem. Eur. J. 19 (2013), 13937-13945.
2) M. Kubů, **J. Přech,** Transformation of analcime into IMF structure during the synthesis of IMF zeolite, Microporous Mesoporous Mater. 206 (2015) 121–126.
3) A. Peral, J.M. Escola, D.P. Serrano, **J. Přech**, C. Ochoa-Hernández, J. Čejka, Bidimensional ZSM-5 zeolites probed as catalysts for polyethylene cracking, Catal. Sci. Technol. 6 (2016) 2754-2765.
4) J. Fermoso, H. Hernando, P. Jana, I. Moreno, **J. Přech,** C. Ochoa-Hernandez, P. Pizarro, J.M. Coronado, J. Čejka, D.P. Serrano, Lamellar and pillared ZSM-5 zeolites modified with MgO and ZnO for catalytic fast pyrolysis of eucalyptus woodchips, Catal. Today (2016), DOI: 10.1016/j.cattod.2015.09.036.

Abstract

Development of sustainable and environmentally friendly chemical processes is of vital importance nowadays. Although there is a palette of different synthetic methods for the formation of epoxides, sulphoxides and sulphones, from both economic and environmental points of view, a direct oxidation with a simple oxidant is highly appreciated.

The main goals of the thesis were design and synthesis of novel titanium containing zeolitic materials with the ability to catalyse selective oxidation of sterically demanding organic compounds, particularly epoxidation of cyclic olefins and terpenes and oxidation of bulky thioethers to corresponding sulphoxides and sulphones with hydrogen peroxide as the oxidant.

Two novel extra-large pore titanosilicates were prepared by means of hydrothermal synthesis (Ti-**CFI**, Ti-**UTL**), three large-pore titanosilicates (Ti-**CON**, Ti-**AFI**, Ti-**IFR**) were prepared using two step deboronation – liquid phase titanium impregnation procedure and two groups of lamellar materials were prepared. One group was based on modified nanosheet TS-1; the other was prepared from Ti-IPC-1P lamellar precursor, which was prepared by means of top-down transformation of Ti-**UTL**. Last but not least, the Ti-**UTL** was transformed into new titanosilicates Ti-IPC-2 (**OKO** structure) and Ti-IPC-4 (**PCR** structure) by means of ADOR transformation. This is the first example of an ADOR transformation of a titanosilicate material. Especially Ti-**UTL** based pillared materials (denoted Ti-IPC-1PI) are purely mesoporous, possessing titanium sites located on the surface of crystalline layers and thus providing a synergy of both crystalline titanosilicate zeolites and mesoporous molecular sieves. So-called silica-titania pillaring post-synthesis modification (applied on both groups of layered titanosilicates) was developed to boost number of active titanium centres.

The structure, morphology and texture of the materials were investigated by powder XRD analysis, nitrogen and argon physisorption and SEM. The character and amount of the titanium active sites were investigated by diffuse reflectance UV/Vis spectroscopy and XRF or ICP-OES elemental analysis. Catalytic activity of the prepared materials was investigated in selective oxidation of various sterically demanding substrates.

The silica-titania pillared Ti-IPC-1PITi catalyst provided cyclooctene conversion 26% and cyclooctene oxide yield 19.5% after 1 h of the reaction being the most active of all the prepared materials and one of the most active catalysts reported for epoxidation of bulky olefins with hydrogen peroxide.

High epoxide selectivity (95-97% at 10% conversion) and high yield of the cyclodecene oxide (TS-1-PITi 15%, Ti-IPC-1PITi 23% after 4 h) were achieved also in epoxidation of cyclodecene using the silica-titania pillared materials. Contrary, conventional TS-1 provided yield below 1%.

The Ti-IPC-1PISi catalyst exhibited an order of magnitude higher activity in both methylphenyl sulphide (MPS) and diphenyl sulphide oxidations (e.g. MPS oxidation: TON = 1418 vs. TON (TS-1-PISi) = 151, both after 30 min).

We conclude the catalysts with most open structures and therefore the lowest diffusion limitations and sufficient amount of the titanium centres (Ti-IPC-1PITi and TS-1-PITi) provided the highest yields as well as the selectivity. Simple silica-titania pillaring treatment improves the catalyst performance dramatically.

Abstrakt

Význam udržitelných chemických technologií a snižování ekologické náročnosti chemických procesů neustále roste. Ačkoli je známa řada různých metod výroby epoxidů, sulfoxidů a sulfonů, přímá selektivní oxidace výchozích látek s využitím jednoduchého oxidačního činidla je velmi žádoucí z pohledu ekonomického i ekologického.

Hlavním cílem této práce je design a příprava nových zeolitů s obsahem titanu, schopných katalyzovat selektivní oxidaci objemných organických látek s využitím peroxidu vodíku jako oxidačního činidla. Studována byla zejména epoxidace cyklických olefinů a terpenů a oxidace objemných thioetherů na příslušné sulfoxidy a sulfony.

V rámci této práce byla připravena dvojice nových titanosilikátů s extra velkými póry (Ti-**CFI**, Ti-**UTL**). Titanosilikáty Ti-**CON**, Ti-**AFI**, Ti-**IFR** byly připraveny deboronací a následnou impregnací roztokem titanového prekursoru. Dále byly připraveny dvě skupiny dvojrozměrných titanosilikátů na bázi modifikovaného vrstevnatého TS-1 a vrstevnatého prekursoru Ti-IPC-1P, který vzniká „top-down“ modifikací Ti-**UTL**. V neposlední řadě byl Ti-**UTL** přeměněn na dvojici nových materiálů Ti-IPC-2 (struktura **OKO**) a Ti-IPC-4 (struktura **PCR**) s menšími póry ve smyslu „ADOR“ přeměny. Toto je první příklad „ADOR“ přeměny titanosilikátů. Zejména materiály připravené pilířováním Ti-IPC-1P (označené Ti-IPC-1PI) jsou čistě mesoporézní a při tom obsahují titanová centra na povrchu krystalických vrstev. Představují tak synergii klasických titanosilikátových zeolitů a mesoporézních molekulových sít. Takzvané „silica-titania“ pilířování (použité při modifikaci obou skupin vrstevnatých materiálů) bylo vyvinuto pro zvýšení počtu aktivních titanových center.

Struktura, morfologie a textura materiálů byla analyzována pomocí práškové rentgenové difrakční analýzy, fyzisorpce dusíku a řádkovací elektronové mikroskopie. Povaha a množství titanových center bylo analyzováno pomocí difusně-reflexní UV/Vis spektroskopie a ICP-OES elementární analýzy. Katalytické vlastnosti připravených materiálů byly zkoumány při selektivní oxidaci různých stericky náročných substrátů.

Silica-titania pilířovaný materiál Ti-IPC-1PITi poskytnul konverzi cyklooktenu 26% a výtěžek cyklookten oxidu 19.5% po 1 h reakce, což jej pasuje na nejaktivnější z připravených katalyzátorů a jeden z nejaktivnějších epoxidačních katalyzátorů, které byly vůbec popsány pro oxidaci objemných substrátů peroxidem vodíku.

Vysoká selektivita na epoxid (95-97% při 10% konverzi) a vysoký výtěžek cyklodecen oxidu (TS-1-PITi 15%, Ti-IPC-1PITi 23% po 4 h reakce) byly dosaženy také při epoxidaci cyklodecenu s využitím silica-titania pilířovaných materiálů. Naopak klasický TS-1 poskytnul výtěžek nižší než 1% za shodných podmínek.

Pilířovaný katalyzátor Ti-IPC-1PISi vykazoval o řád vyšší aktivitu při oxidaci methylfenyl sulfidu (MPS) a difenyl sulfidu (Ph_2S), než materiály ze skupiny vrstevnatého TS-1 (např. pro MPS po 30 min: TON = 1418 vs. TON (TS-1-PISi) = 151).

Uzavíráme tedy, že katalyzátory s nejvíce otevřenou strukturou, nejnižšími difusními bariérami a dostatečným množstvím aktivních titanových center (Ti-IPC-1PITi a TS-1-PITi) poskytovaly nejvyšší výtěžky a selektivitu. Jednoduché „silica-titania“ pilířování výrazně zlepšilo katalytické vlastnosti diskutovaných dvojrozměrných zeolitů.

1. Aims of the thesis

This thesis was focused on design and synthesis of novel zeolitic materials with the ability to catalyze selective oxidation of sterically demanding organic compounds, particularly epoxidation of cyclic olefins and terpenes and oxidation of bulky thioethers to corresponding sulphoxides and sulphones with hydrogen peroxide as the oxidant. The main goals may be summarized as follows:

Synthesis

1) Preparation of novel large pore and extra-large pore titanosilicates by means of hydrothermal synthesis and post-synthesis modifications
   a) Preparation of Ti-**CFI**
   b) Preparation of Ti-**UTL**
   c) Preparation of Ti-**CON**
2) Preparation of novel 2-dimensional zeolitic materials with particular attention to their post-synthesis modifications in order to enhance the accessibility of the active centres
   a) Preparation of layered TS-1 using the restricted crystal growth method
   b) Preparation of Ti-IPC-1 materials by means of top-down synthesis
   c) Study of possible post-synthesis modification with particular attention to stabilisation and pillaring
3) Preparation of hierarchical TS-1 and other benchmarking materials to evaluate the catalytic performance of the developed materials

Characterisation

1) Characterisation of the prepared materials by XRD, nitrogen physisorption and SEM
2) Characterisation of the amount and nature of the active titanium centres using DR-UV/Vis spectroscopy and ICP-OES elemental analysis

Catalysis

1) Testing of the prepared materials in epoxidation of cyclic olefins (cyclooctene, cyclodecene)
2) Epoxidation of selected terpenes (norbornene, verbenol, linalool, α-pinene)
3) Oxidation of bulky thioethers (methylphenyl sulphide, diphenyl sulphide, dibenzothiophene)

2. Introduction

The modern world is practically based on products of chemical industry; *inter alia*, plastic materials, fuels, fertilizers, pharmaceuticals, cosmetics, etc. The current society requires extensive consumption of energy and despite the increasing demand for sustainable sources; crude oil has remained the dominant energy source. The oil refining, petrochemistry and fine chemical industry are the most important branches of the nowadays industry. According to current estimates, about 85% of all processes are catalysed by solid, heterogeneous catalysts [1]. In 60s, zeolites were first introduced as acid catalysts in oil refining. Introduction of the zeolites is considered to be a significant milestone, since zeolites have gradually replaced both toxic and corrosive acids (e.g. sulfuric acid) and solid amorphous silica-alumina catalysts. Nowadays, zeolites and related materials are widely used as large-scale industrial catalysts. Compared to previously used catalysts, zeolites present environmentally friendly alteration. Moreover, their well-defined microporous frameworks and chemically modifiable structures enable very good control over their acidic, basic, or redox properties [2, 3]. From the structural point of view, zeolites are microporous crystalline aluminosilicate materials and they belong to a wider group of materials called molecular sieves. The overall charge of the aluminosilicate framework is negative and it is balanced by extra-framework cations like H^+, NH_4^+, Na^+, K^+, Ca^{2+}, organic cations etc. Until today, there are 231 different zeolitic structures recognized by the structure commission of the International Zeolite Association (IZA) [4]. In addition to aluminium, some silicon atoms in the framework can be substituted with tetravalent or trivalent cations of similar size e.g. Ti^{4+}, Ge^{4+}, B^{3+}, Fe^{3+}, Ga^{3+} and others. As a result, zeolites offer a broad range of possible chemical compositions and their chemistry is very rich.

The commercial applications of zeolites are abundant and they go hand in hand with the development of tailored zeolite-based catalysts. Particularly, the selective oxidation of C=C double bond in small linear olefins is a well described reaction catalysed by medium-pore size titanium-containing zeolites. The propylene oxide process, for instance, has been already commercialized. However, larger epoxides of alkenes, cycloalkenes and terpenes are still unattainable using medium-pore zeolites due to steric obstacles although they are highly requested in pharmacy, perfumery and resin industry [5]. To tackle bulk substrates it is necessary to prepare catalyst with highly accessible Ti-centers, i.e. with large or extra-large pores and/or with auxiliary mesoporous system. Synthesis of a new generation of titanium zeolite-based catalysts and their tailoring for particular oxidation reaction (selective epoxidation, oxidation of sulphides and sulfoxides) is the subject of the presented dissertation thesis.

3. Theoretical part

3.1.Zeolites

Each existing zeolitic structure has its unique 3 letter code assigned by the structure commission of IZA. Zeolites can be divided according to their pore sizes. The pore size is determined by number of tetrahedrally coordinated atoms (T atoms) in their channel openings. On the other hand, size and shape of the pores determines possible applications of the particular zeolite.

Typical number of T atoms in the channel opening is T = 7, 8, 9, 10, 12, 14. 8-ring zeolites with pore dimensions up to 0.4 nm are referred to as small-pore zeolites (e.g. **LTA**, **CHA**). Small-pore zeolites are typically used as ion-exchangers and drying agents. 10-ring zeolites with pore dimensions up to 0.55 nm are called medium-pore zeolites (e.g. **MFI**, **MWW**). 12-ring zeolites with pore dimensions up to 0.75 nm are called large-pore zeolites (e.g. **FAU**, **BEA**) and zeolites with more than 12 T-atoms in the ring are referred to as extra-large-pore zeolites (e.g. **UTL**, **CFI**) [6]. The mentioned examples of medium-pore and large-pore zeolites are typical industrial catalysts.

Type of the channel system is another important feature. Zeolites with non-intersecting channels (usually running along one of the crystallographic axes) have a one-dimensional channel system (e.g. **LTL**, **CFI**). Zeolites with channels intersecting in two and three dimensions have two-dimensional and three-dimensional channel systems (e.g. **FER**, **UTL** have a two-dimensional system and **BEA**, **FAU** have a three-dimensional channel system). In some cases, channels of a different size can intersect (e.g. **UTL** has intersecting 14-ring and 12-ring channels) and also large cavities may be created at channel intersections.

Zeolites exhibit so-called shape selectivity [7], which is an important feature especially in catalytic and separation applications. There exist several types of the shape selectivity. Reactant selectivity means that only one type of reactant molecule can diffuse into the zeolite catalyst channels and access the active sites (e.g. cracking of heptane isomers). Product selectivity occurs when, among all the product molecules formed inside the zeolite channel system, only those with the proper dimensions can diffuse out and appear as observed products (e.g. xylene isomerization). Restricted transition-state selectivity is observed when certain reactions are prevented because the corresponding transition state requires more space than available (e.g. bimolecular isomerization of xylenes) [8].

3.2.Hierarchical Zeolites

In some cases, the microporous character of a zeolite is highly desirable from the selectivity point of view, but in other cases, diffusion limitations for certain substrates may be a critical limitation. Therefore, several different approaches were developed to prepare so-called hierarchical zeolites (possessing micro and mesopores). In a hierarchical material, the mesopores act as kind of a highway in a city with narrow streets (micropores) on a molecular level [9]. The additional mesopores can be created by e.g. by desilication (treatment with NaOH solution) or by secondary templating (use of additional material, which can be removed by calcination leaving mesopores in the crystal). Desilication with the sodium hydroxide is a reproducible methodology to obtain mesopores preserving the structural integrity of the zeolite [10]. Incorporation of carbon during synthesis of the zeolite (carbon templating) is another attractive method of creating mesopores. Typically, carbon nanoparticles, porous carbon, carbon nanotubes or carbon fibres are added into the synthesis gel. After calcination of the resulting carbon–zeolite composite a hierarchical material with well-defined mesopores is obtained [11].

3.3.Layered Zeolites

When a substrate is too bulky to enter the zeolite channel system, any catalysed transformation of this substrate can occur only on the external surface of the zeolite crystals. Increasing the external surface therefore increases the catalyst activity. By decreasing the crystal thickness into a unit cell level we can obtain so called 2-dimensional (lamellar) zeolites. Such materials mostly lose their shape selectivity; however, they possess high external surface area, which is accessible even for sterically demanding molecules. Current state-of-art in the area of 2-dimensional zeolites has been currently reviewed by Roth et al. [12]. Generally, there are 3 approaches to prepare 2-dimensional zeolites.

Some zeolites (e.g. **MWW**, **NSI**, **FER**, **SOD**) form lamellar precursors during hydrothermal synthesis [13], [14]. These lamellar precursors are turned into fully connected three-dimensional zeolites upon calcination, when the organic template in between the layers is removed and terminal silanol groups on the surface of the layers condense into oxygen bridges.

Lamellar zeolites (e.g. **MFI**) can be prepared also using specially designed surfactant templates. The hydrophilic part of the surfactant (usually diquarternary ammonium salt) directs the zeolite crystallisation while the hydrophobic part of the template restricts the crystal growth in

one of the crystallographic directions [15]. As a result, each crystal has a shape of a nanosheet of unit cell thickness.

Recently, our group has disclosed and continue to further develop so-called top-down synthesis of lamellar zeolites. The top-down synthesis is a unique method enabling to post-synthetically transform a 3-dimensional zeolite into a lamellar precursor [16], similar to those obtained by hydrothermal synthesis of **MWW** and **FER** with the topology of the parent zeolite. A crucial condition for this transformation is that the parent zeolite is a germanosilicate with character of dense silica layers connected with double-4-ring (D4R) bridging units (e.g. **UTL**, **IWW**, **IWR**). Germanium is located mainly in the D4R units and it can be removed by acid hydrolysis leaving a material consisting of free silica layers, which can be further manipulated and even reconnected into a new fully connected zeolite (so-called Assembly-Disassembly-Organisation-Reassembly – ADOR strategy) [16, 17].

3.4.Layer manipulation

Great advantages of lamellar zeolitic materials lay in their flexibility and rich possibilities of their post-synthesis modification. The most important modifications are presented in Figure 1. When identifying the modified materials, the **MWW** zeolite based materials will serve as example.

Lamellar zeolite precursor consists of alternating crystalline silica layers and the SDA molecules in between the layers. Contrary to conventional zeolites (where the structure is fully covalently bonded directly after the synthesis), there are no covalent bonds between the individual layers and the SDA molecules are kept together only by hydrogen bonds [12]. The SDA molecules prevent full 3-dimensional covalent connection but keeps the layers in regular orientation one to another. Upon calcination (typically occurring at temperatures above 400°C), the SDA molecules are removed and consequently a dehydration of two corresponding silanol groups occur to form covalent oxygen bridge connecting the discreet layered into fully connected 3D Framework (Figure 1, “standard route”).

In some cases, the SDA can be removed from the lamellar precursor not only by calcination, but also at low temperature (below 80°C; Figure 1 “detemplated”), under the conditions when the silanol condensation into oxygen bridges does not occur. In the case of **MWW**, the template can be removed by diluted HNO_3 solution (<2 M) [18]. In the resulting material, the layers are assumed to be randomly oriented one on another and the material exhibit increased external surface area (150 vs. 117 m^2/g) and decreased micropore volume (0.13 vs. 0.17 cm^3/g) with respect to the 3D-**MWW**.

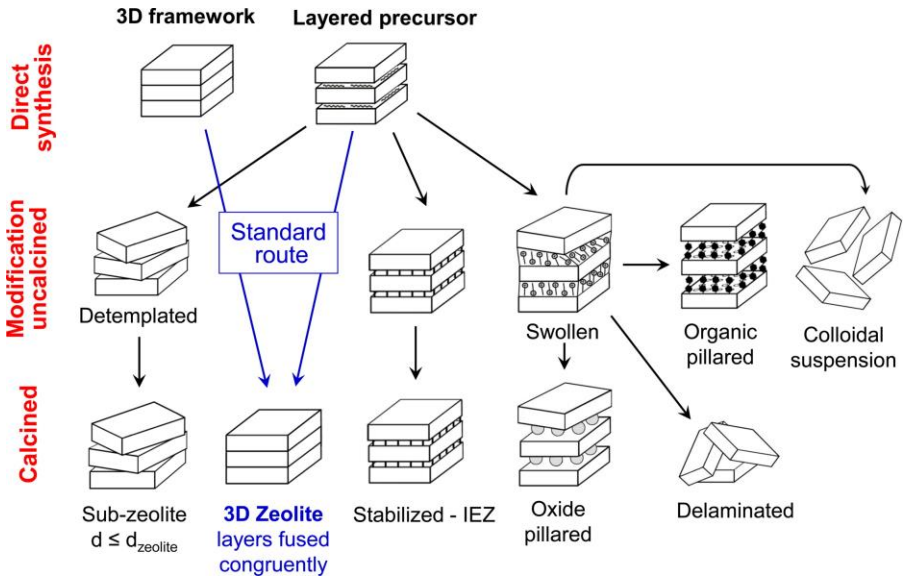

Figure 1: Post-synthesis modifications of layered zeolites. Scheme adapted from [19].

When an appropriate bridging group is inserted in between the layers and connected to the silanol groups (typically additional silicon atom), a so-called interlayer expanded zeolite (IEZ) is obtained [20]. The process of interlayer expansion is sometimes referred to as stabilisation. The IEZ are characterised by larger interlayer pore openings in comparison with their parent structures. For instance IEZ-**MWW** has 12-ring pores and 2.7 nm basal *d*-spacing while conventional **MWW** has 10-ring pores and basal *d*-spacing of 2.5 nm. Except of IPC-2 material [17], the IEZs do not possess fully connected framework and free silanol groups are present on the bridging atoms.

A critical step in the layered zeolite precursor modification is the breaking of the interlamellar hydrogen bonds and expansion of the interlayer space. This process is called swelling (Figure 1) and it is well developed also for lamellar materials such as clays, phyllosilicates and layered metal oxides [21]. In case of lamellar zeolites, the swelling is usually performed using a high concentrated (25 wt. %) quarterly ammonium surfactant (e.g. cetyltrimethylammonium) in a high pH medium [22]. Typically, the swollen material exhibits highly increased interlamellar distance (e.g. **MWW**: *d*-spacing 5.2 nm vs. 2.6 nm in **MWW**(P) [23]). It should be noted, that the materials prepared using a surfactant [15] are swollen intrinsically.

The swelling is not a final step of the post-synthesis modification and once the interlamellar hydrogen bonds are broken, a number of other materials can be prepared. The layers are kept apart from each other by organic surfactants and when these are removed e.g. by calcination, the layers collapse. To preserve the interlayer expansion even after calcination, the layers need to be supported by a material, which is not removed by calcination. In was found that

the TEOS easily penetrates among the surfactant chains in the interlayer space, where it is converted into mesoporous amorphous silica pillars [21]. The first pillared zeolite material is **MWW** denoted MCM-36 [22] and since it was reported, pillaring became a standard modification of lamellar zeolitic materials; however, the true structure of the pillars remain undisclosed because of lack of regularity [12].

Also other linkers like silsesquioxanes or organic linkers may be inserted [24]. The later provide hybrid organic-inorganic materials with interesting adsorption properties. Recently, also covalent insertion of iron, titanium, tin, zinc and europium has been reported in RUB-36 (type of IEZ-**MWW**) [25].

Delaminated material is comprised of randomly edge-to-plain oriented lamellae. Highly open structure is the main feature of this material. The outer surface of the lamellae is well accessible from interparticle space. Corma et al. established this group of materials by ultrasonic treatment of swollen **MWW** layers, forming a material denoted ITQ-2 [26]. However, the **MWW** delamination procedure is not generally applicable and examples of other delaminated zeolites are sparse (only **NSI**, **FER**, **RWR** precursors) [12]. We made several attempts to delaminate nanosheet **MFI** zeolite prepared by the restricted crystal growth method [15] using conditions similar to the ITQ-2; however, TEM analysis revealed that the product (although having BET area up to 800 m^2/g and total adsorption capacity 1.50 cm^3/g) is only a physical mixture of starting nanosheet **MFI** and amorphous silica coming out from partial dissolution of the zeolite [27].

The swollen material may be dispersed also into of single lamellae colloidal solution [28]. The so-called exfoliation into single layers has been reported for several zeolites including **MWW** and **MFI** [29].

3.5.Titanosilicate zeolites

3.5.1. Titanosilicate zeolites: TS-1

Originally, the zeolites possessed powerful acidobasic properties; however, incorporation of other heteroelements (e.g. titanium, boron, iron, vanadium, tin, germanium and others) into their crystalline framework is possible and it opens other areas of catalysis [30]. In 1983, Taramasso et al. [31] reported successful preparation of titanium silicalite-1 (TS-1), a zeolite with **MFI** structure (Figure 2, three-dimensional channel system of intersecting elliptical 10-ring pores with diameters of 5.3 x 5.5 and 5.1 x 5.5 Å) and titanium isomorphously substituted in the framework [32]. This discovery represents a considerable breakthrough in the field of

oxidation catalysis. Formerly known catalysts such as Ti(IV)/SiO_2 [33] were able to catalyse selective oxidation of propylene with organic hydroperoxides; in contrast, the TS-1 was the first heterogeneous oxidation catalyst being able to activate peroxides in the presence of other strongly coordinating compounds, especially water [31, 34].

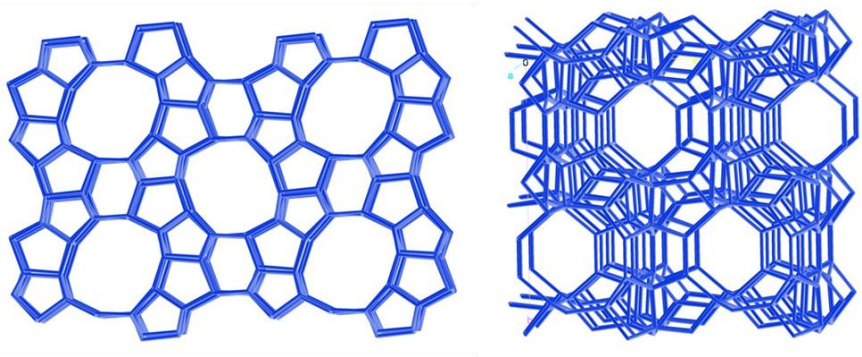

Figure 2: MFI structure. View into the straight channel along b-axis (left) and view into the zig-zag channel along a-axis (right); adapted from [4].

Besides oxygen, the use of H_2O_2 as the oxidant is highly convenient from both the economic and environmental point of view. The hydrogen peroxide has high content of the active oxygen and the only by-product is water [35]. In contrast, conventional synthetic routes towards epoxides, for instance, require the use of chlorine and a strong base, hydroperoxides or peracids [30]. The use of such reactants is accompanied by production of stoichiometric amounts of organic and inorganic by-products, which need to be recycled or disposed. The TS-1 / H_2O_2 oxidation system catalyses a number of different selective oxidation reactions: e.i. epoxidation of olefins [36-38], oxidation of alkanes to alcohols and ketones [39], oxidation of aromatic hydrocarbons to phenols [40], oxidation of phenols to hydroquinones [41], ammoxidation of cyclohexanone [42], oxidation of amines to hydroxylamines [43] and thioethers to sulfoxides [44, 45]. At present, the TS-1 is industrially applied as a catalyst by Eni in propylenoxide process, production of hydroquinone and catechol from phenol and cyclohexanone ammoxidation [46].

Although TS-1 is an excellent catalyst for oxidation of small molecules (e.g. propylene, linear olefins, unsubstituted benzene), due to its relatively narrow (10-ring) pores, the access of larger molecules to the active sites is limited. Therefore, titanosilicates with enhanced accessibility of the active sites, namely large and extra-large pore titanosilicates (possessing 12-ring resp. 14-ring channels) and hierarchical, inter alia, lamellar titanosilicates, are subject of interest. [47], [48], [12].

3.5.2. Titanosilicate zeolites: Ti-beta

Ti-beta (**BEA,** Figure 3) is one of the interesting large-pore zeolites, which has been successfully prepared with the titanium isomorphously incorporated in the framework. The Ti-**BEA** is formed in the presence of tetraethylammonium hydroxide as a structure directing agent (SDA); however, in contrast to the TS-1, it is usually obtained in a low yield [49]. To improve both yield and the catalytic properties of the Ti-**BEA**, alternative synthetic methods e.g. seeding of the synthesis gel with dealuminated zeolite Beta [50], use of alternative template (di(cyclohexylmethyl)dimethylammonium cation) [51], synthesis in fluoride media [52] and dry gel conversion method [53] were developed. The aluminium free Ti-**BEA** zeolite provides much higher epoxide selectivity (e.g. epoxidation of 1-hexene, selectivity 93%) in comparison with Ti,Al-**BEA** (prepared in the first syntheses), especially in combination with an appropriate solvent (acetonitrile) [54].

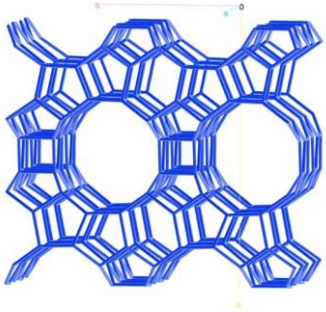

Figure 3: BEA structure view along a-axis; adapted from [4].

3.5.3. Titanosilicate zeolites: Ti-MWW

Preparation of titanosilicate with **MWW** zeolitic structure (Figure 4, medium pore zeolite with 2-dimensional system of 10-ring pores and 7.1 x 18.1 Å supercages) was a challenge until it was found, that titanium is effectively incorporated into the framework in the presence of boric acid together with using conventional SDAs for the **MWW** aluminosilicate: hexamethylene imine or piperidine [55], [56]. The resulting material contains also boron atoms incorporated in the framework. The observed XRD patterns are well consistent with those of **MWW**(P) lamellar precursor, generally known as MCM-22(P). Regarding the Ti content, the system is very effective in Ti incorporation (little difference was observed between the Ti content in the synthesis gel and solid product) and no anatase formation was observed in the UV spectra of the prepared as-synthesized materials. However, extra-framework Ti species, present in the material, are transformed into anatase phase upon calcination [56]. The presence of anatase phase in the titanosilicate catalysts is undesirable, because anatase decomposes ineffectively the oxidant [30]. Strong mineral acids (HNO_3,

H_2SO_4) are able to wash out the octahedrally coordinated extra-framework titanium species. When the treatment is applied prior to the calcination, a material containing only the framework (tetrahedrally coordinated) titanium atoms is obtained [55].

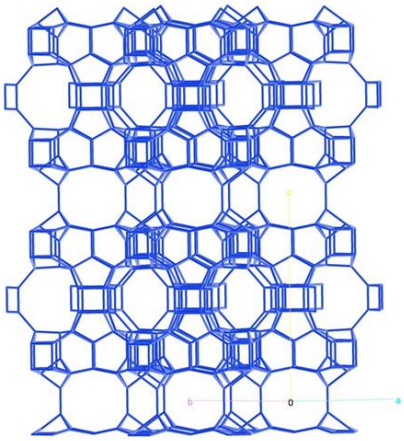

Figure 4: MWW structure view into the 10-ring channels; adapted from [4]

Upon treatment with mineral acids, not only extra-framework titanium but also boron atoms are washed out of the material. As a result the Ti-**MWW** possess Si/B ratio > 500; however, defect silanol nests are present in the positions originally occupied by the boron atoms. Great effort has been developed to prepare the Ti-**MWW** without the defect sites [34]. Basically, such material can be obtained either by synthesis of boron-free Ti-**MWW**(P) or, more conveniently, additional Ti atoms can be inserted into the defect sites forming new active centres. A method using $TiCl_4$ vapours to fill these silanol nests (successfully employed e.g. for preparation of Ti-**MOR** [57]) has been patented for Ti-**MWW** [58]; however, the distribution of Ti in the crystal is questionable, because the $TiCl_4$ molecule (kinetic diameter 6.7 Å) is expected to suffer for steric obstacles while entering the 10-ring channels of Ti-**MWW**. Therefore, other methods have been intensively studied. Wu and Tatsumi developed so-called „reversible structural conversion“ [59] approach where calcined B-**MWW** material is deboronated by 6M HNO_3 solution and subsequently treated with tetrabutyl orthotitanate (TBOTi) mixture with hexamethylene imine or piperidine and water under hydrothermal conditions (175°C for 7 days). Upon this treatment, lamellar structure of Ti-**MWW**(P) is restored and titanium is incorporated into the structure without the presence of boron. Subsequent acid treatment does not lead to formation of defect sites, because only extra-framework titanium atoms are removed. The authors claim, the conversion between lamellar **MWW**(P) and 3-dimensional **MWW** (which occur upon calcination) to be reversible under the reversible structural conversion conditions. However, considering the fact, the zeolite is treated with an aqueous solution of its SDA, under the conditions characteristic for the zeolite **MWW** synthesis, for

time similar to the duration of the **MWW** zeolite synthesis, we speculate, that the process is not a transformation of 3-dimensional **MWW** to lamellar **MWW**(P) with the titanium incorporation into the defect sites but it is, in fact, a full recrystallization of the zeolitic structure. Nevertheless, defect free Ti-**MWW** is obtained by this process. It has been mentioned that the Ti-**MWW** material is formed via lamellar precursor. This is an important feature opening rich area of post-synthesis modifications which lead to a group of **MWW** based materials with enhanced accessibility of the active sites. These materials are reviewed in a separate chapter below together with their catalytic performance.

3.5.4. Other titanosilicate zeolites

It is possible to prepare also other zeolites in the titanosilicate form, either by direct hydrothermal synthesis of by post-synthesis modification (usually by incorporation of titanium into a dealuminated or deboronated zeolite). Shortly after the TS-1 disclose, also TS-2 (Ti-**MEL**, medium pore zeolite with 3-dimensional system of 10-ring channels) has been directly synthesized [60] followed by successful hydrothermal syntheses of Ti-**BEA** and another large pore titanosilicate Ti-**MTW** (zeolite with 1-dimensional 12-ring pores) [61]. Corma et al. reported direct synthesis of Ti-**FER** (medium pore zeolite with 10-ring and 8-ring intersecting channels) and its delaminated form denoted Ti-ITQ-6 [62]. Diaz-Cabanas et al. synthesised large-pore titanosilicate Ti-**ISV** (originally denoted Ti-ITQ-7, large-pore zeolite with 3-dimensional channel system) [63]. Balkus et al. prepared an extra-large pore Ti-**DON** (extra-large pore zeolite with 1-dimensional channels) material using a special bis(pentamethylcyclopentadienyl)cobalt(III) hydroxide SDA [64]. Recently, our group succeeded in hydrothermal synthesis of two novel extra-large pore titanosilicate zeolites Ti-**CFI** (1-dimensional 14-ring channels) [37] and Ti-**UTL** (2-dimensional system of intersecting 14-ring and 12-ring channels) [65]. Discussion of their synthesis, characterisation and catalytic properties is subject of this thesis.

Rigutto et al. prepared first aluminium-free Ti-**BEA** by treatment of a deboronated **BEA** with vapours of $TiCl_4$ at elevated temperature [66]. Later, Wu et al. demonstrated preparation of Ti-**MOR** in a similar way from a dealuminated material. ^{18}O exchange of the samples and subsequent IR analysis confirmed that the Ti-**MOR** contains titanium atoms bound via 3 or 4 oxygen bridges in the aluminium vacancies which are the desired species for peroxide activation [57]. The Ti-**MOR** was found to be able to catalyse ketone ammoxidation [67] and oxidation of aromates to fenols with hydrogen peroxide [68]. Similarly, Kubota et al. prepared of Ti-**MSE** (generally denoted Ti-MCM-68) from a dealuminated parent **MSE** zeolite [69]. Furthermore, Ti-YNU-2 (Ti-**MSE** analogue) represents an example of a catalyst tailoring for a

certain reaction (phenol oxidation) [41]. In this case, a highly defective silicious precursor YNU-2(P) was stabilised by steaming followed by gas phase Ti insertion using $TiCl_4$. The prepared Ti-YNU-2 exhibits nearly an order of magnitude higher TON in comparison with Ti-**MSE** prepared via dealuminated material and with TS-1 in oxidation of phenol. Dartt and Davis used the same method as Rigutto for Ti-**BEA** for the titanium incorporation into large-pore borosilicate **CON** (generally denoted SSZ-33) [70]. The deboronated material was exposed to the $TiCl_4$ vapours in argon at 300°C. Diffuse reflectance ultraviolet (DR-UV) spectra analysis proved that the prepared Ti-**CON** is containing titanium atoms mainly in tetrahedral framework positions and anatase phase is not present. The Ti-**CON** catalysed cyclooctene epoxidation with hydrogen peroxide.

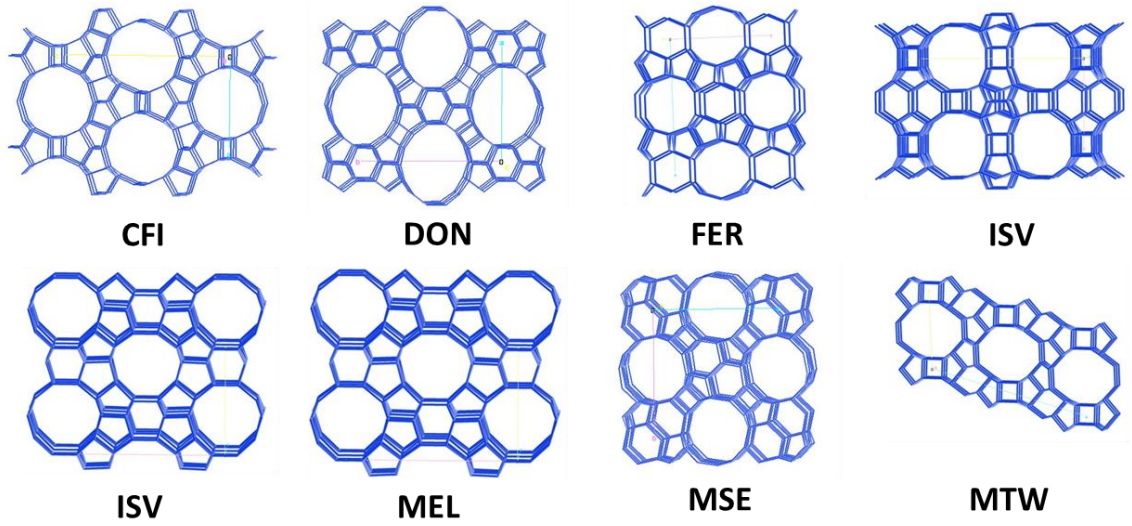

Figure 5: Structure views of the discussed titanosilicate zeolites adapted from [4].

An alternative approach to the titanium insertion from gas phase is the introduction of titanium atoms from a liquid solution of the titanium precursor. For instance, Corma et al. used titanocene dichloride grafting from a $CHCl_3$ solution on ITQ-2 delaminated material to prepare Ti/ITQ-2 catalyst [71] with highly accessible isolated titanium sites. However, this material is active epoxidation catalyst only with *tert*-butyl hydroperoxide in water free conditions. Recently, our group successfully combined the approach of liquid phase impregnation, with the use of deboronated parent zeolite. Deboronated zeolites **CON**, **AFI**, **IFR** and **CFI** were impregnated with a solution of $TiCl_4$ or tetrabutyl orthotitanate (TBOTi) and tested in epoxidation with hydrogen peroxide [38]. Discussion of their preparation and properties is a subject of this thesis and it was already successfully used by Kim et al. [72].

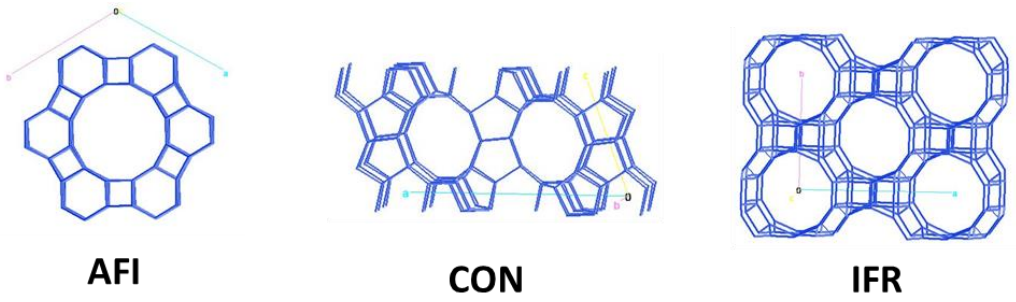

Figure 6: Structures of borosilicate zeolites ; adapted from [4].

3.6.Titanosilicates with enhanced accessibility of the active sites

Large-pore zeolites exhibit lower diffusion restrictions in comparison with medium-pore titanosilicates especially for bulkier substrates. Nevertheless, selective oxidation of sterically demanding substrates, such as terpenes, unsaturated fatty acid esters and bulky substituted or cyclic olefins remains a challenge. These bulky molecules penetrate with difficulties even into the channels of large-pore titanosilicate crystals. In such a case, reactions take place mainly on the outer surface of the titanosilicate crystals or in its close proximity. To provide the access to the active centres inside the crystal, additional mesopores need to be created or thickness of the crystal needs to be reduced. In the first case, we speak about hierarchical materials (*vide supra*), in the second case lamellar (two-dimensional) structures are applied (*vide supra*).

3.6.1. Lamellar titanosilicates

Only layered forms of zeolites **MWW** [56] and **FER** [62] have been prepared in a titanosilicate form. Recently, two alternative "non-classical" approaches (*vide supra*) were disclosed [12], which are applicable also on titanosilicates (Figure 7).

Corma et al. reported delamination of Ti-**FER** lamellar precursor forming Ti-ITQ-6 material [73]. The Ti-**FER** precursor was swollen by cetyltrimethylammonium hydroxide and then subjected to an ultrasound treatment which allows the delamination. The BET area of the Ti-ITQ-6 was 618 m^2/g while the **FER** exhibited 270 m^2/g and according to the *t*-plot analysis, the micropore area was lower than 10 m^2/g.

Fan et al. disclosed direct synthesis of a layered material denoted Ti-YNU-1 [74], which is similar to Ti-**MWW** lamellar precursor and exhibits slightly increased *d*-spacing (2.75 nm) in comparison with Ti-**MWW** precursor (2.5 nm). Further study revealed that the Ti-YNU-1 is in fact an interlamellar expanded zeolite with titanium atoms in the bridging positions between the layers [75]. Corma et al. prepared an expanded Ti-**MWW**(exp) material similar to Ti-YNU-1

by hydrothermal treatment of pure silica **MWW** (denoted also ITQ-1) with piperidine and titanium source [76]. Wu et al. delaminated Ti-**MWW** lamellar precursor [77] by applying the original method for ITQ-2 [78] (delaminated **MWW** aluminosilicate) preparation. Kim et al. described a preparation of pillared Ti-MCM-36 (**MWW** layers) catalyst by swelling of the Ti-MCM-22P layers with a surfactant and supporting of the layers (pillaring) with amorphous silica. The resulting material possesses mesopores with pore size of about 2.8 nm between the crystalline layers. Recently, Ouyang et al. reported a delamination of **MWW** borosilicate in acidic solution of $Zn(NO_3)$. The resulting material denoted DZ-1 was subsequently impregnated with titanium (IV) butoxide forming Ti-DZ-1 which was found to be active in cyclohexene epoxidation [79].

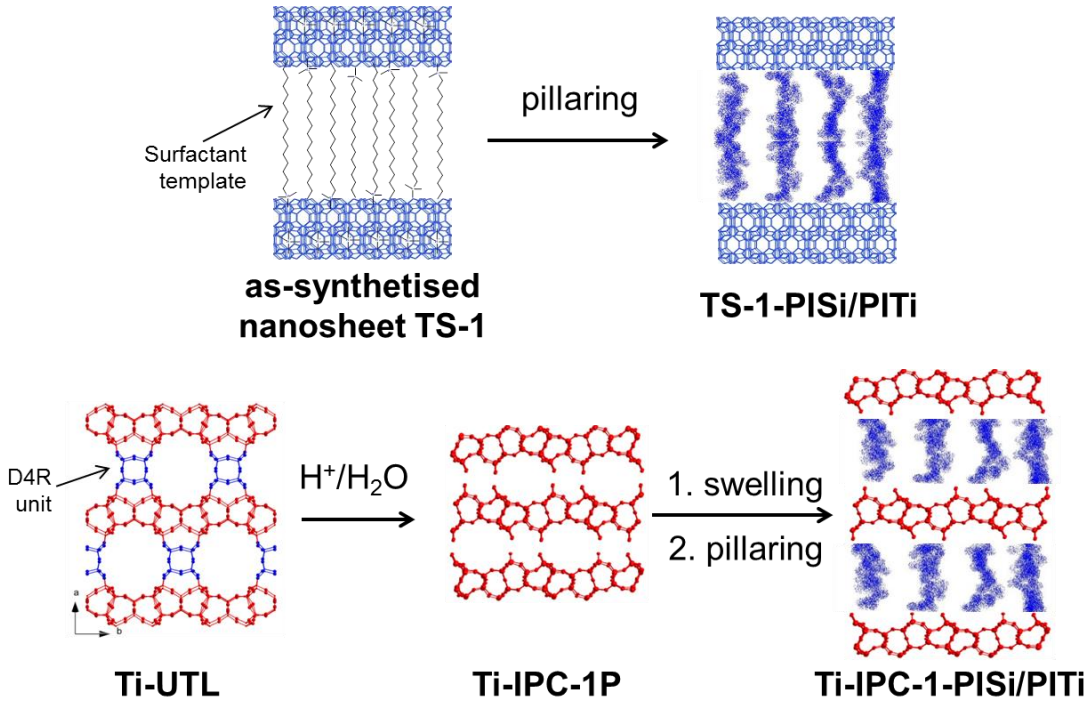

Figure 7: Non-classical syntheses of titanosilicates: simplified view of layered TS-1 preparation and pillaring and top-down transformation of Ti-UTL into pillared Ti-IPC-1PI materials.

Ryoo et al. reported the preparation of TS-1 in the form of nanosheets [80]. The nanosheet TS-1 is formed using surfactant based template $C_{18}H_{37}N^{+}(CH_3)_2C_6H_{12}N^{+}(CH_3)_2C_6H_{13}\ OH^{-}{}_2$ (denoted $C_{18\text{-}6\text{-}6}OH_2$) instead of conventional tetrapropylammonium hydroxide [81]. The resulting material consists of 2 nm thick layers; it possesses a large interlamellar volume on one hand and regular microenvironment around the tetrahedrally coordinated titanium centres located in the crystalline layers. This material has been reported to exhibit activity similar to the conventional 3-dimensional TS-1 in epoxidation of 1-hexene (a molecule which easily

penetrates into **MFI** micropores) with hydrogen peroxide; however, its activity is an order of magnitude higher in epoxidation of cyclooctene in comparison with conventional TS-1 [80].

Recently, Kim et al. [72] grafted titanium (IV) butoxide on the nanosheet TS-1 creating additional and well accessible Ti centres on the outer surface of the layers. The procedure practically follows the one developed for post-synthesis titanium impregnation of borosilicates by our group [38]. For details, see the results and discussion part. Further post-synthetic modifications of the nanosheet TS-1 [82] as well as top-down transformation of Ti-**UTL** and consequential post-synthesis modifications of the resulting lamellar precursor denoted Ti-IPC-1P [65] are subject of this thesis.

3.6.2. Hierarchical titanosilicates

First hierarchical TS-1 was synthetized by Jacobsen et al. [83] using carbon nanoparticles (carbon black pearls) with average diameter of 18 nm. The resulting mesoporous TS-1 had average size of the mesopores 20 nm and it provided the same yield as conventional TS-1 in the epoxidation of 1-octene (ratio between product yield over mesoporous and conventional catalyst after the same reaction time $y_{mesoporous}/y_{conventional}$ = 1). However, a 10 times higher yield of cyclohexene oxide ($y_{mesoporous}/y_{conventional}$ = 9.5 after 70 min of reaction) was obtained in the epoxidation of cyclohexene with H_2O_2 . The carbon nanoparticles templating approach is widely used by a number of other groups e.g. [84-86].

Ke et al. prepared TS-1 with mesopore size of 3.3–6.5 nm by hydrothermal and steam-assisted dry gel conversion techniques in the presence of triethanolamine. It is claimed that the addition of triethanolamine promotes the stability of tetrahedral Ti and create more mesopores in the dry gel [87].

Eimer et al. prepared a mesoporous titanosilicate by assembly of polymeric zeolite precursor species. The TEM analysis showed that the resulting material is composed of agglomerates of TS-1 nanocrystals having about 120 nm in diameter. Catalytic activity was demonstrated on α-pinene oxidation with hydrogen peroxide showing a little difference was observed between the mesoporous titanosilicate and reference Ti-MCM-41 [88].

Cheneviere et al. prepared hierarchical TS-1 in the presence of an organosilane surfactant. The material was characterised by regular mesopores having diameter of 2.5 - 3.5 nm; however, the advantages of a hierarchical material manifested only in cyclohexene epoxidation when *tert*-butyl hydroperoxide was used as the oxidant and the reaction was carried out in the absence of water [89]. The authors explain the observed results by increased

concentration of surface silanol groups but no detailed data are provided on the hydrophilicity of the material. Zhao et al. used the same synthesis approach and different setup of the catalytic experiment and increased TON was observed for the mesoporous TS-1 (TON=60 after 2 h) in comparison with conventional TS-1 (TON=30). Furthermore, ^{29}Si MAS NMR showed little difference in the ratio between Q4 $Si(OSi)_4$ species and Q3 $Si(OSi)_3OH$ species. For the conventional TS-1 ratio Q4/Q3 ratio 3.0 was observed while for mesoporous TS-1 exhibited Q4/Q3 ratio 3.7 [90].

Kang et al. used mesoscale random copolymer which contained quarterly ammonium groups as an SDA. The resulting mesoporous TS-1 was well crystalline and contained mesopores of diameter between 6 and 8 nm [86].

Only a few references deal with the TS-1 desilication as a method to prepare mesoporous TS-1: Chao et al. treated the TS-1 by 0.2 mol/l solutions of various alkali metal hydroxides for 30 min, obtaining mesoporous TS-1. The use of CsOH led to partial destruction of the crystalline structure (BET area (274 m^2/g) decreased strongly in comparison with the other materials (BET= 423-446 m^2/g)) [91]. Silvestre-Albero and co-workers used higher concertation of NaOH desilication solutions (0.4 – 0.8 mol/l) and although it is claimed that the resulting materials provided elevated conversion of *tert*-butyl cyclohexene, the XRD patterns show that the zeolitic structure is completely destroyed especially when 0.6 and 0.8 mol/l desilication solutions are used [92].

Recently, Li et al. reported preparation of core/shell structured titanosilicate by desilication-recrystallisation method. Use of a diammonium surfactant ($C_{18}H_{37}N^+(CH_3)_2C_6H_{12}N^+(CH_3)_2C_3H_7$ OH^-_2; similar to the one used for synthesis of nanosheet TS-1 [80]) together with mild desilication conditions led to a growth of TS-1 nanosheets on the surface of the parent TS-1 crystal [93].

3.6.3. Titanium containing mesoporous molecular sieves

In 1992, ordered mesoporous molecular sieves were disclosed by Mobil researchers [94]. These siliceous materials show uniform mesopores with sizes up to 10 nm; however, their walls are built of amorphous silica. Corma et al. first reported Ti containing MCM-41 [95]. Similar molecular sieve called Ti-HMS (hexagonal mesoporous silica) was prepared by Tanev et al. [96]. Tatsumi et al. prepared Ti-MCM-48 which possesses a 3-dimensional channel system with a cubic symmetry [97] and Ti-SBA-15, which is similar to Ti-MCM-41, but it has the main channels connected with micropores [98]. All the above materials were active in epoxidation of bulky substrates (e.g. norbornene) with bulky oxidants such as *tert*-butyl hydroperoxide,

clearly showing the expected benefits of mesoporous structure. The data on effectivity of the titanium containing mesoporous sieves in epoxidation with hydrogen peroxide differ dramatically for different substrates although these should penetrate easily through the wide channels. For instance, Corma et al. [95] claims 91% selectivity at 30% conversion of 1-hexene over Ti-MCM-41 in 5h [95] while Tatsumi et al. [99] report less than 2% conversion of cyclohexene over Ti-MCM-41 and Ti-MCM-48 in 3 h (both reactions were carried out using similar substrate/catalyst mass ratio (S/C=14 resp. S/C=10) at similar temperature 56 resp. 50°C). Silylation of Ti-MCM-41 and Ti-MCM-48 with trimethylsilane to reduce the amount of surface silanol groups resulted in an increase in the activity (e.g. TON=112 (silylated Ti-MCM-41) vs. 5.5 (non silylated Ti-MCM-41)), but the reported values of selectivity in cyclohexene epoxidation were still below 20% [99].

3.7. Titanium active sites

Not only the titanium content but simultaneously the character of the titanium species determines the performance of the catalyst [100]. It is generally assumed that isolated framework tetrahedrally coordinated titanium species are the active sites catalysing the (ep)oxidation reactions [101]. However, there exist a number of indicia that also other isolated titanium species (not connected to any other titanium atom via oxygen bridges) might be active in oxidation catalysis [38, 41, 102].

According to Pauling's criterion [103], Ti^{4+} should not be able to be incorporated in the zeolite framework because its ionic radius is too large. The ratio of ionic radii ρ of the cation and anion (oxygen) is 0.515 which falls out of the range ρ=0.225-0.414, when tetrahedral coordination is expected. However, it is very rough approximation since the T-O bond is not completely ionic and the model also assumes a perfect round shape of the atoms. It was proved that zeolite framework flexibility (especially **MFI**) is high enough and the titanium incorporation is possible [31]. It was demonstrated that TS-1 has an increased volume of unit cell in comparison with pure silica MFI. The more titanium is incorporated, the higher is the unit cell volume. This can be observed in the XRD pattern [32]. However, beyond a certain limit, further addition of the titanium is not further incorporated and extra-framework species are formed instead. Millini et al. showed that this limit is about Si/Ti molar ratio 40 for the **MFI** (TS-1) structure. It is expected that such limits exist also for other zeolites.

Presence of a band characteristic for tetrahedrally coordinated titanium in the DR-UV/Vis spectrum is another straightforward proof of the titanium incorporation [104]. The presence of the band results from a charge transfer from oxygen ligand to an unoccupied orbital of the

titanium atom. For isolated $Ti(OSi)_4$ species it occurs between 205 and 210 nm for the TS-1 and at about 220 nm for the Ti-**MWW** [56, 104, 105]. Titanosilicate zeolites may contain also other titanium species. The $Ti(OH)(OSi)_2$ titanol species were found to absorb around 228 nm, extra-framework species (five and six-coordinated) exhibit a broad absorption at 260-290 nm and anatase-like phase (several titanium atoms connected via oxygen bridges) absorbs at 330 nm [104, 105]. Generally, the higher is the coordination number of the Ti atom, the higher is the absorption wave length. The presence of the anatase phase is undesirable because it causes unproductive decomposition of the hydrogen peroxide [30]. The behaviour of the extra-framework species in the catalytic reaction is a subject of debates.

Another fingerprint indicating the presence of titanium in the framework position is a vibrational band at 960 cm^{-1}, which can be observed in infrared (IR) and Raman spectra [31, 100]. However, precise origin of this band is still subject of debates. Different theories of its precise origin are reviewed in [105].

3.8.Epoxidation over titanosilicates

Linear and cyclic olefins and especially 1-hexene and cyclohexene are usually the first substrates to test and to demonstrate a new titanosilicate catalyst activity in epoxidation reactions. The reactions are carried out in a liquid phase in a batch reactor using polar solvents such as methanol or acetonitrile. 0.5 Or 1 molar equivalent of 30-35% aqueous hydrogen peroxide as the oxidant is usually used. Reactions are performed at temperatures between 30 and 70°C. Typical experimental setup is close to 0.05 g of a catalyst, 10 mmol of substrate, 10 mmol of the H_2O_2 and 10 ml of a solvent [106]. Data from continuous experiments are rarely reported (e.g. epoxidation of methallyl chloride [107]).

3.8.1. Linear olefins

Tatsumi et al. were the first to study systematically the shape selectivity in epoxidation of olefins over the TS-1. The rate of epoxidation decreased with increasing length of the hydrocarbon chain [108]. Clerici et al. [109] studied in detail epoxidation of C_4–C_8 linear and branched olefins together with allylchloride and allylalcohol over TS-1. Competitive experiments of two similar substrates were carried out as well. TS-1 acts as an electrophile and therefore relative reactivity of different alkenes is dependent on nucleophilicity of the double bond. However, both restricted transition state shape selectivity and diffusion effects of reactants and products also contribute to the ordering of the reactivity and thus the electronic effect might be masked.

Corma et al. studied epoxidation of 1-hexene and 1-dodecene over TS-1 and Ti-**BEA** with a content of aluminium (Si/Ti=25-55, Si/Al=60-120) using methanol resp. ethanol as a solvent at 25 and 80°C. The authors expected the large-pore Ti-**BEA** to be more active than the TS-1; however, the observed TON were lower in comparison with TS-1 (e.g. 1-hexene: TON (TS-1)=50 vs. TON(Ti-**BEA**)=12). Moreover, the presence of highly acidic aluminium sites promoted ring opening reactions and as a result only 12% selectivity to the epoxide was observed oxidising the 1-hexene, while 80% selectivity to the hydroxymethoxyhexane was observed. Similarly for 1-dodecene, 1,2-dihydroxydodecane was the only product obtained over the Ti-BEA, while 77% epoxide selectivity was provided by the TS-1 [110]. In a more detailed study [36], also branched olefins (4-methyl-1-hexene, 2-methyl-2-pentene) were tested. In this case, the advantage of the Ti-**BEA** large pores manifested. The Ti-**BEA** provided 17.2% conversion of 2-methyl-2-pentene after 2 h at 50°C while the TS-1 only 3.9%. However, the main product using the Ti-BEA was corresponding glycol-monomethyl ether in all the cases.

Dartt and Davis [70] tested their large-pore Ti-**CON** with titanium incorporated post-synthetically using $TiCl_4$ vapours against TS-1 and aluminium free Ti-**BEA** in epoxidation of 1-hexene. The most active Ti-**CON** samples (Si/Ti=22) provided conversion 5.7% with 27% selectivity after 2 h at 50°C while the Ti-**BEA** provided 4.2% conversion with 31% selectivity and TS-1 11.9% conversion with 97% selectivity. These results represent considerable improvement in comparison with earlier Ti,Al-**BEA** [36]. The advantages of the wide pores in Ti-**CON** and Ti-**BEA** were manifested in epoxidation cyclohexene and cyclooctene (*vide infra*).

Van der Waal and van Bekkum [111] studied solvent effect in epoxidation of 1-octene using the aluminium free Ti-**BEA**. It was found that in methanol at 40°C, the reaction does not occur at all (while the TS-1 provided 4.1% conversion after 1h) and at 60°C, the main product is the hydroxy-methoxyoctane. The low activity of Ti-**BEA** at 40°C is explained by the hydrophilic character of the material, when water and methanol are strongly adsorbed on the surface, hindering the access of the 1-octene to the active sites. When less polar solvents were used (ethanol, 2-propanol, *tert*-butanol) at 40°C, conversion 0.7%, 1.9% and 0.3%, respectively, was observed after 1 h. Furthermore, the selectivity gradually increased from 40% (ethanol) to 67% (*tert*-butanol). The authors pointed out that the ring opening reactions are catalysed by the Ti site itself as it exhibits a slight Lewis acidity. When, slightly basic acetonitrile was used as the solvent, 0.7% conversion and 89% selectivity were achieved after 1 h and even after 5 h of the reaction, the epoxide represented 98% of the oxidation products. This evidences that acetonitrile is able to suppress the Lewis acidity of Ti-**BEA** and therefore the undesired ring-

opening reactions. Further study [54] of linear alkene epoxidation over Ti-**BEA** in acetonitrile at 70°C focused on the effect of position and configuration of the double bond in the molecule. It was found that epoxidation of internal double bond occurs slightly faster than that of terminal bond; however, steric effects also play a role (e.g. Initial turnover frequency (TOF, [mol mol_{Ti}^{-1} h^{-1}]): 2-octene[1] 169 > 1-octene 148 ≈ *trans*-4-octene 152). Also the olefins with shorter chain are epoxidised faster than those with longer chain (e.g. TOF, [mol mol_{Ti}^{-1} h^{-1}]: 1-hexene 235 > 1-octene 148 > 1-heptene 129 ≈ 1-decene 127). This effect was observed using the TS-1 earlier [108].

Corma et al. [62] synthetized Ti-**FER** and its delaminated ITQ-6 form and demonstrated their activity in epoxidation of 1-hexene with hydrogen peroxide. The Ti-**FER** provided conversion of 1-hexene only 3.2% while the delaminated Ti-ITQ-6 gave conversion 19.7% after 5 h. The delaminated material was active similarly to the Ti-**BEA** (conversion 18.0 %, TON (Ti-ITQ-6)=23 vs. TON (Ti-**BEA**)=20). To our knowledge, this is the first example of a lamellar titanosilicate epoxidation catalyst.

Wu et al. [47] reported increased activity of Ti-**MWW** in comparison with TS-1 in 1-hexene epoxidation in acetonitrile at 60°C. The Ti-MWW exhibited TON 150–250 after 2 h depending on the titanium content while the TS-1 exhibited only TON=73. The catalyst with the highest Ti content (Si/Ti=38) provided conversion 44.8% with 99% selectivity while the conversion over the TS-1 was only 5.8%. This is an example of a catalyst which is more active than the TS-1 in epoxidation of 1-hexene.

The pillared Ti-MCM-36, reported by Kim et al. [112], exhibited more than 3 times higher TON (Ti-MCM-36: 257, TS-1: 81) than conventional TS-1 in 1-hexene epoxidation at 45°C even when the optimal solvents for both catalysts were used for comparison (acetonitrile for Ti-MCM-36, methanol for the TS-1). TON=125 was observed for the 3-dimensional Ti-**MWW**.

Fan et al. [106] focused on the solvent influence on the activity of the Ti-**MWW** (and TS-1 and Ti-**BEA**). It was found that in contrast to the TS-1 not only the Ti-**BEA** but also Ti-**MWW** exhibits much higher activity when acetonitrile is used as a solvent instead of methanol. Also other solvents (e.g. acetone, ethanol, *tert*-butanol) and mixtures of the preferred solvents (methanol/acetonitrile/water) were investigated showing that hydrophilicity of the catalyst is another important parameter which need to be taken into account while optimising a reaction.

[1] Mixture of *cis* and *trans* isomer.

Xiao et al. [113] reported catalytic activity of Ti-COE-3 resp. Ti-COE-4 materials prepared by interlamellar expansion of Ti-RUB-36 lamellar material with dichlorodimethyl silane. The materials differ in the presence of methyl resp. hydroxyl groups on the bridging silicon atoms between the layers and therefore in the hydrophilicity. The Ti-COE-3 provided 8% conversion after 4 h while the Ti-COE-4 gave 14.2% in epoxidation of 1-hexene in methanol at 60°C; however the less hydrophilic Ti-COE-3 exhibited higher epoxide selectivity (20%) then Ti-COE-4 (7%). The main product was 1-hexen-3-one in both cases (selectivity 72 resp. 69%).

The use of nanosheet TS-1 provided lower conversion (13.9% in methanol after 2 h at 60°C) of 1-hexene in comparison with 3-dimensional TS-1 (19.7%) although keeping 95% selectivity [80]. Wang et al. [114] reported even higher difference in 1-hexene conversion in both methanol (layered TS-1 conversion 6.5% vs. TS-1 25.2%) and acetonitrile (layered TS-1 conversion 4.1% vs. TS-1 12.1%). We consider this to be a final proof that for linear olefins, conventional TS-1 or Ti-**MWW** are the catalysts of choice. On the other hand, the use of large-pore and lamellar structures is highly advantageous in epoxidation of cyclic olefins and terpenes (*vide infra*).

3.8.2. Cyclic olefins

Hulea et al. [115] studied epoxidation of cyclopentene with hydrogen peroxide over TS-1 and Ti-**BEA** catalysts using different solvents at 40°C. When the reaction was carried out in methanol, TS-1 provided higher conversion (87% after 3 h) then the Ti-**BEA** (57%); however, in acetonitrile, the difference was negligible (19% resp. 17%). Methanol was found to be the best solvent in term of the reaction rate, but the highest selectivity was achieved in Ti-**BEA**/acetonitrile system (97%) and TS-1/*tert*-butanol system (99%). The TS-1/methanol system provided only 21% selectivity.

Since it was found in the early studies that TS-1 is unable to epoxidise cyclohexene [39] and other bulky substrates effectively due to the diffusion restrictions, a strong effort has been made to synthesise catalysts with better accessibility to the active centres (*vide supra*). Dartt and Davis reported aluminium free Ti-**BEA** and vapour phase titanium incorporated Ti-**CON** to be active in oxidation of cyclohexene and cyclooctene [70] in methanol at 70°C. Ti-**BEA** provided cyclohexene conversion 29.3% after 3 h and the most active of the Ti-**CON** catalysts provided conversion 25.5% at the same time while only 2.4% of the substrate was converted using the TS-1. Hydrogen peroxide efficiency (amount of H_2O_2 used effectively for the oxidation reaction) was above 90% in all cases. However, cyclohexene oxide underwent total methanolysis to 1-hydroxy-2-methoxycyclohexane. Contrary, cyclooctene oxide was stable

under the reaction conditions. Using the Ti-**BEA**, cyclooctene conversion was 33.3% after 3 h, what corresponds to total conversion of the hydrogen peroxide (substrate/H_2O_2 ratio was 3). The Ti-**CON** provided conversion 25.3% while TS-1 only 2 %. Epoxide selectivity above 99% was observed using all 3 catalysts. The results evidence the use of large-pore titanosilicates is a feasible approach how to oxidise bulkier substrates. Sasidharan and Bhaumik [116] reported a detailed study on tuning the properties of Ti-**BEA** using various SDAs in hydroxide and fluoride media. The prepared catalysts were examined in 4-vinyl-1-cyclohexene epoxidation. Conversion of the substrate at 65°C ranged between 15 and 37.8% after 1.5 h and a ratio of ring/side chain oxidation products ranged from 0.19 to 0.40 depending on the used template; however, no direct connection between the template structure and catalytic performance is described. The TS-1 provided conversion of 18% selectively oxidising the side chain of the substrate.

The Ti-**MWW** proved its ability to oxidise cyclohexene giving conversion up to 7.1% at 60°C after 2 h with 63% selectivity. The TS-1 provided only 0.5% conversion and Ti-BEA 11.9% in the same set of experiments [47]. A study of solvent effects [106] using Ti-**MWW** in epoxidation of cyclohexene revealed that in the case of Ti-**MWW**, acetonitrile is the most beneficial solvent (providing the highest conversion and selectivity) as in the case of 1-hexene.

Fan et al. tested interlamellar expanded Ti-YNU-1 catalyst (Ti-**MWW** structure) [74] in epoxidation of C_5-C_{12} cycloalkenes at 60°C in acetonitrile. The Ti-YNU-1 provided cyclohexene conversion 21.2 % after 2 h what is more than 3-dimensional Ti-**MWW** (8.1%, Si/Ti=45) and Ti-BEA (16.5%, Si/Ti=35) although it had a Si/Ti ratio as high as 240. The Ti-YNU-1 was the most active of the tested catalysts (Ti-YNU-1, TS-1, Ti-**MOR**, Ti-**BEA**, Ti-**MWW**) in all cyclopentene, cyclohexene, cycloheptene and cyclooctene epoxidations (e.g. cycloheptene TON: Ti-YNU-1 1100 vs. Ti-**MWW** 50) demonstrating the advantages of a layered catalyst. Shen et al. used the Ti-YNU-1 for epoxidation of α,β-unsaturated ketones. The Ti-YNU-1 was able to oxidise 2-cyclopenten-1-one and 2-cyclohexene-1-one but it failed to oxidise their 3-methylated analogues. Ti-**BEA** oxidised all 4 mentioned substrates [117].

Moliner and Corma reported an alternative synthesis of expanded Ti-**MWW**(exp) material (analogue to Ti-YNU-1) [76]. The Ti-**MWW**(exp) provided cyclohexene conversion of 35% after 5 h at 60°C what is 7 times more than the conversion provided by Ti-**MWW.** Over the Ti-YNU-1, the conversion was only 2.6 times higher in comparison with Ti-**MWW** [74].

Xu et al. prepared Ti-IEZ-**MWW** by stabilisation of the lamellar precursor with dichlorodimethylsilane resp. dichlorotertramethyldisilane in 2M HNO_3 solution. The material stabilised with dichlorodimethylsilane did not exceeded the performance of Ti-YNU-1 and Ti-**MWW**(exp) providing even lower conversion of cyclohexene than Ti-**MWW** (7.8% vs. 12.7% after 2 h at 60°C). The material stabilised with dichlorotetramethyldisilane provided cyclohexene conversion of 20.3%. These results are in a sharp contrast with the work of Wang et al. [118]. Wang and co-workers reported the preparation of interlayer expanded Ti-IEZ-**MWW** using diethoxydimethylsilane. The material expressed an order of magnitude higher TON (Ti-IEZ-**MWW**: 233, Ti-**MWW**: 33) compared with Ti-**MWW** in epoxidation of cyclohexene at 60°C and the observed conversion was 5 times higher (20.7% vs. 4.1% after 2 h at 60°C).

Except of the above mentioned modifications of Ti-**MWW** material, Na et al. significantly contributed to the area of bulky substrates epoxidation introducing nanosheet TS-1 catalyst [80]. The nanosheet TS-1 catalyst provided 25% conversion of cyclohexene with 69% selectivity and 15.3% conversion of cyclooctene with 95% selectivity after 2 h of reaction in acetonitrile at 60°C. Even epoxidation of cyclododecene is reported using the nanosheet TS-1 [72]. The observed conversion after 2 h was 5.2% what is more than mesoporous Ti-MCM-41 (3.1%), which was used as a benchmark.

The above results shows, that large-pore titanosilicates and interlamellar expanded zeolites are able to oxidise cyclic olefins up to C_8 ring. Except the nanosheet TS-1, no efficient catalyst is reported for epoxidation of cyclodecene or cyclododecene.

3.8.3. Terpenes and other bulky substrates

Terpenes and their oxygenated derivates are used in food and fragrance industry [119]. Therefore, the epoxidation of terpenes using titanosilicate catalysts is given certain attention; however, it still represents a challenge.

Van der Waal used zeolite Ti-**BEA** in epoxidation of a number of bulky substrates including norbornene, camphene and limonene [54]. 13.3% conversion was observed in epoxidation of norbornene in methanol at 60°C using the Ti-**BEA** after 1h. The epoxide selectivity was 37%. TS-1 was unable to oxidise norbornene at all and mesoporous Ti-MCM-41 provided conversion of 6.7% with 48% selectivity. When the epoxidation using the Ti-**BEA** was carried out in acetonitrile at 70°C, conversion of 8% and selectivity of 89% was observed after 1 h.

Corma et al. also tested Ti-**FER** delaminated ITQ-6 material in epoxidation of norbornene in acetonitrile at 60°C and compared the results with Ti-**BEA** [73]. The Ti-ITQ-6 provided

conversion of 16.5% after 2 h while the Ti-**BEA** provided 13.3% conversion. One would expect that Ti-**FER** will be unable to oxidise bulky and rigid bicyclic substrate such as norbornene; however, norbornene conversion of 13% is reported after 2 h, unfortunately without any comments on the Ti-**FER** unexpected activity. Selectivity is reported between 88 and 91% for all 3 catalysts. Kim et al. showed that also nanosheet TS-1 is able to epoxidise norbonene in acetonitrile at 60°C giving conversion of 22% with 83% selectivity [72].

Sasidharan and Bhaumik compared epoxidation of 4-vinyl-cyclohexene limonene, 4-vinyl-norbornene, 4-ethylidene-norbornene and 1-phenyl-cyclohexene in methanol and acetonitrile using Ti-BEA at 65°C. It was found that solvent used plays a very little role in driving the selectivity between two different double bonds. Furthermore, terminal double bond on the side chain was always found to be more reactive than the double bond in the ring [120].

Eimer et al. studied α-pinene selective oxidation using mesoporous titanosilicate composed of TS-1 protozeolitic particles (basically a kind of hierarchical TS-1) [88]. The reactions were carried out in acetonitrile at 70°C. A wide palette of products was observed of which α-pinene oxide and 1,2-pinanediol were the most abundant (up to 21.6 mol.% resp. 18.7 mol.% in products). Other important products (over 10 mol. % in products) were verbenol, verbenone, myrthenal and *trans*-carvenol.

Except of terpenes, also selective oxidation of other natural products is subject of interest. Selective oxidation of FAME is one of them. Kamegawa et al. demonstrated epoxidation of methyl oleate using titanium containing mesoporous-macroporous silica [121]. Wilde et al. showed that also industrial TS-1 is able to perform this reaction. The highest selectivity (87%) was observed in acetonitrile at 50°C (conversion 93% after 24 h) [122].

3.9.Oxidations of bulky organic sulphides

Organic sulphoxides and sulphones are valuable intermediates [123] and building blocks of pharmaceuticals [124] and agrochemicals [125]. Besides that oxidative desulphurization can represent an alternative route to hydrodesulphurization (HDS); especially, where the sulphur compounds are difficult to remove using the conventional HDS [126]. In addition to heterogenous oxidation catalysts, there exists a palette of different oxidants (e.g. peroxides, NaOCl, H_5IO_6, $KMnO_4$ [127], peroxynitrous acid [128]) and homogenous catalysts (e.g. complexes of titanium [129], vanadium [130], tungsten [131] and zinc [132]), which are capable to selectively oxidise sulphides to corresponding sulphoxides and sulphones; however, from the engineering point of view it is always convenient to work with a heterogeneous catalyst.

Corma et al. reported oxidation of methylphenyl sulphide (MPS) and phenyl-*iso*-pentyl sulphide over Ti-**BEA** and mesoporous Ti-MCM-41 with both hydrogen peroxide and *tert*-butylhydroperoxide [133]. The Ti-**BEA** provided higher conversion (95% vs. 80% after 30 min at 40°C) in oxidation of MPS confirming higher intrinsic activity of crystalline titanosilicates, but in oxidation of phenyl-*iso*-pentyl sulphide the diffusion limitations manifested themselves and the Ti-MCM-41 provided higher conversion (20% vs. 60% after 6 g at 40°C).

Hulea et al. studied oxidation of dialkyl, alkyl-aryl and diphenyl sulphides to corresponding sulphoxides with hydrogen peroxide using titanosilicates Ti-**BEA** and TS-1 [134]. Dialkyl sulphides bearing short linear substituents (methyl, ethyl, *n*-butyl) were oxidised rapidly (conversion over 75% after 2 h at 30°C). On the other hand, the diphenyl sulphide was oxidised slowly, especially when the TS-1 was used (conversion 5 % after 2h at 30°C). Moreau et al. reported a kinetic study on oxidation of dibutylsulphoxide to sulphone and preceding oxidation of sulphide to sulphoxide. The oxidation of sulphoxide to sulphone was found to be of the first order with respect to the sulphoxide and catalyst and zero order with respect to the hydrogen peroxide [135].

Kang et al. [86] studied oxidation of bulky alkyl-aryl and di-aryl sulphides using mesoporous TS-1. Of the bulkiest substrates, diphenyl sulphide conversion was 99% after 10 h at 30°C with 98% sulphoxide selectivity. Total conversion of benzylphenyl sulphide was observed after 14 h with 90% selectivity. Upon addition of higher amount of H_2O_2 and prolongation of the reaction time, the sulphoxides were further oxidised to corresponding sulphones. Interestingly, water was found to slow down the oxidation of sulphide to sulphone.

Kon et al. investigated oxidation of a number of dialkyl and alkyl-aryl sulphides over Ti-**MWW** and Ti-IEZ-**MWW** under solver free conditions at 25°C. Especially for the bulkiest diphenyl sulphide, the diffusion facilitation provided by the interlayer expansion was clearly demonstrated (conversion over Ti-**MWW** 36% vs. Ti-IEZ-**MWW** 64% after 18 h at 40°C) [136]. Also competitive oxidation of methylphenyl sulphide (MPS) and *para*-substituted methylphenyl sulphides was studied and evaluated using the Hammett free energy plot [137]. It was found that the substrates with electron donating groups (methyl, methoxy groups) were oxidised faster in comparison with MPS (e.g. methyl-*p*-methoxyphenyl sulphide conversion 5.5% vs. MPS conversion 2.7% after 5 min in a competitive experiment) and *para*-halogen substituted MPS were oxidised slower than the MPS (e.g. methyl-*p*-chlorophenyl sulphide conversion 7.3% vs. MPS conversion 8.6% after 5 min). This further confirms the electrophillic character of the titanium active species.

Hulea et al. also demonstrated the possibility of dibenzothiophene (DBTH) oxidation with H_2O_2 using Ti-**BEA** and Ti-HMS (hexagonal mesoporous silica). TS-1 was found inactive. The DBTH oxidation can be used in oxidative desulphurisation (ODS) processes e.g. for removal of sulphur from kerosene. ODS may represent an alternative when commonly used hydrodesulphurisation process is costly because it occurs at mild conditions without hydrogen consumption and high-pressure apparatus [44]. Du et al. extended the concept of mesoporous TS-1 use to the ODS reporting effective oxidation of thiophene, DBTH and 4,6-dimethyldibenzothiophene [138].

4. Experimental

4.1. Reagents and solvents

Origin and purity of the reagents and solvents used for the preparation of the catalysts and catalytic testing are listed in Table 1.

Table 1: List of used chemicals

Reagents used in the catalyst preparation

Chemical	Purity	Origin	Abbreviation
(-)-Spartein sulfate pentahydrate	99%	SAFC	
1-aminooctane	99%	Aldrich	
Ammonium nitrate	p.a. 99.5 %	Lach-Ner	NH_4NO_3
Boric acid	99%	Fluka	H_3BO_3
Cab-O-Sil M-5 (SiO_2)		Havel Composites	
Carbon black pearls 2000		Cabot	CBP
Cetyltrimenthylammonium chloride	25 wt. % in H_2O	Aldrich	C_{16}TMA Cl
Diethoxydimethylsilane	98%	Aldrich	
Germanium oxide	99.999%	Alfa Aesar	GeO_2
Iodomethane	99%	Fluka	
Lithium hydroxide hydrate	99%	Fluka	
Piperidine	99%	Riedel de Haen	
Sodium hydroxide	p.a. 98%	Penta	
Sodium tetraborate decahydrate	p.a. 99.5 %	Penta	
Tetrabutyl orthotitanate	97%	Aldrich	TBOTi
Tetraethyl orthosilicate	98%	Aldrich	TEOS
Tetraethyl orthotitanate	98%	Aldrich	TEOTi
Tetrapropylammonium hydroxide	40 wt.% in H_2O	Aldrich	TPA-OH
Titanium (IV) chloride	98%	Aldrich	$TiCl_4$

Reagents used in the catalytic tests

Chemical	Purity	Origin	Abbreviation
1,3-diisopropylbenzene	95%	Fluka	
1-octene	98%	Aldrich	
Cis-cyclooctene	95%	Aldrich	
Dibenzothiophene	98%	Aldrich	DBTH
Dioctylsuphide	96%	Aldrich	
Diphenyl sulphide	98%	Aldrich	Ph_2S
H_2O_2 aqueous solution	35 wt.%	Aldrich	H_2O_2
Linalool	97%	Aldrich	
Mesitylene	99%	Acros Organics	
Methylphenyl sulphide	99%	Aldrich	MPS
Norbornene	99%	Aldrich	
Trans-cyclodecene	98%	Aldrich	

Reagents used in the catalytic tests (continued)			
Chemical	**Purity**	**Origin**	**Abbreviation**
Verbenol	95%	Aldrich	
α-pinene	95%	Acros Organics	

Other reagents and solvents

Chemical	Purity	Origin
1-butanol	98%	Lachema
Acetonitrile	HPLC grade	Fisher chemical
Anion exchange resin AG1-X8	OH^- form	Biorad
Ethanol	absolute, p.a.	Penta
Ethyl acetate	p.a.	Penta
Hydrochloric acid	p.a.	Penta
Nitric acid	p.a.	Penta
Toluene	p.a.	Penta

4.2. Synthesis of conventional TS-1

Conventional titanosilicate TS-1 was prepared from a reaction gel with initial Si/Ti ratio 43 using the procedure originally described in Ref. [81] with slight modifications [139]. Tetrabutyl orthotitanate (TBOTi) and tetraethyl orthosilicate (TEOS) were used as the titanium and silica source, respectively. Tetrapropylammonium hydroxide (TPA-OH, 40 wt. % in water) served as a structure directing agent. The TBOTi (580 mg) was added dropwise into the TEOS (15.3 g) and stirred for 45 min under ambient conditions prior to the addition of water (43.0 g) and TPA-OH (9.32 g). The initial gel composition was 100 TEOS: 2.32 TBOTi : 35 TPA-OH : 4000 H_2O. The hydrothermal crystallization occurred in a 90 ml Teflon-lined autoclave at 175°C under agitation. The crystallization time was adjusted to 70 h (TS-1(200)) resp. 94 h (TS-1(600)) forming two materials with different crystal size (number in brackets in nm, determined by SEM). The final zeolite was filtered off, washed with a copious amount of distilled water, dried at 80°C and finally calcined in air, at 550°C for 8 h, using a temperature ramp of 1°C/min.

4.3.Synthesis of mesoporous TS-1

Mesoporous titanium silicalite-1 (meso-TS-1) was prepared using carbon black pearls (CBP, diameter 20 nm) as a secondary templating agent. The procedure was based on [81] and originally reported in [139]. The initial gel with a molar ratio of Si/Ti = 43 was prepared from TEOS (15.3 g) and TBOTi (580 mg) distilled water (43.0 g) and TPA-OH (9.32 g) as the structure-directing agent. First, the TBOTi was added dropwise into the TEOS and stirred for 45 min at ambient conditions. Next, water and TPA-OH were added, the mixture was stirred another 30 min. Last, the CBP (6.00 g) were added and the black gel was homogenized for 30 min. The

final synthesis gel with molar composition 100 TEOS : 2.35 TBOTi : 25 TPA-OH : 3700 H_2O : 680 CBP was hydrothermally crystallized in a Teflon-lined autoclave (90 cm^3) at 175°C for 90 h under agitation. After the hydrothermal synthesis, the zeolite was filtered off, washed with a copious amount of distilled water, dried at 85°C and finally calcined in an air flow (150 cm^3/min) at 550°C for 24 h using a temperature ramp of 2°C/min.

4.4. Desilication of TS-1

Desilication of the TS-1 was performed in an aqueous solution of NaOH in the following way. 1 g of the parent TS-1 was added into 30 ml of preheated NaOH solution (concentration 0.2 or 0.05 M) and stirred typically for 40 min at 65°C. After the given time, the suspension was diluted with 100 ml of cold distilled water, centrifuged for 20 min, washed with water and centrifuged again. The solid material was dried at 65°C. Residual Na^+ cations present in the material slow down the epoxidation. They were removed by ion-exchange of the desilicated TS-1 with NH_4NO_3. The samples were treated four-times with 1.0M NH_4NO_3 solution for 4 h at room temperature using 100 ml of the solution per 1 g of the sample and re-calcined at 450°C for 90 min before use in catalytic experiments.

4.5. Synthesis of layered and pillared TS-1

The synthesis of layered TS-1 (also parent to the pillared TS-1) was carried out according to the Na et al. procedure [80] from TEOS and TBOTi, using surfactant SDA in hydroxide form, denoted $C_{18\text{-}6\text{-}6}OH_2$. The surfactant SDA $C_{18}H_{37}$ -$N^+(CH_3)_2$ -C_6H_{12} -$N^+(CH_3)_2$ -C_6H_{13} in hydroxide form was prepared as described in the literature [80]. Typically, the TBOTi (1.081 g) was added dropwise into TEOS (26.39 g) and stirred for 30 minutes. Then an aqueous solution of the SDA (7.6 mmol in 130 g of water) was added to the mixture was let to hydrolyse at 60°C for 3 h. The evaporated mass of ethanol and water was replaced with the same mass amount of water at the end. The synthesis mixture with initial composition 100 TEOS : 2.5 TBOTi : 6 $C_{18\text{-}6\text{-}6}OH_2$: 5000 H_2O was hydrothermally crystallized in a 90 ml Teflon-lined autoclave at 160°C for 236 h under agitation. After the given time, the zeolite was filtered off, washed with water, dried at 80°C and finally calcined or subjected to the pillaring treatment. Calcination was carried out in static air at 570°C for 8 h, using a temperature ramp of 1°C/min.

To prepare a pillared material from the as-synthetized layered TS-1, no swelling of the material was necessary as the layers are swollen intrinsically by the surfactant template. The pillaring (silica as well as silica-titania pillaring), originally reported in [82], was performed modifying the Kim procedure [112]. TEOS (for the silica pillaring) or a mixture of TEOS and TBOTi with a given Si/Ti molar ratio was mixed with the as-synthetized dry layered zeolite (10 g of the TEOS

mixture per 1 g of the zeolite) and stirred at 65°C for 24 h. Then the mixture was centrifuged and the solid material was separated and dried at room temperature for 48 h. Subsequently, the product was hydrolysed in water with 5% of ethanol (100 ml/1 g) at ambient temperature for 24 h under vigorous stirring. Ethanol in the mixture helps to disperse the hydrophobic titanosilicate. Finally, the solid material was centrifuged again, dried at 65°C and calcined in an air flow (200ml/min) at 550° C for 10 hours using the temperature ramp of 2° C/min. The silica pillared materials are denoted TS-1-PISi, the silica-titania pillared materials are denoted TS-1-PITi (Si/Ti) with the pillaring mixture Si/Ti ratio in brackets.

4.6. Synthesis of Ti-MCM-36

The synthesis followed the procedure described by Wu et al. [56]. Piperidine (SDA, 26.1 g) was added to distilled water (73.3 g) and stirred for 15 min. The piperidine solution was divided into two equal parts and TBOTi (1.54 g)) was added into one part and H_3BO_3 (17.73 g) was added to the other part. Both solutions were stirred for about 50 min. Then, equal amounts of pyrogenic SiO_2 (Cab-O-Sil M-5, total 12.86 g) were slowly added into both solutions and stirred for another 60 min. Finally, both resulting slurries were mixed together and stirred for 60 min. The final gel of molar composition 3.5 TBOTi : 134 H_3BO_3 : 143 piperidine : 100 SiO_2 : 1900 H_2O was charged into a Teflon-lined autoclaves (90 cm^3). The crystallization proceeded under agitation and the temperature was increased stepwise. The crystallization started at 130 °C for the first 24 h, then, the temperature was increased to 150°C for another 24 h and finally, to 170°C for 120 h. After the hydrothermal synthesis, the solid product was collected by filtration, washed with distilled water and dried in an oven at 60 °C. To remove extra-framework Ti-species, the as-synthesized product (denoted as Ti-**MWW**(P)) was stirred in a 2M HNO_3 at 85°C for 15 h (20 $cm^3\ g^{-1}$) and then filtered, washed with distilled water and dried at 60°C again yielding lamellar precursor Ti-**MWW**(P).

To transform the Ti-**MWW**(P) into Ti-MCM-36, the Ti-**MWW**(P) was swollen using 20 $cm^3\ g^{-1}$ of 25 wt.-% aqueous solution of cetyltrimethylammonium hydroxide (C_{16}TMA-OH, prepared by ion-exchange from the chloride form). The slurry was stirred at ambient temperature for 16 h. The swollen Ti-**MWW**-sw was separated by centrifugation, washed with distilled water and dried in air at 60°C.

Pillaring of Ti-**MWW**-sw was carried out with TEOS (50 $cm^3\ g^{-1}$) at 85°C for 16 h under stirring. The solid product was isolated by centrifugation and dried at ambient temperature for 24 h. Subsequently, the material was hydrolysed in water (100 $cm^3\ g^{-1}$) at ambient temperature for another 24 h. Finally, the solid product was separated again by centrifugation, dried at 60°C

and calcined in flow of air at 550°C for 10 h using a temperature ramp of 2° C min^{-1} resulting in Ti-MCM-36.

4.7. Synthesis of Ti-UTL

The Ti-**UTL** was prepared using a procedure reported earlier [65], [140]. The titanium was introduced into the framework directly during the hydrothermal synthesis. The initial reaction gel with Si/Ti molar ratio 50 was prepared from Cab-O-Sil M5, TBOTi, germanium oxide, distilled water, and (6R,10S)-6,10-dimethyl-5-azoniaspiro[4.5]decane hydroxide as an SDA. The preparation of the SDA is described in Ref. [141]. The aqueous solution of the SDA (0.033 mol) was diluted with water (45.0 g) and Cab-O-Sil M-5 (4.00 g) and GeO_2 (3.48 g) were added under stirring. After 30 minutes of homogenization, TBOTi (453 mg), diluted 1:3 with 1-butanol, was added dropwise and the gel was stirred for another 30 minutes. The initial molar composition of the synthesis gel was 2 TBOTi : 50 GeO_2 : 50 SDA : 100 SiO_2 : 3750 H_2O. The zeolite crystallized in a 90-ml Teflon-lined autoclave at 175°C under agitation for 7 days. The final product was filtered off, washed with water, dried at 85°C and finally calcined with a stepwise increase of the temperature. At first at 200°C for 2 h, then at 350°C for 4 h and finally at 550°C for 8h, using a temperature ramp of 2°C/min.

The synthesis of B-**UTL**, which was used as a parent material in the preparation of IPC-1PITi catalyst, is described in the Ref. [140].

4.8. Post-synthesis modifications of Ti-UTL

All the post-synthesis modifications of the Ti-**UTL** were performed according to procedures reported earlier [16], [17]. The Ti-**UTL** was converted into lamellar precursor Ti-IPC-1P by acid hydrolysis with 0.01 M HCl. 250 ml of the HCl solution was used per 1 g of the calcined Ti-**UTL** and the material was hydrolysed at 75°C for 16 h under agitation. The resulting lamellar precursor Ti-IPC-1P was collected by filtration, washed with water and dried at 65°C.

The Ti-IPC-1PISi (silica pillared) and Ti-IPC-1PITi (silica-titania pillared) materials were prepared in a following way. The Ti-IPC-1P was swollen with a solution of C_{16}TMA-OH (30 g/g of theTi-IPC-1P). The swelling occurred at room temperature for 24 h under stirring. The swollen product was centrifuged, washed with water and dried at 65°C. The pillaring was done using TEOS or its mixture with TBOTi (Si/Ti = 30) to form pillared lamellar Ti-IPC-1PISi resp. Ti-IPC-1PITi catalyst. 10ml of the pillaring medium were used per 1 g of the swollen material and the mixture was stirred at 85°C for 24 h. Then the mixture was centrifuged and the solid material was dried for 48 h at room temperature. Subsequently, the product was hydrolysed in water with 5% of ethanol (100 ml/1 g) at ambient temperature for 24 h under vigorous stirring.

Finally, the solid material was centrifuged again, dried at 65°C and calcined in an air flow (200 ml/min) at 550° C for 8 h using a temperature ramp of 2°C/min.

The Ti-IPC-2 catalyst was prepared by stabilization of the Ti-IPC-1P with diethoxydimethylsilane in 1M HNO_3 in a 25-ml Teflon-lined autoclave at 175°C for 16 h without agitation. 10 ml of the HNO_3 solution and 0.5 g of the diethoxydimethylsilane were used per 1 g of the Ti-IPC-1P. A strongly hydrophobic product was obtained. Final calcination was performed at 550°C for 8 h using a temperature ramp of 2°C/min.

The Ti-IPC-4 was formed via intercalation of the Ti-IPC-1P with 1-aminooctane. 1 g of the Ti-IPC-1P was mixed with 30 ml of 1-aminooctane and stirred at 90°C for 16 h. The solid material was centrifuged and dried at room temperature for 24 h. Finally the material was calcined at 750°C for 8 h with a temperature ramp of 2°C/min.

4.9. Synthesis of Ti-CFI

The Ti-**CFI** zeolite was prepared from TBOTi, lithium hydroxide hydrate, Cab-O-Sil M-5 and *N*(16)-methylsparteinium hydroxide as the SDA [37]. The *N*(16)-methylsparteinium hydroxide was prepared according to the procedure described in ref. [142]. In the first step, N(16)-methylsparteinium iodide was prepared by a reaction of (-)-spartein and methyl iodide in acetonitrile at room temperature for 72 h. The resulting iodine salt was ion exchanged into hydroxide form using strongly basic anion exchange resin AG1-X8 in OH^- form. Properly ion exchanged SDA solution exhibited pH=14.0 and no opacity after acidification with 1M HNO_3 to pH=1 and addition of 1 volume of 0.06M $AgNO_3$ solution.

The synthesis of the **CFI** was based on the procedure described in ref. [142]. *N*(16)-methylsparteinium hydroxide (N-MeSpa-OH , 0.3 M aqueous solution, 30.3 g) was mixed with demineralised water (14.7 g) and lithium hydroxide hydrate (210 mg) in a Teflon-lined autoclave. A solution of TBOTi (283 mg), diluted 1:3 with 1-butanol, was added dropwise to the synthesis mixture under vigorous stirring during 2 min. The resulting mixture was homogenized at room temperature for 30 min. Finally, Cab-O-Sil M-5 silicon oxide (3.00 g) was added and the mixture was stirred for another 30 min. In some cases the mixture was seeded with earlier prepared “as-synthetized” **CFI** crystals. The milky homogeneous mixture, with molar composition 0-2.0 TBOTi : 10 N-MeSpa OH : 5 LiOH : 50 SiO_2 : 2500 H_2O, was closed in an autoclave and heated under agitation to 155 – 170 °C for 6 to 17 days. The solid product was collected by filtration, washed out with demineralised water and dried overnight at 65°C. Calcination of the samples was carried out in a stream of air (200 ml/min) at 570°C for 8 h.

To remove extra-framework titanium species from the **CFI** samples, some samples were treated with nitric acid solution prior to the calcination. 30 to 90 ml (depending on Si/Ti ratio) of 2.0M HNO_3 solution was used per 1 g of dry as-synthetized material. The mixture was heated at 100°C for 16 h. After the given time, the solid material was filtered off, washed with water and calcined as described above.

In order to remove Li^+ anions, some samples were ion-exchanged with ammonium nitrate. Calcined samples were treated four-times with 1.0M NH_4NO_3 solution for 4 h at room temperature using 100 ml of the solution per 1 g of the sample. The samples were re-calcined at 540°C for 6 h before use.

4.10. Synthesis of large-pore borosilicate zeolites and their deboronation

Parent B-**AFI** (SSZ-24 zeolite) was prepared using a modified procedure described by Lobo and Davis [143]. N-MeSpa OH (0.71 M aqueous solution, preparation described in paragraph 4.9, 11 ml) was mixed with demineralised water (24.4g), lithium hydroxide (82.5 mg) and sodium hydroxide (78.5 mg) in a Teflon-lined autoclave. After dissolution, sodium tetraborate decahydrate (150 mg) was introduced to the synthesis mixture. Finally, Cab-O-Sil M5 silicon oxide (2.36 g) and seeds of earlier prepared B-**AFI** (30 mg) were added and the mixture was homogenized for 30 min. The milky homogeneous mixture, with molar composition 0.625 $Na_2B_4O_7$: 10 N-MeSpa-OH : 2.5 NaOH : 2.5 LiOH : 50 SiO_2 : 2500 H_2O, was closed in a 90 ml Teflon-lined autoclave and heated at 160 °C for 7 days under agitation. The solid product was recovered by filtration, washed out with demineralised water and dried overnight at 65°C. Calcination of the sample was carried out in a stream of air at 570°C for 8 h.

Parent B-**CFI** (CIT-5 zeolite) was prepared according to Yoshokawa et al. [144] and our experience with direct synthesis of Ti-**CFI** [37] using the same SDA as for **AFI**. Synthesis gel with molar composition 1 H_3BO_3 : 10 N-MeSpa-OH : 5 LiOH : 50 SiO_2 : 2500 H_2O (62 mg H_3BO_3 : 33 ml 0.3 M aq N-MeSpa-OH : 210 mg LiOH.H_2O : 3.00 g Cab-O-Sil M5 : 12 g H_2O), was closed in a 90 ml Teflon-lined autoclave and heated at 160 °C for 10 days under agitation. The solid product was collected by filtration, washed out with demineralised water, dried overnight at 65°C and calcined in a stream of air at 570°C for 8 h.

B-**CON** (SSZ-33 zeolite) zeolite was synthesized according to the patent [145] using N,N,N-trimethyl-8-ammonium tricyclo-[5.2.1.$0^{2.6}$]-decane hydroxide as the SDA. The starting gel had the following composition: 24.5 SDA-OH : 22 NaOH : 1 $Na_2B_4O_7$: 161.5 SiO_2 : 7000 H_2O (11.2 ml 1.2 M aq SDA-OH : 0.48 g NaOH : 0.215 g $Na_2B_4O_7$.10 H_2O : 5.40 g Cab-O-Sil M5 : 60.8 g H_2O).

The synthesis was seeded with 2 wt. % of **CON**. The hydrothermal synthesis was carried out in a 90 ml Teflon-lined autoclave heated at 160°C for 4 days under agitation. The solid product was collected by filtration, washed out with demineralised water, dried overnight at 65°C and calcined in an oven under a stream of nitrogen. Samples were heated in stages with a rate of 1°C/min to 120°C, maintained at 120°C for 2 h, then heated to 540°C, kept there for 4 h, and finally heated to 600°C and held for an additional 6 h.

The procedure for the synthesis of B-**IFR** (SSZ-42 zeolite) was based on the method proposed by Zones [146]. The zeolite was synthesized using N-benzyl-1,4-diazabicyclo[2.2.2]octane cation as the template molecule. The reaction mixture has the composition 22 SDA-OH : 1 $Na_2B_4O_7$: 107 SiO_2 : 6550 H_2O (46.1 g 0.35 M aq SDA-OH : 0.969 g $Na_2B_4O_7$.10 H_2O : 8.32 g Cab-O-Sil M5 : 70.15 g H_2O). The reaction mixture was heated in a 90 ml Teflon-lined autoclave at 150 °C for 17 days without agitation. The solid product was filtered, washed out with demineralised water, dried overnight at 65°C and calcined in an oven under a stream of nitrogen. Samples were heated in stages with a rate of 1°C/min to 125°C, maintained 2 h, then heated to 540°C, kept for 4 h, and finally heated to 600°C and held for an additional 4 h.

The initial Si/B molar ratio for all the materials ranged from 20 to 50. All the samples were deboronated in a 0.01 M solution of HCl. Typically, 1 g of zeolite was suspended in 60 ml of the solution and stirred for 24 h at room temperature. After the given time, the zeolite was filtered off, washed out with distilled water and dried at 65°C. Successful deboronation was indicated by a strong decrease in the intensity or total disappearance of a characteristic IR band at 1380 cm^{-1}.

4.11. Titanium impregnation of deboronated zeolites

Impregnations with tetraethyl orthotitanate (TEOTi) resp. TBOTi in liquid phase were performed using following procedure. TEOTi or TBOTi was dissolved in absolute ethanol or butanol, respectively. The deboronated zeolite was activated at 450°C for 60 min, cooled in a desiccator and added to the mixture of titanium alkoxide and alcohol. The mixture was stirred and heated to 45°C for 16 h in a glass round bottom flask under Dimroth condenser. In particular, 158 mg of TBOTi (0.465 mmol) and 33 ml of butanol were used per 1.0 g of the zeolite. After the given time, the mixture was centrifuged, washed out two times with fresh alcohol and the impregnated zeolite was dried at 65°C. At the end, the material was calcined at 240°C for 2 h and then at 560°C for 6 h with the temperature ramp of 2°C/min.

Impregnation with $TiCl_4$ was performed similarly to the above procedure by a solution of $TiCl_4$ in dry toluene. 0.47 ml of 1M solution of $TiCl_4$ (0.47 mmol) was added to a suspension of 1 g of

the activated zeolite in 33 ml of dry toluene. The mixture was stirred at 45°C for 16 h under nitrogen atmosphere. After the given time, the mixture was centrifuged, washed out two times with pure dry toluene, dried at 65°C and calcined at 240°C for 2 h and then at 560°C for 6 h with the temperature ramp of 2°C/min.

Selected samples were treated with vapour of $TiCl_4$ according to a procedure described by Dartt and Davis [70]. 500 mg of the activated deboronated zeolite (activation at 450°C, 60 min) were heated in a quartz reactor to 300°C in a flow of dry argon (50 ml/min). Then the flow of argon was switched to bubble through a vessel with $TiCl_4$, kept at room temperature, before the contact with the sample (still at 300°C). The sample was exposed to the $TiCl_4$ vapour for 60 min a then cooled down to room temperature in pure argon flow. Then, the sample was re-calcined at 560°C for 6 h with temperature ramp of 2°C/min. Direct treatment of B-**IFR** with $TiCl_4$ and subsequent methanolysis according to Dartt and Davis [70] was examined as well. In this case, the sample was cooled to 100°C after the above described exposure to $TiCl_4$ vapour and then the stream of argon was redirected to a methanol bubbler before the reactor. The sample was treated with methanol vapour for 16 h and then cooled and re-calcined as above.

4.12. Characterization techniques

X-ray powder diffraction (XRD) patterns were collected using a Bruker AXS D8 Advance diffractometer equipped with a graphite monochromator and a position sensitive detector Våntec-1 using CuKα radiation in Bragg–Brentano geometry. Typically, data were collected in continuous mode over the 2θ range of 1-40° for the lamellar materials and 2θ range of 5-50° for the conventional zeolites with a step size of 0.00853° and time per step 0.25 s.

The textural properties were determined from nitrogen sorption isotherms. The isotherms were recorded at liquid nitrogen temperature (-196°C) with Micromeritics Gemini volumetric instrument. Prior to the sorption measurements, individual zeolites were degassed in a stream of helium at 300°C for 3 h. BET area was evaluated using adsorption data in the range of a relative pressure from p/p_0 = 0.05 to 0.20. The t-plot method [147] was applied to determine the volume of micropores (V_{micro}) and external surface area (S_{ext}). The adsorbed amount of nitrogen at p/p_0 = 0.95 reflects the total adsorption capacity (V_{total}) of the material.

Detailed nitrogen sorption isotherms and argon sorption isotherms were obtained with a Micromeritics ASAP 2020 volumetric sorption analyzer. To attain sufficient accuracy in the accumulation of the adsorption data, the ASAP 2020 was equipped with pressure transducers covering the 133 Pa, 1.33 kPa and 133 kPa ranges. The measurements were carried out at liquid nitrogen temperature (-196°C) resp. liquid argon temperature (-186°C). Prior to the

analysis, the individual samples were outgassed in vacuo (1.33 Pa) at 250°C overnight. The pore size distribution of mesoporous samples was calculated from the desorption branch of the hysteresis loop using the BJH algorithm [148] with Halsey equation. To analyze the characteristics of pores smaller than 3 nm, low-pressure argon sorption was performed for selected samples at -186°C. The pore size distributions were calculated from the argon adsorption isotherms by the non-local density functional theory (NLDFT) model for cylindrical pores in oxides.

The size and shape of zeolite crystals were examined by scanning electron microscopy (SEM) on a JEOL, JSM-5500LV microscope. The images were collected with acceleration voltage of 20 kV. Energy dispersive X-ray spectroscopy (EDX) analyses were performed using Hitachi S-4800 field emission scanning electron microscope at 25 kV with Noran EDX system. Also some SEM images were collected using the Hitachi S-4800 system at 5 kV.

DR-UV/Vis absorption spectra were collected using Perkin-Elmer Lambda 950 Spectrometer with 2mm quartz tube and 8 x 8 mm slit. The data were collected in the wavelength range of 190-500 nm. All the samples were analyzed after calcination.

Chemical composition of the materials was determined by ICP-OES ThermoScientific iCAP 7000 instrument or using XRF spectrometer Philips PW 1404 with the analytical program UniQuant at Výzkumný ústav anorganické chemie, a. s. (Ústí nad Labem, Czech Republic). For the XRF analysis, the samples were mixed with dentacryl resin as a binder and pressed on the surface of cellulose pellets.

The FTIR spectra of borosilicates and deboronated samples were recorded with a Nicolet 6700 instrument equipped with AEM module with a resolution 4 cm^{-1}. Zeolites were pressed into self-supporting wafers with a density of 8.0–12 mg/cm^2 and activated by outgassing at 450°C in the IR cell under vacuum.

4.13. Catalytic tests

4.13.1. Epoxidation of C=C double bond

The epoxidations of *cis*-cyclooctene, norbornene, α-pinene and verbenol were carried out in a Heidolph Synthesis 1 system at 60°C with the shaking speed of 610 rpm. The alkene/catalyst mass ratio was 10 (S/C = 10) and alkene/H_2O_2 molar ratio was 2. Acetonitrile was used as a solvent and mesitylene served as an internal standard. In a typical experiment, 500 mg of the substrate was mixed with 250 mg of the internal standard, 50 mg of the catalyst and 8 ml of

acetonitrile. The reaction started by addition of H_2O_2 aqueous solution (35%wt.) into the mixture after equilibration at the reaction temperature.

The epoxidation of 1-octene, *cis*-cyclooctene (some experiments), *trans*- cyclodecene and linalool was carried out similarly in a 25 ml magnetically stirred glass three-necked round bottom flask equipped with a Dimroth condenser at 60°C. Typically, 1-octene (1.122g, 10 mmol) was dissolved in 11.75 ml of methanol, followed by 0.5 g of 1,3-diisopropylbenzene as a standard and 50 mg of the catalyst (S/C=22). Epoxidation of linalool (6 mmol, 0.925g) was performed in methanol (9 ml) using 60 mg of the catalyst (S/C = 15) and mesitylene (250 mg) as an internal standard. The reaction started by addition of aqueous solution of H_2O_2 (1 molar eq of linalool) keeping the C=C double bond/H_2O_2 ratio 2. Epoxidations of cyclooctene and cyclodecene were performed using the same amounts of reagents as described above.

Samples of the reaction mixtures were taken in regular intervals, immediately centrifuged to remove the catalyst, cooled and analysed using an Agilent 6850 GC system with 50m x 0.32 mm x 1.0 µm DB-5 column, an autosampler and a FID or a Thermo DSQ single quadrupole GC-MS system. Helium was used as a carrier gas.

4.13.2. Oxidation of sulphides

The oxidation of methylphenyl sulphide (MPS) was carried out in a 25 ml magnetically stirred glass three-necked round bottom flask equipped with a Dimroth condenser at 30°C. Typically, 8 mmol of the sulphide was dissolved in 10 ml of acetonitrile together with 250 µl of 1,3-diisopropylbenzene (internal standard) and 50 mg of the catalyst were introduced into the mixture. For MPS, this setup corresponds to substrate/catalyst mass ratio S/C = 20. The mixture was heated to the reaction temperature and the reaction was started by addition of H_2O_2 aqueous solution (35 wt. %). Typically, the sulphide/H_2O_2 molar ratio was 2. Experiments under the solvent free conditions followed a procedure used in ref. [136]. The MPS oxidation was carried out in a 10 ml glass reactor with magnetic stirring (1000 rpm) at 25°C. Typically, 50 mg of the catalyst, 5 mmol of MPS and 5-6 mmol of the H_2O_2 aqueous solution were used. 1,3-diisopropylbenzene served as the internal standard.

The oxidations of diphenyl sulphide (Ph_2S) and dibenzothiophene (DBTH) were carried in a similar setup at 40°C. In the case of Ph_2S, 4 mmol of Ph_2S were mixed with 10 ml of acetonitrile, 250 µl of 1,3-diisopropylbenzene and 50 mg of the catalyst (S/C = 15) and the reaction was started by the addition of 4 mmol of H_2O_2 aqueous solution (sulphide/H_2O_2 = 1). In case of DBTH, 2 mmol of the substrate were dissolved in 15 ml of acetonitrile together with 125 µl of 1,3-diisopropylbenzene and 25 mg of the catalyst (S/C = 15) and the reaction started

by the addition of 2 mmol of H_2O_2 aqueous solution (sulphide/H_2O_2 = 1). The higher dilution in the case of DBTH was used to prevent crystallisation of the DBTH and products out of the samples while cooled.

Oxidation of dioctylsuphide to dioctyl sulphone was performed at 50°C. 4 mmol of dioctylsulphide were mixed with 10 ml of acetonitrile, 10 mmol of H_2O_2 and 50 mg of the layered TS-1 catalyst. 2 mmol of H_2O_2 were added after 12 h. The reaction mixture was stirred intensively for 16 h. Then, it was diluted with additional 10 ml of acetonitrile the catalyst was removed by centrifugation and the remaining solution was evaporated. The crude product was dissolved in 10 ml ethyl acetate, dried over $MgSO_4$ and finally the product crystallised after addition of 2 ml of methanol at 4°C in a refrigerator.

Samples of the reaction mixtures were taken in regular intervals and treated and analysed as described above.

4.13.3. Kinetic data evaluation

The internal standard calibration method was used for the evaluation of the kinetic data. Conversion was calculated as the ratio between consumed and initial molar amount of the substrate (eqn 1). Yield of a particular product was calculated as the ratio between obtained product and consumed substrate (eqn 2). Product selectivity at certain conversion was calculated as the ratio between product yield and substrate conversion. Hydrogen peroxide efficiency at 100% conversion of the H_2O_2 was calculated as the ratio between sum of oxidation product yields and initial amount of the hydrogen peroxide (eqn 3). TON of the oxidation reaction was calculated as the molar amount of the converted substrate per the molar amount titanium (eqn 4).

$$\mathrm{X} = \frac{n(\mathrm{substrate})_{initial} - n(\mathrm{substrate})_{sample}}{n(\mathrm{substrate})_{initial}} \quad \text{(eqn 1)}$$

$$\mathrm{y\ (product)} = \frac{n(\mathrm{product})_{sample}}{n(\mathrm{substrate})_{initial} - n(\mathrm{substrate})_{sample}} \quad \text{(eqn 2)}$$

$$\mathrm{E}_{\mathrm{H_2O_2},100\%} = \frac{\sum y_{i-product}}{n(\mathrm{H_2O_2})_{initial}} \quad \text{(eqn 3)}$$

$$\mathrm{TON} = \frac{n(\mathrm{substrate})_{initial} - n(\mathrm{substrate})_{sample}}{n(\mathrm{Ti})} \quad \text{(eqn 4)}$$

5. Results and discussion

5.1. Synthesis and characterisation of novel titanosilicates

5.1.1. Synthesis and characterisation of Ti-CFI

The synthesis conditions for Ti-**CFI** were tuned based on elder reports on high silica and pure silica **CFI** [142], [144]. Kubota et al. [142] reported synthesis of Al-**CFI** and pure silica **CFI** under static conditions with quartz tubes inside the autoclave but the attempts to use this method for Ti-**CFI** were not successful providing either amorphous material or cristobalite.

The Ti-**CFI** has been successfully synthesised under agitation with Si/Ti ratio between 106 and 23 in the final material. Titanium content, crystal size, duration of the synthesis and obtained crystalline phase are summarized in Table 2. After initial experiments (synthesis of Ti-**CFI** (100)), the synthesis temperature was lowered from 170°C to 155°C in order to obtain more uniform crystal size distribution (see Figure 8). Increasing amount of titanium in the synthesis mixture caused prolongation of the synthesis time (e.g. from 11 days of Ti-**CFI** (60), to 17 days of Ti-CFI (40)). The same effect was observed also in the aluminium containing (12 days) vs. aluminium free (5 days) syntheses [149]. Seeding of the reaction mixture, on the other hand, significantly shortened the synthesis time. As a result, Ti-**CFI** (25) sample crystallized in only 11 days.

Table 2: Optimisation of Ti-CFI synthesis

Sample	Si/Ti (RM)[a]	Temperature [°C]	Crystal size [µm]	Si/Ti	Time [day]	Structure[b]
Ti-**CFI** (100)	100	170	10-40	106	6	**CFI**+Am.
Ti-**CFI** (60)	60	155	10-20	63[c]	11	**CFI**
Ti-**CFI** (40)	40	155	10-20	36[c]	17	**CFI**
Ti-**CFI** (25)	25	160	10-20	23[c]	11[d]	**CFI**
Ti-**CFI** (10)	10	160	-	-	20[d]	Am.
Ti-**AFI** (a)	80	160	1-2.5	106	14	**AFI**

[a] initial Si/Ti molar ratio in the synthesis mixure
[b] determined by XRD; Am. stands for amorphous material
[c] Si/Ti molar ratio determined by XRF, otherwise by EDX.
[d] The synthesis was seeded with Ti-**CFI** (40)

SEM images show that the zeolite Ti-**CFI** crystals has thin plate morphology with the largest dimension up to approximately 20 µm (Figure 8), sometimes forming aggregates. This morphology is the same as for aluminosilicate, pure siliceous, or borosilicate forms of the CFI [142], [144]. The thickness of the crystals is about 0.2 µm, which are about 100 unit cells.

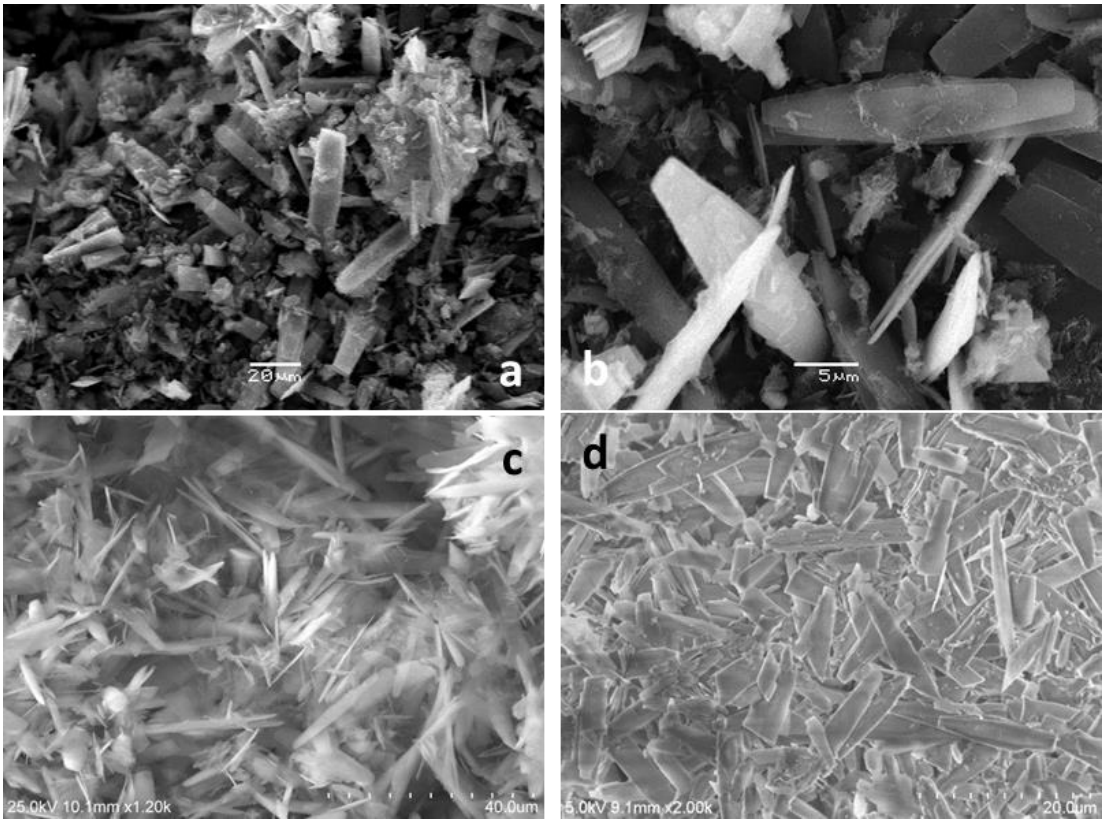

Figure 8: SEM images of Ti-CFI (100) (a), Ti –CFI (60) (b), Ti-CFI (40) (c) and Ti-CFI (25) (d)

N(16)-methylsparteinium cation can template also the synthesis of zeolite **AFI** [143]. The driving parameter is the presence of particular (bulky) anions (I^-, Br^- vs. OH^-) or cations (Na^+, K^+ vs. Li^+) [144]. When the SDA was used without ion-exchange, **AFI** phase was obtained after 14 days of the crystallization at 160°C (sample Ti-**AFI** (a)). The SEM image of Ti-**AFI**(a) hexagonal crystals is presented in Figure 10. The sample is not fully crystalline yet. This is because the synthesis was terminated, when a formation of crystalline phase other than CFI was observed. Lok et al. patented the synthesis of titanium containing aluminophosphate with **AFI** topology (TAPO-5) [150] but to our knowledge, this is the first reported titanosilicate with **AFI** structure.

The XRD patters of the prepared Ti-**CFI** and Ti-**AFI** samples are presented in Figure 9. The **CFI** pattern is characterised by 3 diffraction lines at low 2ϑ angles: 6.91° (002), 7.32° (101) and 13.9° (004) followed by a group of 5 peaks between 18° and 22°. The intensity of the first two diffraction lines depends on the presence of the structure-directing agent in the pores and on the orientation of the **CFI** crystals one to another. Kubota et al. reported that (00*l*) diffraction lines (especially the 2 ϑ = 6.9°, 13.9° and 20.9°) may be significantly amplified if there is a preferred orientation of **CFI** crystals [142]. This may lead to more complex identification of the **CFI** phase. No preferential orientation was observed for Ti-**CFI**. Calcination of the samples leads to a strong increase in the intensity of the 2ϑ = 6.91° and 7.32° lines (Figure 11). Well

crystalline samples Ti-**CFI** (60), (40) and (25) exhibited BET area between 308 and 346 m^2/g and micropore volume between 0.094 and 0.098 cm^3/g based on the argon adsorption isotherm at -186°C. The XRD patterns of the calcined samples, argon sorption isotherms and detailed textural properties are presented in the enclosed article [37].

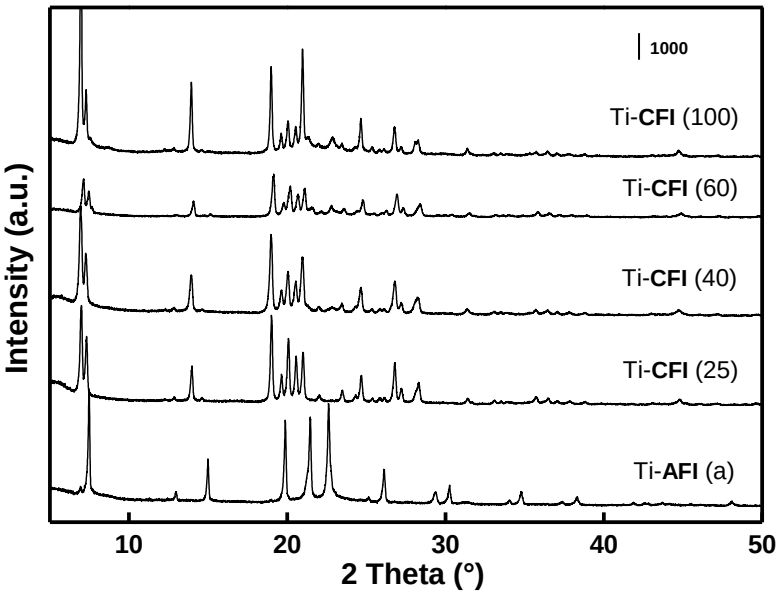

Figure 9: XRD patterns of as-synthetised Ti-CFI and Ti-AFI.

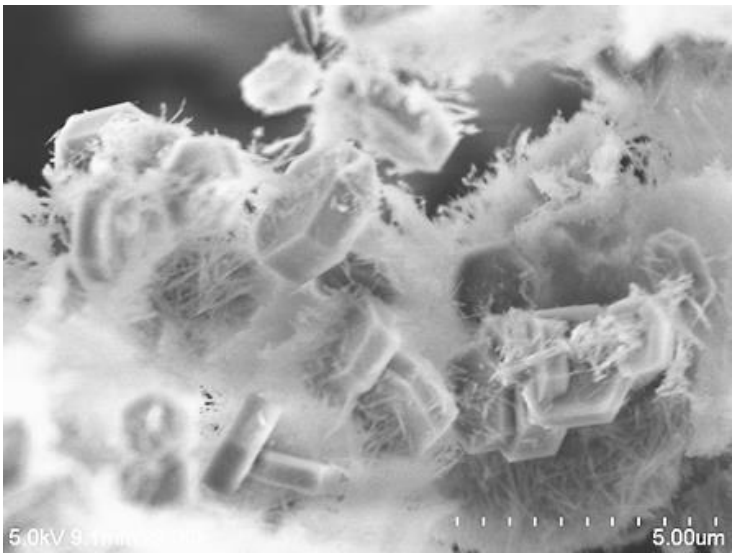

Figure 10: SEM image of Ti-AFI(a)

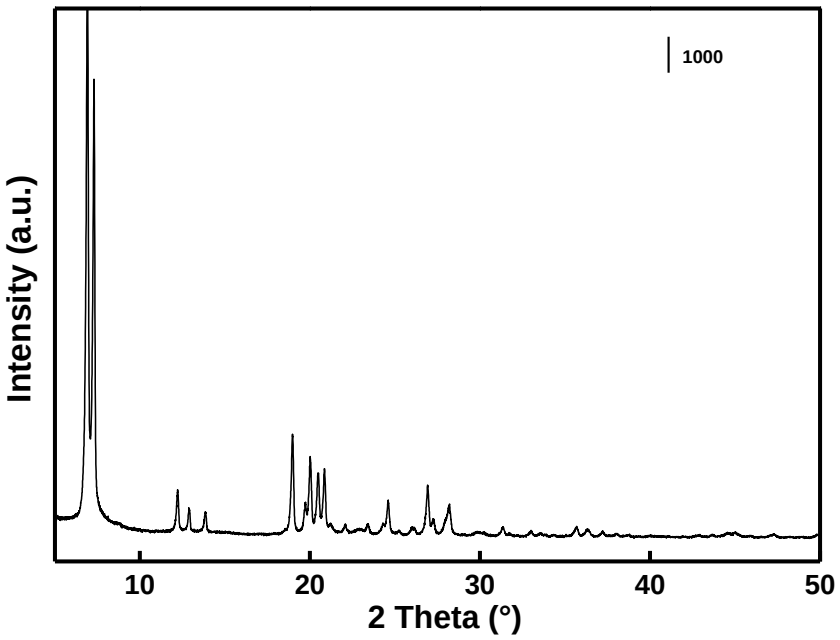

Figure 11: XRD pattern of calcined Ti-CFI(40)

The character of the titanium sites in the Ti-CFI as well as Ti-AFI samples was investigated by DR-UV-Vis spectroscopy. It is generally assumed that the tetrahedrally coordinated framework titanium atoms are the active centres for the H_2O_2 activation and oxidation reaction [101]. However, a number of indicia exist that also other single titanium atom species (not connected to any other titanium atom via oxygen bridge) might be active in oxidation catalysis [38, 41, 102]. It is assumed that the first step of the reaction mechanism is a disintegration of one of the Ti-O-Si bonds and increase in the coordination number from 4 to 5 [105].

All the Ti-**CFI**(60), (40), (25) and Ti-**AFI**(a) samples have after calcination similar spectra (Figure 12). They are characterised by the most intensive band 238 nm and a significant shoulder at 207 nm. Zecchina et al. ascribed the 208 nm band to tetrahedrally coordinated "TiO_4" framework species and the 238 nm band to isolated extra-framework titanium species in octahedral environment [104]. We conclude that part of titanium is in extra-framework positions (238 nm band); however, it is well dispersed (not forming anatase-like phase absorbing above 300 nm) and therefore should be active or at least should not negatively affect the catalytic activity of the material.

The extra-framework titanium species can be removed by treatment with boiling HNO_3 prior to the calcination of the sample [76]. We examined this procedure on the Ti-**CFI** (60) and Ti-**CFI** (25) samples. Figure 12 shows that upon this treatment, the 238 nm band practically disappeared in the case of Ti-**CFI** (60). This proves that nearly all extra-framework Ti from Ti-**CFI** (60) sample was removed. The band at 207 nm was preserved. On the other hand, in the

spectrum of Ti-**CFI** (25), a new band appeared centred at 328 nm. This band indicates the formation of dense TiO_2 (anatase phase) [104]. When the amount of HNO_3 used for the treatment of Ti-**CFI** (25) was increased 3 times (Figure 12, dashed grey line), the spectrum of the final material contained only the band at 208 nm as in case of Ti-**CFI** (60). We conclude that high excess of the acid is necessary to remove all extra-framework Ti. Similar intensity of the Ti-**CFI** (60) and (25) spectra after the removal of extra-framework titanium suggests the existence of an upper limit (approx. Si/Ti=200) for the number of titanium atoms incorporated into the framework, similarly to the case of TS-1 [30] (which is significantly lower than in the case of TS-1) and above this limit, the titanium occupy the extra-framework positions.

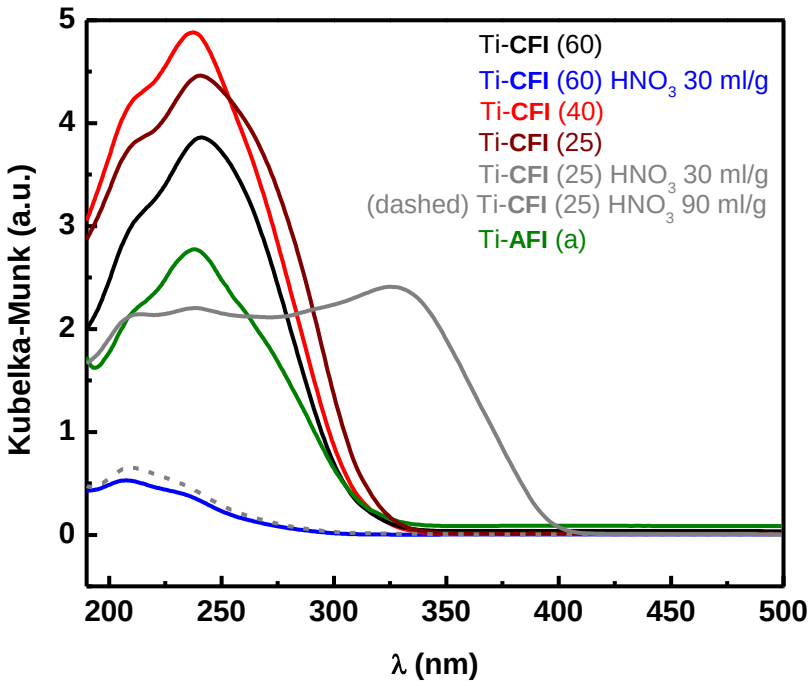

Figure 12: DR-UV/Vis spectra of Ti-CFI and Ti-AFI samples.

5.1.2. Synthesis and characterisation of Ti-UTL and derived materials

We aimed our attention towards an extra-large pore germanosilicate **UTL** containing 14-ring channels intersecting 12-ring channels. This material can be prepared with a number of trivalent heteroelements (B, Al, Ga, Fe, In) incorporated into the framework [140]. This was a promising feature, since the isomorphous incorporation of titanium into a zeolitic framework is a complex problem with many variables affecting the final product. Furthermore, we aimed to perform the top-down and ADOR transformations with this titanosilicate material [16, 17].

We have succeeded in the preparation of Ti-**UTL** using (6R,10S)-6,10-dimethyl-5-azoniaspiro[4.5]decane hydroxide as a structure directing agent and TBOTi as a titanium source. The material was prepared as a titano-germanosilicate, because the presence of Ge is crucial for both UTL structure crystallisation and possibility of the ADOR transformations. The Ti-**UTL** exhibited Si/Ti ratio 139 and the XRD pattern (Figure 13) was consistent with standard **UTL** pattern [4].

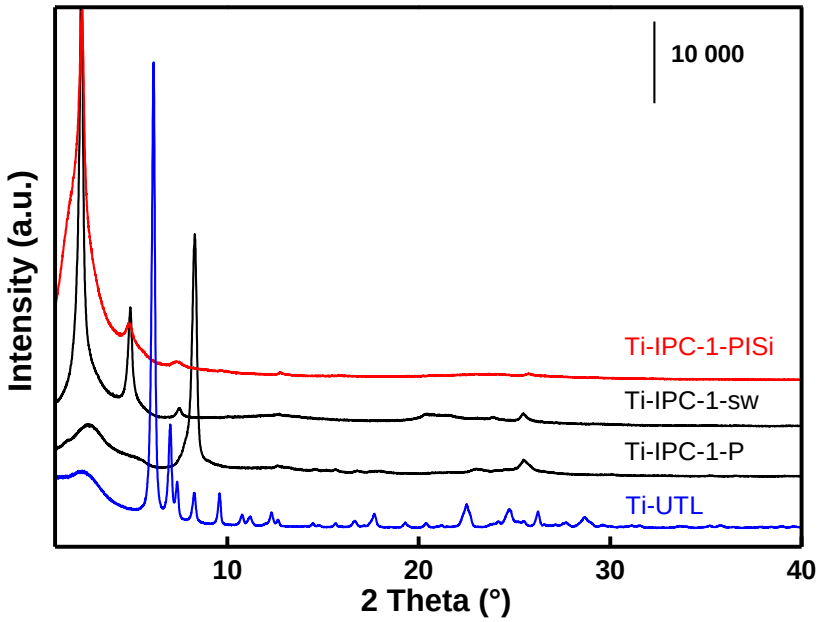

Figure 13: XRD patters of Ti-UTL and Ti-IPC-1P, Ti-IPC-1-sw and Ti-IPC-1PISi, obtained by the top-down transformation.

When the calcined Ti-**UTL** was hydrolysed most of the diffraction lines disappeared and lamellar precursor Ti-IPC-1P was obtained. A shift of the most intensive (200) line from 2 ϑ = 6.1° (Ti-**UTL**) to 2 ϑ = 8.2° (Ti-IPC-1P) reflects a decrease in the *d*-spacing from 2.9 nm to 2.1 nm upon removal of the germanium-containing D4R units. Successful swelling of the material

is characterised by an increase in the *d*-spacing to 3.7 nm. Intensive (100), (200) and (300) diffraction lines present in the XRD pattern of the swollen Ti-IPC-1sw confirm this.

The swollen Ti-IPC-1sw was pillared with TEOS and after calcination, the silica pillared material, denoted Ti-IPC-1PISi, exhibited Si/Ti ratio 480. The reason for such a strong decrease is discussed below.

Besides the swelling and pillaring, the lamellar precursor IPC-1P can be reassembled into **OKO** and **PCR** zeolites with smaller channels (12x10 resp. 10x8-ring 2-dimensional channel systems) by means of the ADOR process [17]. Therefore, we attempted to stabilise the Ti-IPC-1P with diethoxydimethyl silane in 1M HNO_3 at 175°C. As a result, we obtained a material denoted Ti-IPC-2 after calcination. The Ti-IPC-2 is a fully connected 3-dimensional titanosilicate, its XRD pattern (Figure 14) is consistent with **OKO** topology [4] and the material is characterised by Si/Ti ratio 210 according to the IPC-OES.

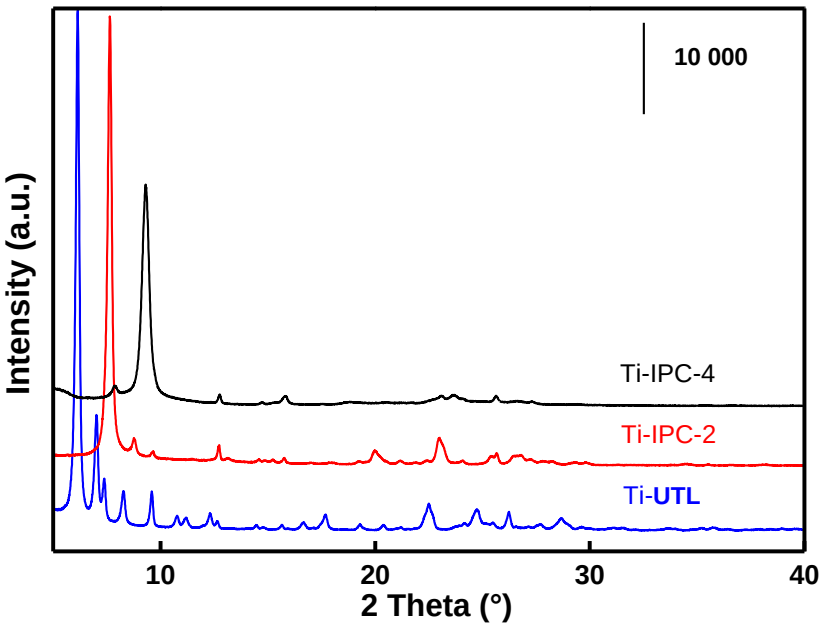

Figure 14: XRD patterns of Ti-UTL and derived Ti-IPC-2 and Ti-IPC-4 materials.

Intercalation of the Ti-IPC-1P with 1-aminooctane led to organisation of layers. After calcination, the layers condensed into a material denoted Ti-IPC-4, possessing the **PCR** topology. The XRD pattern is presented in Figure 14. A shift of the (200) diffraction line from 2 ϑ = 6.1° (Ti-**UTL**) to 2 ϑ = 7.6° (Ti-IPC-2) and 2 ϑ = 9.3° (Ti-IPC-4) reflects the substitution of former D4R units by S4R units in the Ti-IPC-2 and their total removal in Ti-IPC-4 (Figure 15). We conclude that the introduction of Ti into the **UTL** structure did not affect the possibility of its top-down and ADOR transformations.

Scanning electron micrographs (Figure 16) show the preservation of the characteristic thin plate morphology the Ti-**UTL** crystals during all the post-synthesis modifications. In the case of the pillared Ti-IPC-1PISi, the crystals are partially covered with amorphous silica phase resulting from the excess of the pillaring medium.

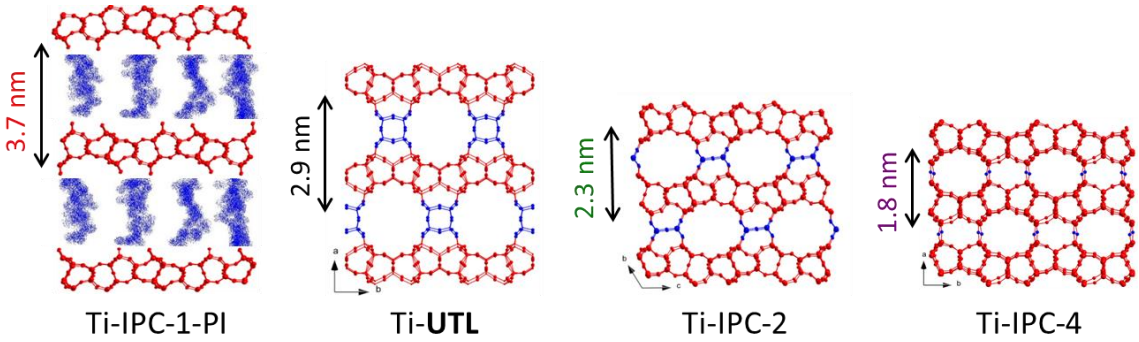

Figure 15: Structure of the Ti-UTL and derived materials. Basal *d*-spacing is highlighted.

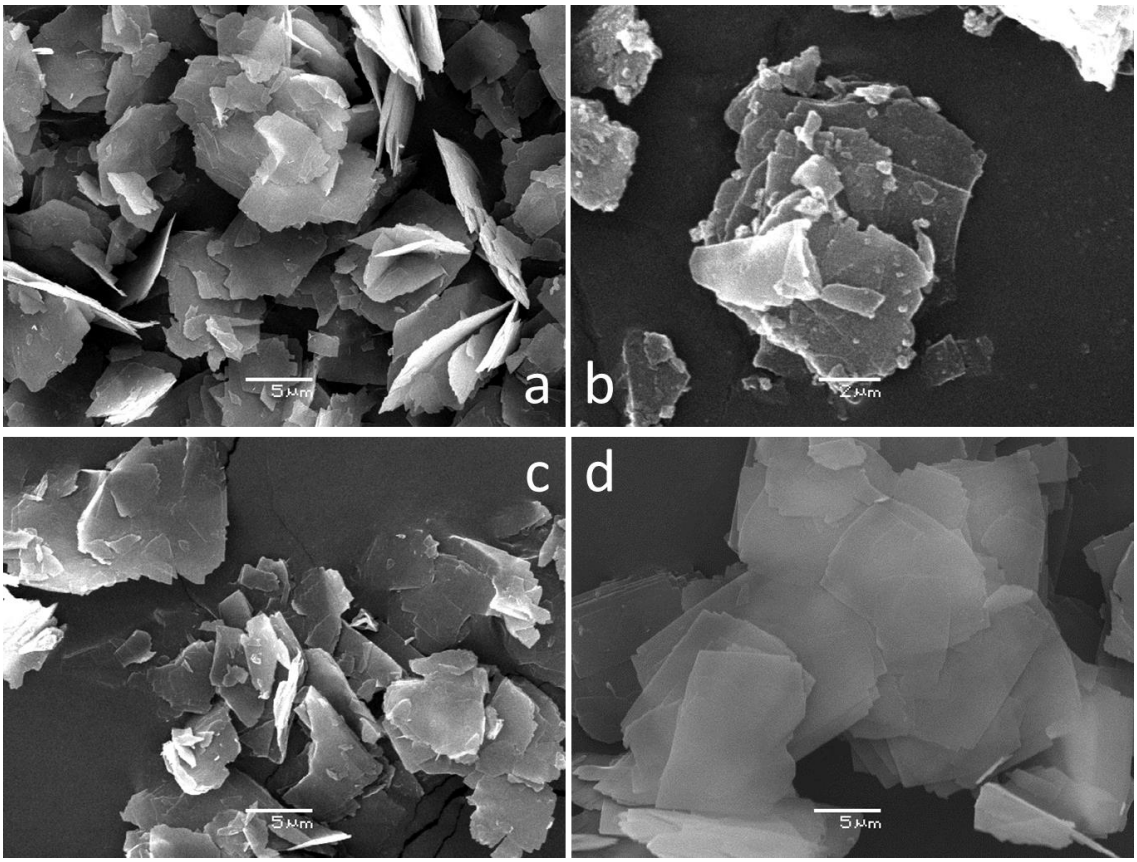

Figure 16: SEM images of Ti-UTL (a), Ti-IPC-1PISi (b), Ti-IPC-2 (c) and Ti-IPC-4 (d)

The textural properties and Ti content of the discussed samples are listed in Table 3. The BET areas, micropore volumes and total adsorption capacities decrease with decreasing size of the pores in the order Ti-**UTL** > Ti-IPC-2 > Ti-IPC-4 > Ti-IPC-1 (e.g. BET area: Ti-**UTL =** 539 m^2/g, Ti-

IPC-2 = 383 m^2/g, Ti-IPC-4 = 237 m^2/g, Ti-IPC-1 = 192 m^2/g). The Ti-IPC-1 material was obtained upon calcination of the Ti-IPC-1P lamellar precursor without any other treatment. Its BET area and micropore volume are lower in comparison with Ti-IPC-4 because the layers were not organized and randomly collapsed one on another. It should be underlined that the Ti-IPC-1PISi is a purely mesoporous composite of crystalline titanosilicate layers and amorphous silica pillars. Therefore, it is expected to combine the advantages of amorphous mesoporous sieves and crystalline titanosilicates, although its titanium content is low. Post-synthesis addition of titanium during the pillaring treatment in order to increase the titanium content is discussed in a separate chapter. Nitrogen sorption isotherm are presented in the attached article [65].

Table 3: Textural properties and titanium content of the Ti-UTL and derived materials

Titanosilicate	BET (m^2/g)	V_{mic} (cm^3/g)	V_{tot} (cm^3/g)	Si/Ti
Ti-**UTL**	539	0.24	0.29	139
Ti-IPC-1PISi	1001	0	0.67	480
Ti-IPC-1	192	0.07	0.13	n.d.[a]
Ti-IPC-2	383	0.15	0.22	210
Ti-IPC-4	237	0.10	0.15	n.d.[a]

[a] Ti content was not determined because the material was not intended to be used in catalytic tests.

The DR-UV/Vis spectra (Figure 17) of the Ti-**UTL**, Ti-IPC-1PISi and Ti-IPC-2 confirm that framework tetrahedrally coordinated titanium species (characterized by a band centered at 210 nm) are the dominant in the material.

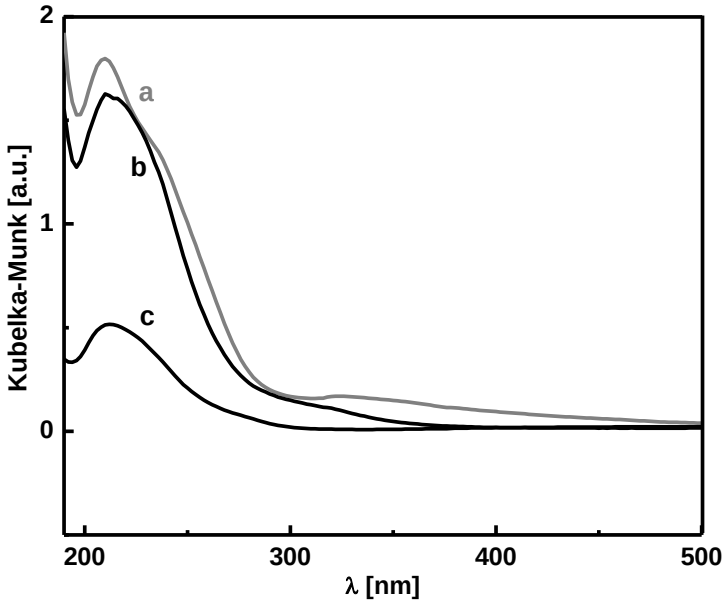

Figure 17: DR-UV/Vis spectra of Ti-UTL (a), Ti-IPC-2 (b) and Ti-IPC-1PISi (c)

5.1.3. Synthesis and characterisation of conventional and hierarchical TS-1

Conventional TS-1 with two different crystal sizes (200 nm resp. 600 nm; determined by SEM (Figure 19); hereafter denoted TS-1 with the crystal size in brackets) were prepared using the Taramasso et al. procedure [81]. The adjustment of the crystallisation time enabled to control the crystal size. The TS-1(200) was obtained after 70 h of the hydrothermal synthesis while the TS-1(600) crystallized for 94 h. The TS-1(600) material served in most of the catalytic experiments as a benchmark. The TS-1(200) was used as a parent material for the desilication experiments (*vide infra*). XRD patterns are presented in Figure 18 and textural properties and titanium content are listed in Table 4.

Hierarchical TS-1 materials were prepared using two methods: (i) secondary templating using Carbon Black Pearls with average particle diameter of 20 nm (denoted meso-TS-1) and (ii) desilication using aqueous NaOH solution (denoted desil-TS-1 with NaOH concentration in brackets).

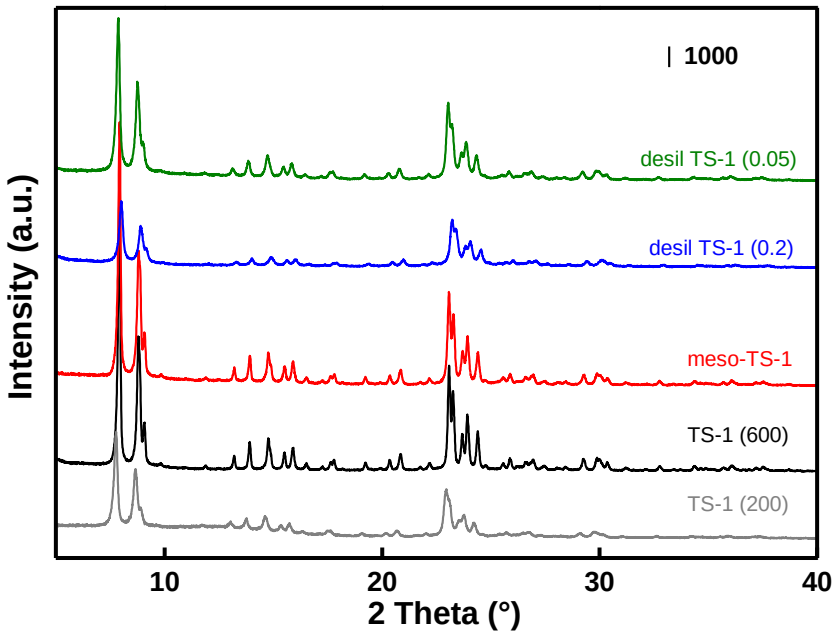

Figure 18: XRD patterns of conventional and hierarchical TS-1 materials

In case of secondary templating, the XRD pattern (Figure 18) clearly evidences the presence of the **MFI** crystalline structure and the SEM image (Figure 19b) reveals a sponge-like morphology of the TS-1 crystals. The unusual morphology results from the presence of mesopores after removal of the secondary template during calcination. The BET area did not change in comparison with the TS-1(600) (465 vs. 450 m^2/g), but the total adsorption capacity

increased from 0.16 cm^3/g (TS-1(600)) to 0.26 cm^3/g (meso-TS-1) and the micropore volume slightly decreased (TS-1(600) 0.13 cm^3/g vs. meso-TS-1 0.10 cm^3/g).

Desilication in 0.2 M NaOH solution led to a strong decrease in the BET area in comparison with the parent TS-1(200) (348 vs. 528 m^2/g). On the other hand, the total adsorption capacity increased twice; from 0.22 cm^3/g to 0.44 cm^2/g. Desilication using lower concentration (0.05 M) of the NaOH solution led to formation of mesopores (V_{tot} = 0.32 cm^3/g) but the decrease in the BET area was lower (BET area 455 m^2/g). The level of desilication can be qualitatively observed also in the SEM images (compare Figure 19 c, d). The desil-TS-1 (0.05) crystals possess only rounded edges. In contrast the desil-TS-1 (0.2) material has a sponge-like morphology, much lower uniformity of the crystal size and the crystals seem more corroded.

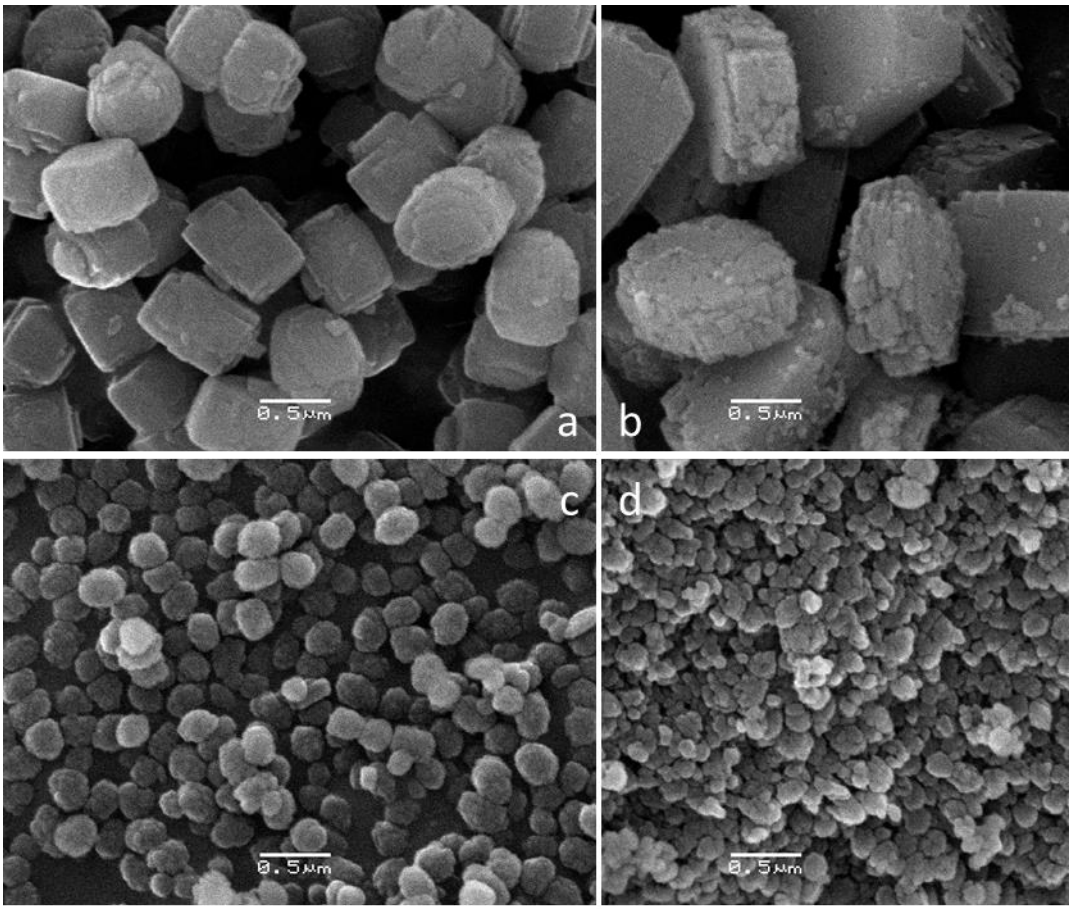

Figure 19: SEM images of TS-1(600) (a), meso-TS-1 (b), desil-TS-1 (0.05) (c) and desil-TS-1 (0.2) (d)

Table 4: Textural properties and titanium content of the conventional and hierarchical TS-1

Titanosilicate	BET (m^2/g)	V_{mic} (cm^3/g)	V_{tot} (cm^3/g)	Si/Ti
TS-1(200)	528	0.15	0.22	36
TS-1(600)	450	0.13	0.16	39
Meso-TS-1	465	0.10	0.26	40
Desil-TS-1(0.2)	348	0.10	0.44	41
Desil-TS-1(0.05)	455	0.15	0.32	35

The nitrogen adsorption isotherms of the hierarchical TS-1 material are presented in Figure 20. Upon desilication the shape of the TS-1 isotherm changed from type I (characteristic for microporous materials) closer to the type II (characteristic for non-porous materials). The increase of nitrogen uptake at higher relative pressure ($p/p_0 > 0.2$) is due to the filling of the mesopores. The mesoporous TS-1 prepared by secondary templating possess a combination of type I and type IV isotherm with a hysteresis loop. The hysteresis loop is present because of a different shape of the mesopores in comparison with desilicated TS-1. BJH pore size distribution analysis (Figure 21) shows presence of mesopores 10-30 nm wide, centred at 20 nm, which reflects the size of the secondary template particles.

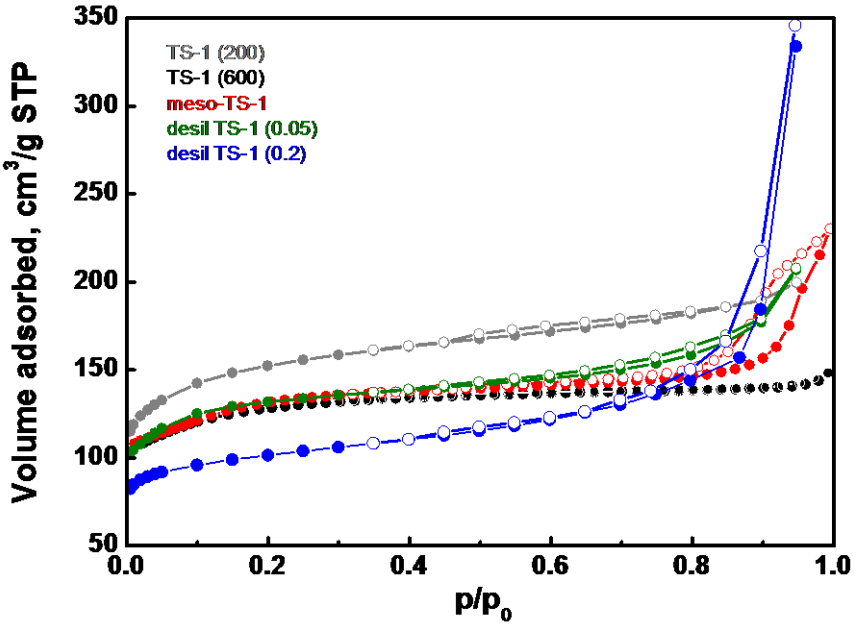

Figure 20: Nitrogen sorption isotherms of conventional and hierarchical TS-1 materials. Empty points denote desorption.

The DR-UV/Vis analysis revealed that all discussed samples contain mainly framework tetrahedrally coordinated titanium (characterized by a band centered at 210 nm). No other band can be observed in the spectrum of the TS-1(600). The TS-1(200) and meso-TS-1 contained some share of anatase phase (absorbing at 330 nm). In the desilicated samples a

shoulder at 260 nm appeared characterizing extra framework titanium species, most probably released during partial dissolution of the TS-1 within the desilication.

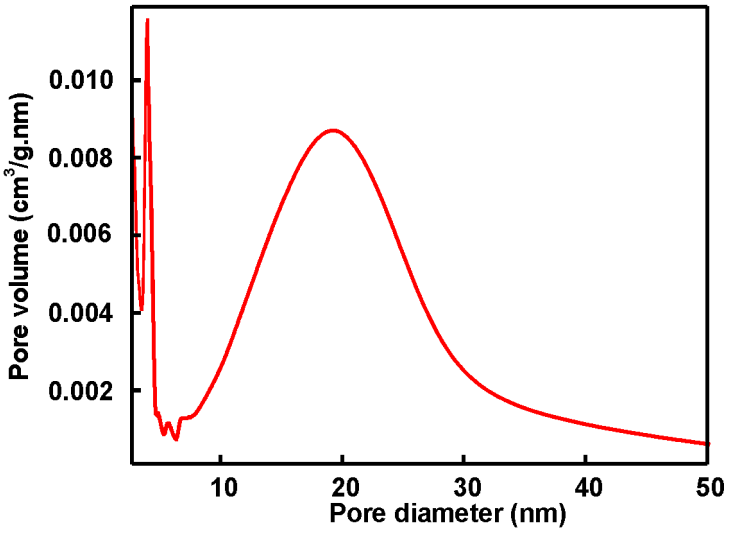

Figure 21: BJH pore size distribution curve for meso-TS-1

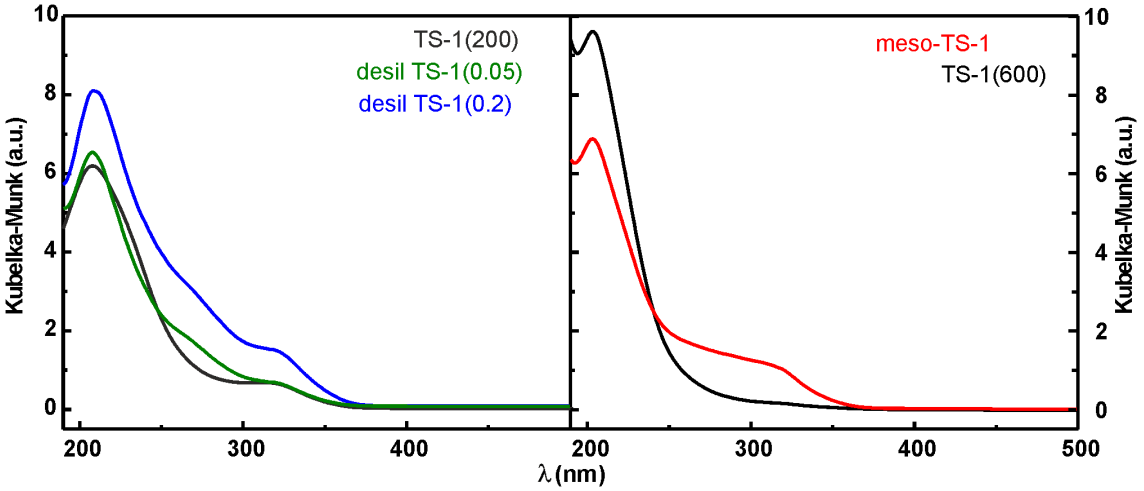

Figure 22: DR-UV/Vis spectra of conventional and hierarchical TS-1 materials

5.1.4. Synthesis and characterisation of lamellar TS-1 materials

Layered TS-1 material was prepared using the Ryoo procedure for preparation of nanosheet TS-1 [80]. The XRD pattern of the as-synthesised material (Figure 23) is consistent with the XRD pattern presented by the Ryoo group. The first diffraction line at 2ϑ =1.4° characterizes the distance between the TS-1 zeolite layers. Ryoo observed a similar position of the line (2ϑ =1.45°) when preparing an aluminosilicate nanosheet MFI zeolite according to the same synthetic protocol [151].

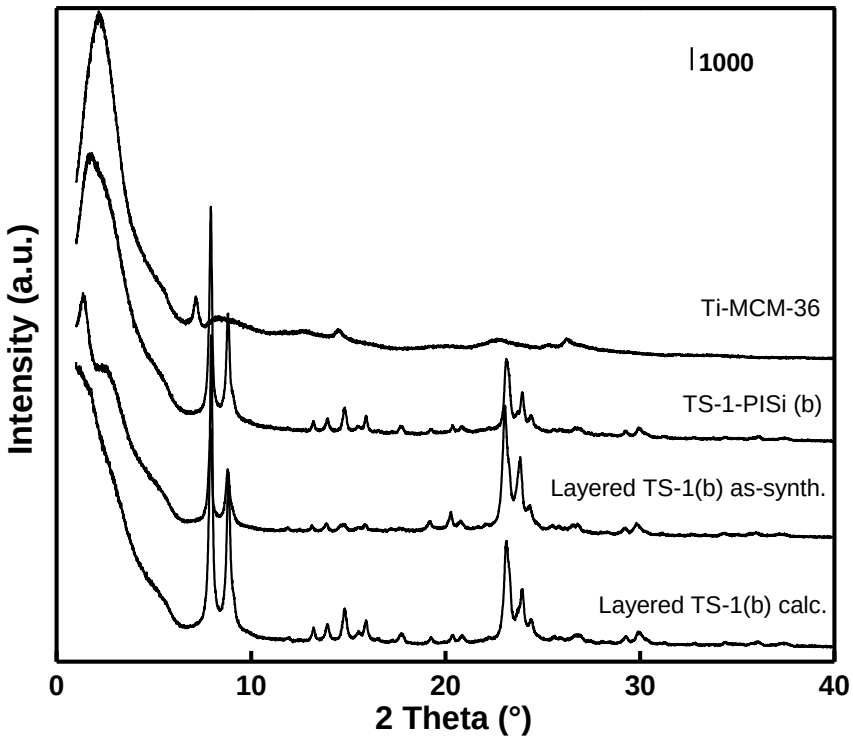

Figure 23: XRD patters of layered and pillared TS-1 and Ti-MCM-36

In the as-synthesized material layers are kept apart regularly by the surfactant template and after calcination stack to each other randomly causing the disappearance of the low 2ϑ diffraction line (Figure 23). During the pillaring treatment, the interlamellar space is intercalated with TEOS, forming amorphous mesoporous silica pillars after hydrolysis and calcination. As a result, the layers remain kept apart after the template removal and thus the diffraction line typical for the regular layer separation (2ϑ = 1.7° and 2.0°) remains present. A slight shift of the diffraction line toward higher angles (from 2ϑ = 1.4° (as-synthetized layered TS-1) to 2ϑ = 1.7° (TS-1-PISi)) reflects a slight decrease in the interlayer distance when the template is burnt and the layers "settle down" remaining supported only by the silica pillars. The position of the line corresponds to basal *d*-spacing of 4.5 to 5.2 nm and interlamellar distance of 2.5 to 3 nm (the thickness of the TS-1 lamella is approximately 2 nm [15]). This

observation is consistent with the shape of the nitrogen adsorption isotherm (Figure 24). It is typical for pillared materials exhibiting an increased uptake of nitrogen at relative pressure between 0.1 and 0.4 which is characteristic for filling of pores belonging to lower mesopore region (2-10 nm).

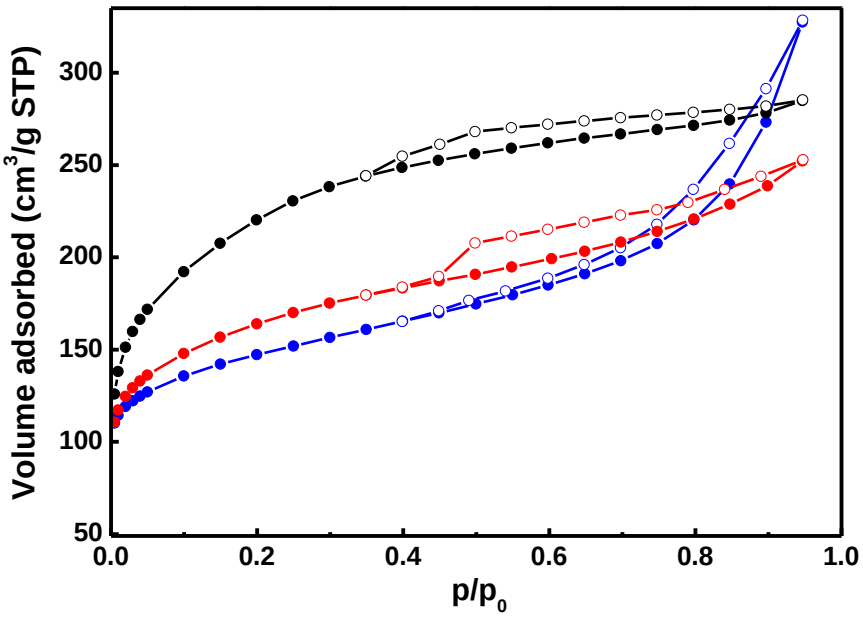

Figure 24: Nitrogen sorption isotherms of layered TS-1(b) (blue), TS-1-PISi(b) (red) and Ti-MCM-36 (black). Empty points denote desorption.

Table 5: Textural properties and titanium content of the layered and pillared TS-1 and Ti-MCM-36

Titanosilicate	BET (m^2/g)	S_{ext} (m^2/g)	V_{mic} (cm^3/g)	V_{tot} (cm^3/g)	Si/Ti
TS-1(600)	450	151	0.13	0.16	39
Layered TS-1(a)	473	293	0.09	0.44	36
Layered TS-1(b)	511	226	0.13	0.51	33
TS-1-PISi(a)	595	384	0.09	0.46	93
TS-1-PISi(b)	575	337	0.11	0.39	55
Ti-MCM-36	786	629	0.07	0.44	57

The Ti-MCM-36 material was prepared according to the procedure described by Wu et al. [56] and Kim et al. [112] by swelling and pillaring of Ti-**MWW**(P) lamellar precursor. The observed properties (Table 5) were consistent with those reported in the literature and the material served as another benchmark in the catalytic experiments.

The layered TS-1 samples possess BET areas between 473 and 522 m^2/g (Table 5) and total adsorption capacities (V_{tot}) between 0.44 and 0.51 cm^3/g. The BET areas are quite similar to

the conventional TS-1 (450-525 m^2/g, *vide supra*); however, the total adsorption volumes are much higher in comparison with TS-1(600) (V_{tot}=0.16 cm^3/g). Similarly, the external surface area (S_{ext}) increased for layered TS-1 (between 226 and 293 m^2/g) compared with TS-1(600) (151 m^2/g).

The pillaring treatment significantly increases the BET area (up to 595 m^2/g) as well as external surface area (up to 384 m^2/g). On the other hand, the total adsorption capacity of the material remains similar (Layered TS-1a 0.44 cm^3/g vs. TS-1-PISi(a) 0.46 cm^3/g). This corresponds to the fact that although the interlayer space is in fact larger for pillared material than for the layered one, it is partially filled with silica pillars resulting in an increase in the surface area but in a decrease in the adsorption volume. DR-UV/Vis spectra of the layered and pillared TS-1 are presented in the attached article [82]. The most intensive band in all the spectra was centred at 210 nm, which means that tetrahedrally coordinated titanium species are dominant in all layered TS-1 (a),(b) and TS-1-PISi (a),(b). In the spectra of layered TS-1(b) and pillared TS-1(b) another band at 260 nm can be observed. This band is typical for isolated extra-framework titanium species [104]. No anatase-like TiO_2 phase (absorbing at 330 nm) was observed.

5.1.5. Synthesis, titanium impregnation and characterisation of large-pore borosilicates

In addition to direct hydrothermal synthesis, titanosilicate zeolites can be prepared also by means of post-synthesis modification. The drawback of the impregnation method is that titanium atoms are not in well-defined positions and coordination state. This might be overcome by two step procedure where titanium atoms are inserted into defect sites previously occupied by heteroatoms such as boron. We reported [38] an impregnation of large-pore borosilicates **AFI**, **CON**, **IFR** and **CFI** with TBOTi in butan-1-ol and titanium chloride in toluene. Titanium incorporation into **AFI** and **IFR** from vapour phase according to the method described in [70] has been also described. In the first step the boron atoms were removed by treatment with 0.01 M HCl and subsequently the material was subjected to the impregnation with a solution of titanium source. The parent borosilicate zeolites and prepared impregnated titanosilicate materials are listed in Table 6.

The amount of titanium in the zeolites was investigated using XRF spectroscopy. Generally, higher titanium content in the impregnated samples was achieved using $TiCl_4$ solution. This is due to a higher reactivity and smaller kinetic diameter of $TiCl_4$ molecule in comparison with TBOTi. $TiCl_4$ can easier diffuse through the channel system of the large-pore zeolites. The catalysts impregnated with TBOTi possess low titanium content. This is because the TBOTi

molecule is large and probably cannot access the defect sites in the core of the impregnated crystals. Nevertheless, the catalytic performance especially of Ti-**CON**(TBOTi) strongly exceeded TS-1 as well as other materials with higher titanium content (*vide infra*). Comparing the performance of Ti-**CON**(TBOTi) (Si/Ti = 450, cyclooctene conversion 37% after 4 h) and Ti-**CON**($TiCl_4$ sol) (Si/Ti = 81, cyclooctene conversion 26% after 4 h), we assume that the concentration of the titanium sites is higher on the external surface of the crystals and in its close proximity where the catalytic reactions mainly take place. For the **CFI** and **AFI**, almost no titanium was incorporated into the material, most probably because TBOTi molecules were unable to diffuse through the 1-dimensional channels of these two materials. This was indicated by no UV/Vis light absorption (*vide infra*).

Table 6: Textural properties and titanium content of the parent borosilicates (upper part) and impregnated titanosilicates (lower part of the table)

Material[a]	BET (m^2/g)	V_{micro} (cm^3/g)	V_{total} (cm^3/g)	Si/Ti (XRF)
deB-**CON**	640	0.24	0.42	--
B-**IFR**	508	0.22	0.24	--
B-**AFI**	336	0.14	0.16	--
B-**CFI**	377	0.15	0.21	--
Ti-**CON**(TBOTi)	640	0.24	0.42	450
Ti-**CON**(TBOTi)[c]	600	0.21	0.32	470
Ti-**CON**($TiCl_4$ sol)	654	0.24	0.42	81
Ti-**IFR**(TBOTi)	508	0.22	0.24	>500
Ti-**IFR** ($TiCl_4$ vap)	497	0.21	0.24	72
Ti-**AFI**(TBOTi)	351	0.15	0.17	>500
Ti-**AFI**($TiCl_4$ vap)	329	0.14	0.16	220
Ti-**CFI**($TiCl_4$ sol)	325	0.12	0.20	109
TS-1[b]	450	0.13	0.16	44
Ti-**CFI** (40)[b]	295	0.10	0.22	36
Ti-**AFI** (a)[b]	282	0.12	0.16	200

[a] notes in brackets: abbreviation indicate the used titanium source; sol indicates impregnation in a $TiCl_4$ solution; vap indicates using $TiCl_4$ vapour; deB-**CON** stands for deboronated **CON**.
[b] Directly synthetized reference titanosilicate.
[c] Sample prepared from different batch of **CON** than the one indicated in the upper part of the table.

The XRD patterns of parent borosilicate zeolites and impregnated titanosilicate zeolites are presented in the attached article [38]. No significant changes were observed between the patterns of parent and impregnated zeolites indicating that neither the deboronation nor the impregnation procedure affects the crystallinity of the zeolites. A slight shift towards lower angles (0.2° for the (002) and (101) lines) in the position of the diffraction lines may be

observed for the **CFI**. The patterns of **CON** (0.3° for the (110) line) and **AFI** (0.1° for the (100) line) are shifted also. We ascribe this shift to the incorporation of titanium, which is larger than silicon and boron and causes a small increase in *d* values. Similar shift was observed e.g. by Dartt and Davis [70] and Rigutto et al. [66]. For the **IFR**, the shift is not distinct. Textural properties were determined from nitrogen adsorption isotherms recorded at -196°C (Table 6). The differences in BET areas, micropore volumes and total adsorption capacities among parent borosilicates (upper part of the table) and impregnated titanosilicates (lower part) are within the experimental error.

The DR-UV/Vis analysis was crucial to analyse the character of the titanium sites present in the impregnated materials. We expected framework species (characterised by absorption at 210 nm) as well as some share of extra-framework species (absorbing between 240 and 290 nm, depending on their coordination number and geometry) [105] to be present in the impregnated materials. Presence of anatase phase (absorbing around 330 nm) is undesired because it causes unproductive decomposition of hydrogen peroxide [30]. Spectra for the Ti-**CFI**, Ti-**CON**, Ti-**IFR** and Ti-**AFI** materials are presented in Figure 25, Figure 26, Figure 27 and Figure 28, respectively.

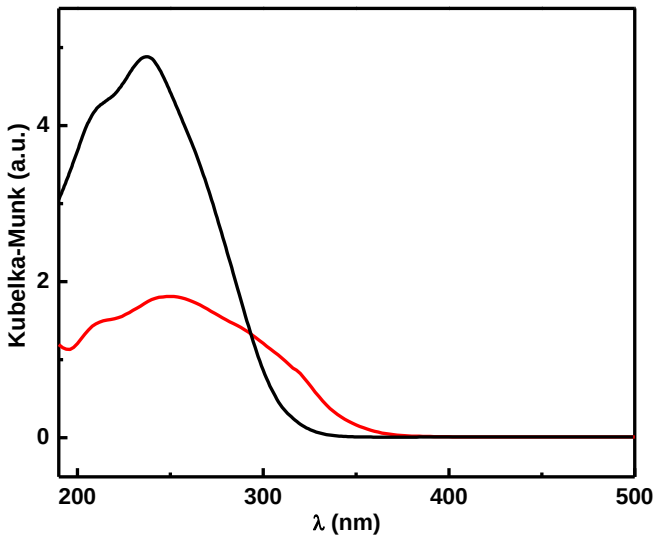

Figure 25: DR-UV/Vis spectra of impregnated Ti-CFI($TiCl_4$ sol) (red) and directly synthetized Ti-CFI (40) (black).

The titanosilicates impregnated with TBOTi solution contained mainly tetrahedrally coordinated single titanium atoms and some share of extra-framework titanium atoms. In the case of **CFI** and **AFI**, almost no UV absorption in the range of 190 – 300 nm was observed (spectra are not presented) indicating that titanium is not present in the final material. In contrast, titanosilicates prepared using titanium (IV) chloride (a solution as well as vapour)

contained more titanium (Si/Ti molar ratio from 220 to 72). Anatase was present in the $TiCl_4$ impregnated samples (evidenced by UV absorption over 300 nm), but no direct correlation between the presence of anatase and catalyst performance was observed (*vide infra*).

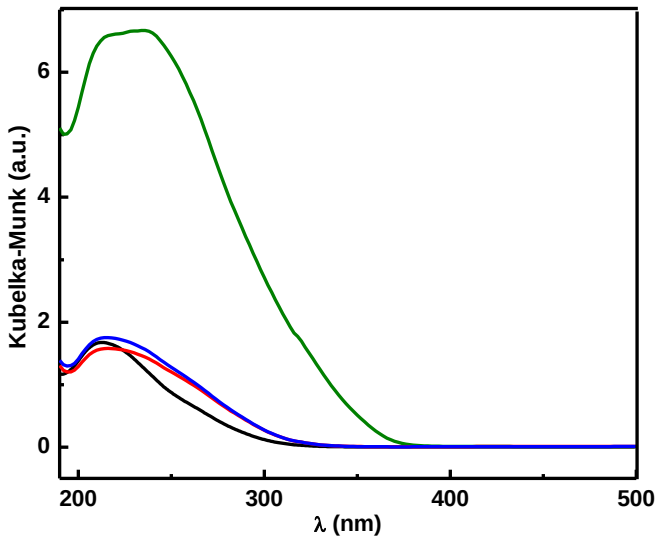

Figure 26: DR-UV/Vis spectra of impregnated CON samples: Ti-CON(TBOTi) (black), Ti-CON(TBOTi) prepared after deboronation with 0.1 M HCl (red), Ti-CON(TBOTi) (blue), Ti-CON($TiCl_4$ sol) (green).

For the zeolite **CFI**, it appears that the most suitable method for titanium incorporation is direct synthesis discussed separately (*vide supra*) [37]. In contrast, the **CON** zeolite was impregnated successfully with TBOTi solution and the DR-UV/Vis spectra of the materials are similar to the best samples prepared by Dartt and Davis using more complex gas phase $TiCl_4$ incorporation [70]. Use of more concentrated HCl (0.1 M instead of 0.01 M solution) for the **CON** deboronation did not lead to a higher content of titanium (no increase in the UV absorption was observed; see Figure 26, red line).

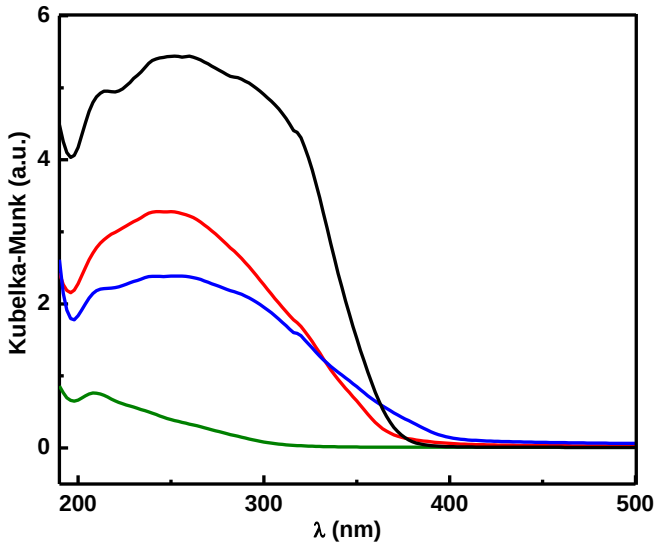

Figure 27: DR-UV/Vis spectra of impregnated IFR samples. Ti-IFR($TiCl_4$ sol) (black), Ti-IFR ($TiCl_4$ vap) (red), Ti-IFR ($TiCl_4$ vap) directly treated borosilicate (blue), Ti-IFR (TBOTi) (green)

Impregnation of **IFR** with TBOTi solution led to a material with the titanium content under the quantification limit of the analytical method and the only proof of titanium presence is the UV absorption band. Therefore, we used the treatment with $TiCl_4$ vapour. The titanium content in the final material increased, but the UV spectra of both $TiCl_4$ vapor treated deboronated **IFR** and directly treated B-**IFR** were similar to the material obtained by impregnation with $TiCl_4$ solution (Figure 27). In all spectra a shoulder at 210 nm shows the presence of framework titanium, but intensive bands of extra-framework titanium and anatase are present. For **AFI**, treatment with $TiCl_4$ vapour appears to be more successful (higher intensity of the band at 210 nm in comparison with the bands at 260 and 330 nm, Si/Ti = 220) than $TiCl_4$ solution (Si/Ti = 500; Figure 28).

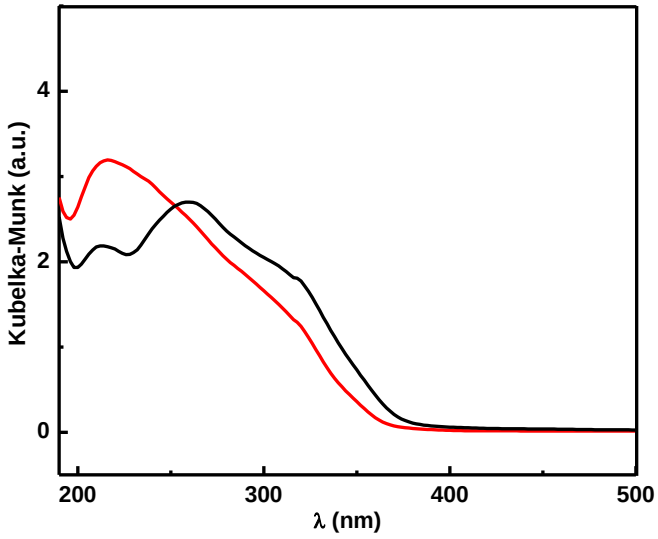

Figure 28: DR-UV/Vis spectra of impregnated AFI: Ti-AFI($TiCl_4$ sol) (black), Ti-AFI ($TiCl_4$ vap) (red).

5.1.6. Silica-titania pillaring of lamellar titanosilicates

It was mentioned that pillaring treatment of lamellar titanosilicates provides or helps to preserve the enhanced accessibility of the active sites and desirable textural properties. On the other hand, the active crystalline titanosilicate phase is, in fact, diluted with catalytically inactive silica. In the case of TS-1-PISi, the Si/Ti ratio increased from 36 (layered TS-1(a)) to 93 (TS-1-PISi(a)) (Table 5) and in the case if Ti-IPC-1PISi, the Si/Ti ratio is 480, what represent about 4-times lower titanium content in comparison with the parent Ti-**UTL** (Si/Ti = 139, Table 3).

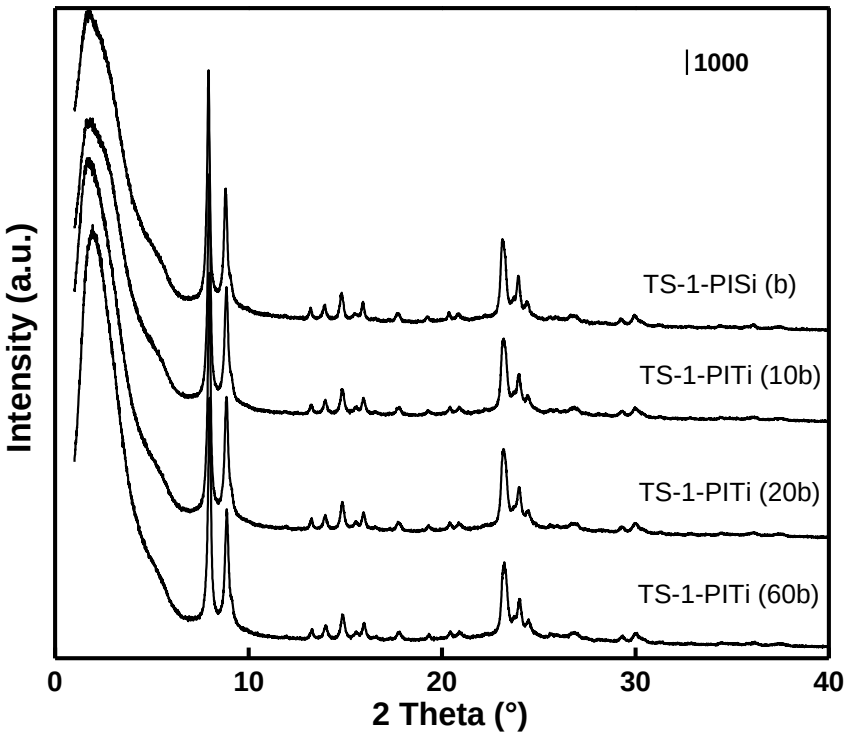

Figure 29: XRD patterns of the silica-titania pillared TS-1 materials.

To compensate the decrease in titanium content of the pillared materials in comparison with layered (parent) materials we developed so-called silica-titania pillaring method. Key step of the silica-titania pillaring is the addition of 1-10 molar % of a titanium source (typically TBOTi) into the pillaring medium (TEOS). The TBOTi reacts either with the TEOS (forming titanium sites inside or on the surface of the silica pillars) or with the silanol groups located on the surface of the crystalline layers, forming additional, well accessible active centres. To confirm the activity of the additional titanium sites, also an IPC-1P without any titanium introduced during its hydrothermal synthesis was silica-titania pillared (IPC-1PITi(40)) and tested as a catalyst. The results of the catalytic tests (e.g. cyclooctene conversion 28.3% vs. Ti-IPC-1PITi(30) 35.8% after 4h) confirmed the catalytic activity of the sites created during the silica-titania pillaring.

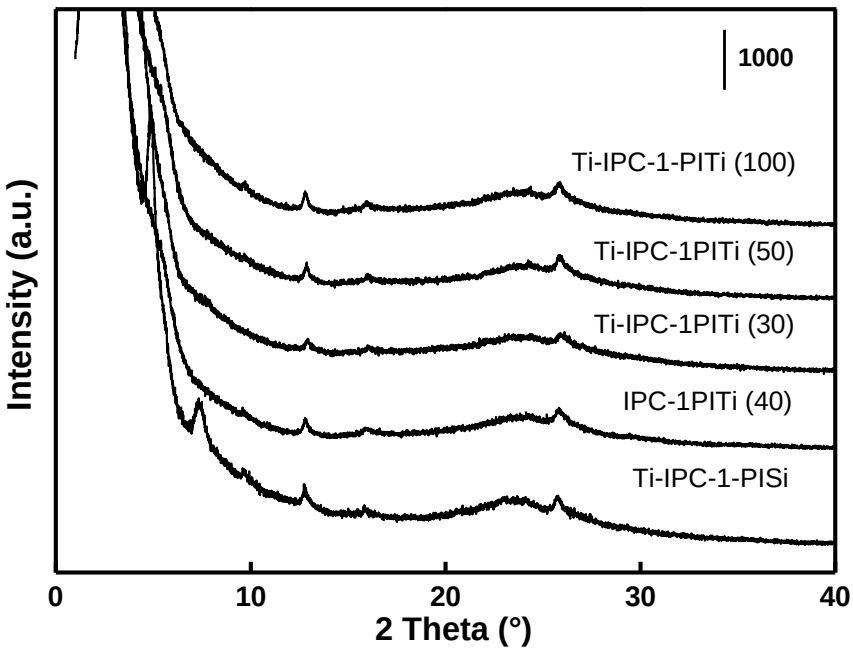

Figure 30: XRD patterns of the silica-titania pillared Ti-IPC-1PITi materials.

The accessibility of the titanium in the pillars is questionable; however, the silica-titania pillaring leads to materials providing much higher conversion in comparison with their silica pillared analogues (e.g. conversion in cyclooctene epoxidation TS-1-PISi 6.5% vs. TS-1-PITi(20) 21%; for details *vide infra*). We assume the process of creation of the additional sites on the surface of the layers is similar to the TBOTi impregnation of deboronated borosilicates (*vide supra*). The TBOTi is more reactive that TEOS [152] and therefore it is expected to react preferentially with the surface silanols.

Table 7: Textural properties and titanium content of the silica-titania pillared TS-1 (upper part) and Ti-IPC-1PITi (lower part of the table).

Titanosilicate[a]	BET (m^2/g)	S_{ext} (m^2/g)	V_{mic} (cm^3/g)	V_{tot} (cm^3/g)	Si/Ti
TS-1-PISi (a)	595	384	0.09	0.46	93
TS-1-PISi (b)	575	337	0.11	0.39	55
TS-1-PITi (10b)[b]	540	323	0.10	0.33	14
TS-1-PITi (20a)[b]	480	239	0.11	0.29	23
TS-1-PITi (20b)[b]	634	402	0.10	0.37	20
TS-1-PITi (60b)[b]	685	524	0.07	0.37	30
Ti-IPC-1PISi	1001	n.d.	0	0.67	480
IPC-1PITi (40)[b,c]	664	388	0.11	0.34	43
Ti-IPC-1PITi (30)[b]	910	n.d.	0	0.46	16
Ti-IPC-1PITi (50)[b]	662	353	0.14	0.35	18
Ti-IPC-1PITi (100)[b]	763	523	0.10	0.43	69

[a] Samples marked (a) resp. (b) were prepared form same batch of parent nanosheet TS-1.
[b] Number in brackets represents Si/Ti ratio in the pillaring mixture.
[c] Pure germanosilicate **UTL** was used as the parent material.

From the structural point of view, there is not a big difference among the silica and silica-titania pillared materials. Figure 29 and Figure 30 present the XRD patterns of silica and silica-titania pillared TS-1 resp. IPC-1 materials. No differences between the silica and silica-titania pillared materials are observed even when a high TBOTi concentration (10 molar %) is used. Table 7 presents basic textural properties and titanium content of the silica-titania pillared materials.

The titanium content was higher than in the parent material in all cases (e.g. TS-1-PITi(20a) Si/Ti=23 vs. layered TS-1(a) Si/Ti = 36) but the BET area as well as the total adsorption capacity decreased significantly in comparison with TEOS pillared materials (e.g. TS-1-PITi(20a) vs. TS-1-PISi(a): BET: 480 vs. 595 m^2/g; V_{tot}: 0.29 vs. 0.46 cm^3/g). We ascribe this behaviour to higher reactivity of the TBOTi. The presence of TBOTi supports formation of thicker pillars than pure TEOS (the silica-TiO_2 phase between the layers is denser). A series of silica-titania pillared TS-1 with different Ti content in the pillaring mixture (namely 10, 5 and 1.67 molar %) in TS-1-PITi(10b), (20b) and (60b), respectively. A trend in the dependence of BET area on Ti content in the pillaring mixture can be observed in Figure 31. The horizontal line marks the BET area of a non-pillared material. The higher Ti content in the pillaring mixture is used, the lower BET area possesses the product. Regarding the catalytic performance, it was found that the optimum titanium content in the pillaring medium is close to 5 molar % (*vide infra*). Similar behaviour was observed also in the case of Ti-IPC-1PITi materials.

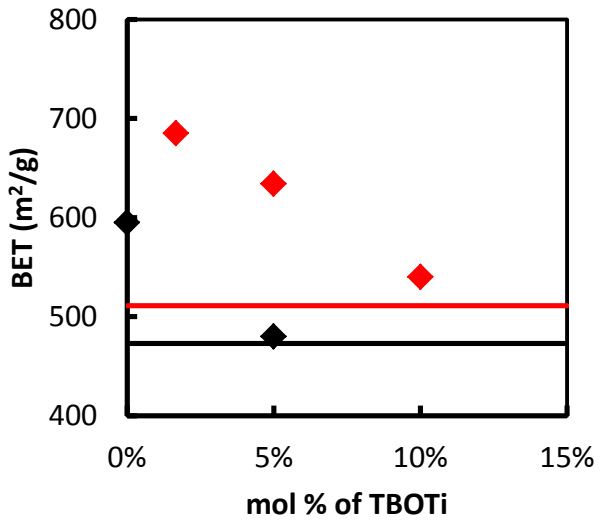

Figure 31: Silica-titania pillared TS-1 BET area dependence on composition of the pillaring medium: TS-1-PITi(a) samples (black), TS-1-PITi(b) samples (red).

The DR-UV/Vis spectra of TS-1PITi (Figure 32) and Ti-IPC-1PITi (Figure 33) show some differences. In the spectra of TS-1-PITi, the most intensive band is centered at 210 nm and it

evidences the presence of tetrahedrally coordinated titanium species. In addition, a shoulder at approximately 260-290 nm can be observed. The UV light absorption between 260 and 290 nm is typical for extra-framework titanium species and its intensity increases with increasing content of titanium in the pillaring medium. In contrast, the relative intensities of the bands (within particular samples) in the Ti-IPC-1PITi are similar in all materials and spectra of the samples differ only in the absolute intensity, what might be caused by other reasons but titanium content (e.g. different bulk density of the samples). This suggests that probably, lower TBOTi is sufficient for proper silica-titania pillaring of the Ti-IPC-1P layers.

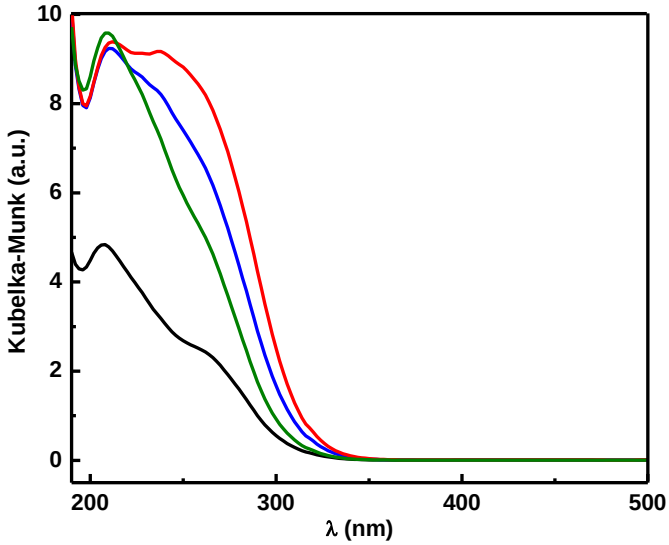

Figure 32: DR-UV/Vis spectra of TS-1-PISi(b) (black), TS-1-PITi(10b) (red), TS-1-PITi(20b) (blue) and TS-1-TiPI(60b) (green)

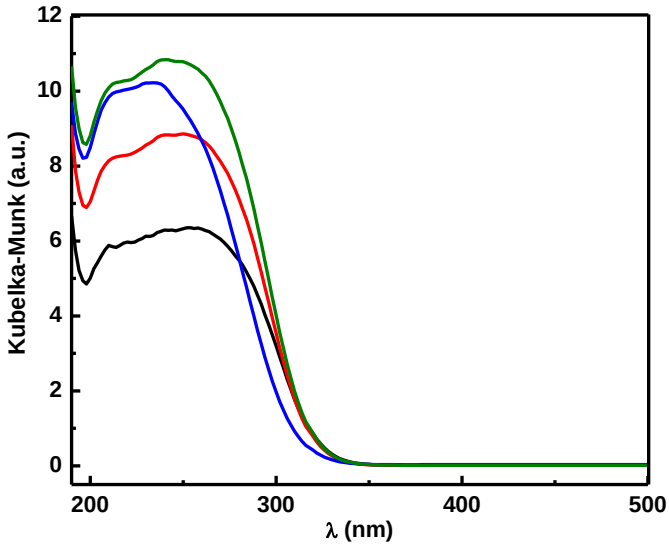

Figure 33: DR-UV/Vis spectra of Ti-IPC-1PITi(30) (black), Ti-IPC-1PITi(50) (red), Ti-IPC-1PITi(100) (blue) and IPC-1TiPI(40) (green)

5.2.Epoxidation of bulky substrates

5.2.1. Epoxidation of cyclooctene

All prepared catalysts were tested in *cis*-cyclooctene epoxidation using aqueous hydrogen peroxide as the oxidant in acetonitrile at 60°C. Acetonitrile was chosen as a solvent inert to the formed epoxide and it suppresses possible ring-opening reactions due to its weak basicity [54]. No conversion of cyclooctene was observed in a blank experiment. Selected results of the cyclooctene epoxidation are summarized in Table 8. Detailed discussion of catalytic performance of each material is provided in the attached articles [37, 38, 45, 65, 82].

The Ti-**CON** provides yields of cyclooctene oxide up to 28.3 % after 4 h (Ti-**CON**(TBOTi)). The presence of anatase phase in Ti-**CON**($TiCl_4$ sol) did not influence significantly the yield and the selectivity (90% at 20% conversion) was even higher than in the case of anatase-free Ti-**CON**(TBOTi) (77% at 20% conversion). Sasaki et al. [41] observed a similar behaviour for Ti-YNU-2 in the oxidation of phenol with hydrogen peroxide. The Ti-YNU-2 exhibited significantly higher activity (TON = 923 vs. TON = 272 and selectivity (92% vs. 74%) in comparison with Ti-MCM-68 (containing mainly tetrahedrally coordinated titanium), although it contained hexacoordinated titanium and anatase. The performance of the impregnated Ti-**CON** is comparable with the results reported by Dartt and Davis [70] and nanosheet TS-1 reported by Ryoo [80] (both using similar experimental conditions). The difference between Ti-**CON**(TBOTi) (Si/Ti=450, conversion 37% after 4 h) and Ti-**CON**($TiCl_4$ sol) (Si/Ti=81, conversion 26% after 4 h) suggests that the epoxidation reaction does not occur in the whole volume (if it did, we would expect the difference of an order of magnitude in conversion between the two samples) of the zeolite crystal but mainly close to the external surface (where local titanium concentration is expected to be higher in Ti-**CON**(TBOTi). The Ti-**CFI**(40) and Ti-**CFI**(60) also provided the same conversion and yield of cyclooctene oxide, although they possess different titanium content. This suggests that the reaction rate is mostly diffusion driven also in the case of Ti-**CFI**.

The Ti-**UTL** gave yield of cyclooctene oxide 4.7% and conversion 14.3% after 4 h. The transformation of the Ti-**UTL** into a pillared material Ti-IPC-1PISi led to a strong improvement of the titanium sites accessibility. As a result, the yield (8% after 4 h) as well as the conversion (21.3 %) increased in comparison with Ti-**UTL** although the Si/Ti ratio increased from 139 to 480.

Unexpectedly, the yield provided by the layered TS-1 was comparable to conventional TS-1 (2.8 % after 4 h). The layered TS-1 provided higher selectivity[2] (75% vs. 42%). We assume that cyclooctene is oxidized due to the flexibility of its molecule, which is able to adopt such a conformation that fits into the TS-1 channels, although our observation do not meet the one reported by Na et al. [80]. When using TS-1-PISi, the yield only slightly increased to 3.5% after 4 h, which may be accounted for the dilution of the active component. The Ti-MCM-36 gave 8% yield after 4 h and the selectivity was similar to the TS-1-PISi (54% resp. 58%).

Table 8: Reaction data for epoxidation of cyclooctene at 60°C in acetonitrile after 4 h

Catalyst	Conversion[a] (%)	Yield[b] (%)	Selectivity (%)[c]
Ti-**CON**(TBOTi)	37.0	28.3	77 (20%)
Ti-**CON**($TiCl_4$ sol)	26.0	22.0	90 (20%)
Ti-**IFR**(TBOTi)	< 2.0	0.7	n.d.
Ti-**IFR**($TiCl_4$ vap)	3.9	1.1	35 (5%)
Ti-**AFI**($TiCl_4$ vap)	0.0	--	--
Ti-**CFI**($TiCl_4$ sol)	3.5	0.9	n.d.
Ti-**CFI**(40)	10.6	2.1	20 (10%)
Ti-**CFI**(60)	10.5	2.0	20 (10%)
Ti-**AFI**(a)	2.9	1.1	59 (5%)
Ti-**UTL**	14.3	4.7	30 (20%)
Ti-IPC-1PISi	21.3	8.0	38 (20%)
Ti-IPC-2	11.2	0.4	n.d.
Ti-IPC-1PITi (30)	35.8	23.3	80 (20%)
Ti-IPC-1PITi(100)	34.7	24.7	80 (20%)
IPC-1PITi (40)	28.3	15.5	67 (20%)
Layered TS-1(a)	3.7	2.8	75 (20%)
TS-1-PISi(b)	6.5	3.5	58 (20%)
TS-1-PITi(10b)	19.1	15.3	80 (20%)
TS-1-PITi(20b)	21.0	16.9	76 (20%)
TS-1-PITi(60b)	18.6	14.0	76 (20%)
Ti-MCM-36	18.0	8.0	54 (20%)
meso TS-1	9.2	1.1	24 (20%)
desil-TS-1 (0.05)	10.0	3.0	43 (20%)
TS-1(200)	8.0	3.0	42 (20%)
TS-1(600)	5.9	2.9	55 (10%)

[a] cyclooctene conversion after 4 h
[b] yield of cyclooctene oxide after 4 h
[c] Selectivity observed at the conversion in brackets; defined as [produced epoxide]/[consumed alkene]

The use of desil-TS-1 and meso-TS-1 resulted in slightly higher conversion in comparison with the TS-1 (X(desil-TS-1) = 10%, X(meso-TS-1) = 9.2% vs. X(TS-1(600))=5.9, X(TS-1(200) = 8%) but the selectivity of the reaction decreased.

[2] Selectivity is always compared at the same or similar conversion levels of conversion for cyclooctene epoxidation are presented in Table 8.

The use of silica-titania pillared catalysts provided the desired increase in both yield of the cyclooctene oxide and the selectivity. The highest yields of the epoxide were obtained using Ti-IPC-1PITi(30) and Ti-IPC-1PITi(100) catalysts (23.3% resp. 24.7 after 4h) with 80% selectivity (compared at 20% conversion). Yields after 4 h are slightly lower than the one obtained using Ti-**CON**(TBOTi) (28.3%); however, we should note that for instance Ti-IPC-1PITi (30) catalyst provided conversion of 26% and yield 19.5% 1 h (Figure 34) and then the rate of the reaction decreased rapidly. Iodometric titration of the sample revealed total conversion of the hydrogen peroxide, which means, that approximately 28% of hydrogen peroxide was ineffectively decomposed (due to the presence of anatase phase) or it were consumed in side reactions (e.g. further oxidation of the ring opening products observed by Pirovano et al.[153]). When a fresh H_2O_2 was added, the reaction was restored. The IPC-1PITi(40) catalyst (possessing no titanium from the hydrothermal synthesis) fits to the group of silica-titania pillared catalysts providing conversion and yield of 28.3% resp. 15.5% after 4 h. This further evidence that the active titanium sites formed during silica-titania pillaring are active in oxidation catalysis.

Using the TS-1-PITi(10b), (20b) and (60b) catalysts, yields of cyclooctene oxide of 15.3%, 16.9% and 14%, respectively, were obtained after 4 h. Selectivity ranged between 76 and 80% at 20% conversion. Considering the dependence of the BET area on TBOTi concentration in the pillaring mixture (Figure 31), we conclude there are two factors contradicting each other which define the catalyst performance. The higher content of titanium the more active sites; however, the lower BET area. It appears that 5 mol. % (Si/Ti = 20) in the pillaring mixture is close to the optimum.

In the epoxidation over Ti-IPC-1PITi(30) as a representative catalyst, methanol was used as a solvent instead of acetonitrile; however, the change of the solvent did not influence the conversion significantly (conversion 35.8 % vs. 34.7 % in acetonitrile). Only the yield of the epoxide decreased (23.3% vs. 19.1% after 4 h) because of ring-opening reaction with methanol [111].

We conclude that the catalysts with most open structures and therefore the lowest diffusion limitations and sufficient amount of the titanium centres (Ti-IPC-1PITi (30), Ti-IPC-1PITi (100), TS-1-PITi (20b) and TS-1-PITi (60b), Table 7) provided the highest yields as well as the selectivity. A comparison of the best catalysts of each structure is provided in Figure 34. Simple silica-titania pillaring treatment improves the catalyst performance dramatically. Based on the observed catalytic results and DR-UV/Vis spectra (*vide supra*), we support the points of

Sasaki et al. [41] and Guo et al. [102] that also titanium species other that the single tetrahedrally coordinated ones are active in oxidation catalysis.

Leaching of titanium out of titanosilicate zeolites is unusual. We did not recognize any leaching of titanium during leaching tests. Usually, the most active catalyst among a series was examined; namely: Ti-**CON** (TBOTi, (l)), Ti-IPC-1PITi (30) and TS-1-PITi (20b). Details are provided in the attached articles [37, 38, 45, 65, 82].

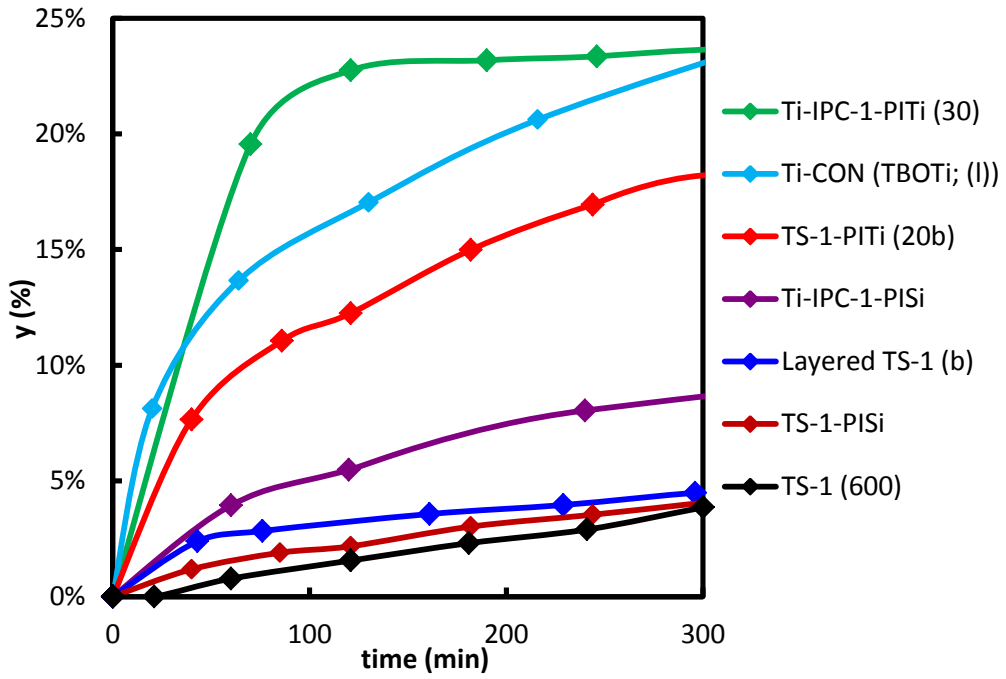

Figure 34: Development of the cyclooctene oxide yield in time using lamellar titanosilicate catalysts

5.2.2. Epoxidation of cyclodecene

Trans-cyclodecene was oxidised only using the silica-titania pillared catalysts and Ti-**BEA** (BET area 339 m^2/g, Si/Ti = 116) was used as a benchmarking material instead of TS-1(600). TS-1(600) provided yield below 1% after 5 h. The reaction was carried out in a mixture of acetonitrile and 2-propanol (2:1 vol.) to achieve homogeneity of the reaction mixture even upon addition of aqueous H_2O_2. Cyclodecene oxide proved to be resistant toward epoxide ring opening under the testing reaction conditions and thus high selectivity (95-97% at 10% conversion) and high yield (TS-1-PITi 15%, Ti-IPC-1PITi 23% at 60°C after 4 h) were achieved in epoxidation of cyclodecene.

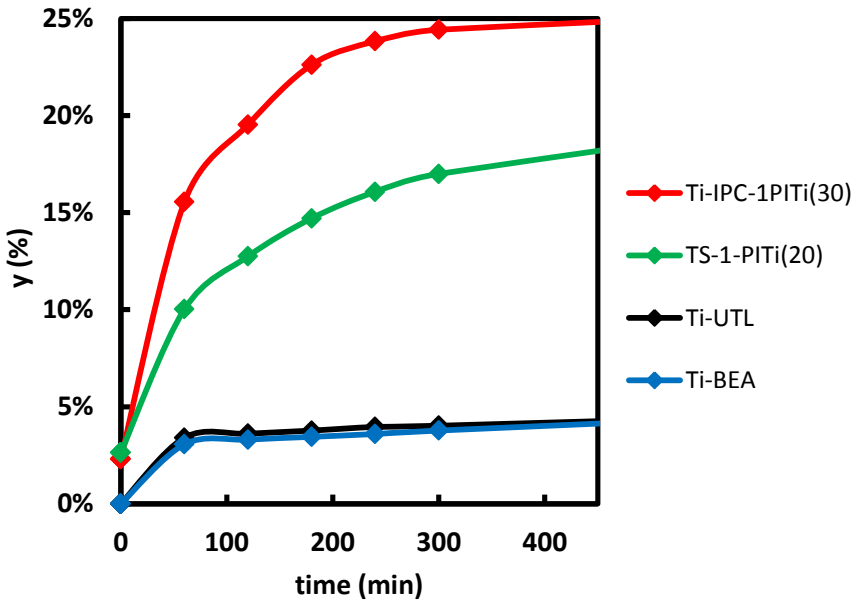

Figure 35: Development of the cyclodecene oxide yield in time at 60°C

5.2.3. Epoxidation of norbornene

Norbornene possesses bulky and rigid structure and therefore it was chosen for further test of the catalysts providing high conversion in epoxidation of cyclooctene (Table 9). Ti-**CON**($TiCl_4$ sol) was the catalyst providing the highest yield of norbornene oxide (15.4% after 4 h). In the serie of the Ti-**UTL** based materials, order of epoxide yields over different catalysts was following: Ti-IPC-1PITi(30) 12.6% > Ti-IPC-1PISi 6.5 % > Ti-**UTL** 0.9% after 4 h. The order in the group of the TS-1 based catalysts was similar: TS-1-PITi(20b) 14.8 > TS-1-PISi(b) 5.5% ≈ layered TS-1 (b) 6.1% > TS-1(600) 1.8%. Interestingly, the Ti-**CON**($TiCl_4$ sol) provided significantly higher selectivity (76%) in comparison with the Ti-**CON**(TBOTi) (42%). Note that similar difference in selectivity using these two catalysts was observed also in cyclooctene epoxidation.

It is clear that the norbornene oxide yield is supported by both good accessibility of the active centres and high titanium content. Norbornene is truly unable to access the 10-ring pores and therefore only the sites on the outer surface of the layers can participate in the catalytic reaction. That is the reason why the Ti-IPC-1PISi catalyst provides higher yield than the TS-1-PISi(b) and layered TS-1(b), which both have almost 10 times higher titanium content. Note that the three catalysts providing the highest yield (Ti-IPC-1PITi(30), TS-1PITi(20b) and Ti-**CON**($TiCl_4$ sol) contain high amount of extra-framework titanium species (*vide supra*). This may suggest that extra-framework titanium species also participate in the oxidation catalysis. The epoxide selectivity of the reactions ranged between 22% and 56% at 10% conversion due to consecutive ring opening reactions.

Table 9: Epoxidation of norbornene over titanosilicate catalysts in acetonitrile at 60°C; conversion and yield after 4 h

Catalyst	Conversion (%)	Epoxide yield (%)	$S_{10\%}$ (%)[a]
TS-1(600)	2.8[b]	1.8[b]	65[c]
Layered TS-1(b)	12.0[b]	6.1[b]	42
TS-1-PISi(b)	10.6[b]	5.5[b]	52
TS-1-PITi(20b)	23.0[b]	14.8[b]	56
Ti-MCM-36	24.1[b]	8.5[b]	26
Ti-**CFI**($TiCl_4$ sol)	4.9	3.3	50
Ti-**CON**(TBOTi)	17	9.4	42
Ti-**CON**($TiCl_4$ sol)	18.7	15.4	76
Ti-**IFR**(TBOTi)	6.9	0.8	n.d.
Ti-**UTL**	60.5	0.9	n.d.
Ti-IPC-1PISi	49.2	6.5	22
Ti-IPC-1PITi(30)	57.2	12.6	33

[a] Selectivity at 10% conversion defined as [yield of epoxide]/[consumed alkene]
[b] conversion and yield after 4.5 h
[c] Selectivity provided at 3% conversion; 10% conversion was not achieved until 8 h

5.2.4. Regioselective epoxidation of linalool

The epoxidation of linalool was performed in methanol instead of acetonitrile (Table 10). The linalool molecule possesses 2 different double bonds, which can be oxidised. C1=C2 terminal double bond and C6=C7 internal double bond bearing 3 alkyl substituents. Using all the catalysts, only epoxidation of the internal double bond (which is more electron rich) was observed together with acid catalysed intramolecular rearrangement of the resulting epoxide [154]. As a major product 2-(5-methyl-5-vinyltetrahydro-1-furyl)-2-propanol (known as linalool oxide) was formed and 2,2-dimethyl-3-hydroxy-6-methyl-6-vinyltetrahydropyran was the minor product. The intramolecular reactions proceeded immediately and thus epoxide itself was not observed. Both products form diastereoisomers distinguishable using conventional GC

column. This is a known behaviour also for other unsaturated alcohols having the general formula $R_1R_2C=CH(CH_2)_nCR_1R_2OH$ where R_1,R_2 are -H or -CH_3 and n = 1 - 3 under conditions of epoxidation over titanosilicate catalysts [155]. Yield and selectivity are calculated for the main product (linalool oxide).

The Ti-**CON**(TBOTi) provided 13.3% yield of the linalool oxides after 5.3 h. Other impregnated large-pore catalysts and the TS-1(600), provided an order of magnitude lower conversion and yield. Ti-**IFR**($TiCl_4$ vap) and Ti-**CFI**($TiCl_4$ sol) were performing slightly better (both conversion 3.7 % after 5.3 h) than Ti-**AFI**($TiCl_4$ sol) and TS-1(600) (conversion lower than 2%). This is in accordance with the above results obtained in epoxidation of cyclooctene and norbornene.

The highest yield of the linalool oxide (23.5% after 4 h) was obtained using the Ti-IPC-1PITi (30) catalyst. Only slightly lower yield was given by Ti-IPC-1PITi (100) although this catalyst was more selective (58% vs. 50% at 10% conversion). The TS-1-PITi (20b) provided yield 21.4% after 4 h and the selectivity was 74% at 10% conversion (the same as for Ti-**CON**(TBOTi)); however, it dropped rapidly with increasing conversion (50% at 40% conversion). Nevertheless, the silica-titania pillared materials were the most effective of the studied catalysts. The yield of linalool oxide over Ti-**UTL** was only 3.3% after 4 h, but the conversion was high (31.7%). Two new products were observed instead of the linalool oxide and its pyrane analogue (*vide supra*). Both substances were identified as linalool derivates; however, it was not possible to determine their structure only from the GC-MS data. None of them was linalool epoxide or any of its simple ring-opening product (diol or ketone). We ascribe the change in the product composition to the presence of germanium in the Ti-**UTL** structure.

Table 10: Reaction data from epoxidation of linalool in methanol at 60°C

Catalyst	Conversion (%)	Yield[a] (%)	Selectivity (%)[b]	reaction time
Ti-**CON**(TBOTi)	22.7	13.3	74	5.3 h
Ti-**AFI** ($TiCl_4$; (l))	< 2.0	0.5	n.d.	5.3 h
Ti-**IFR**($TiCl_4$ vap)	3.7	3.5	n.d.	5.3 h
Ti-**CFI**($TiCl_4$ sol)	3.7	3.6	n.d.	5.3 h
Ti-**UTL**	31.7	3.3	9	4 h
Ti-IPC-1PISi	6.4	3.8	64	4 h
Ti-IPC-1PITi(30)	46.6	23.5	50	4 h
Ti-IPC-1PITi(100)	43.5	22.2	58	4 h
TS-1-PITi (20b)	43.2	21.4	74	4 h
TS-1	< 2.0	1.3	n.d.	5.3 h

[a] yield of both possible diastereoisomers of linalool oxide
[b] selectivity at the 10% conversion; defined as [sum of produced linalool oxide isomers]/[consumed linalool]; n.d. = selectivity not determined due to low conversion
[d] determined at 3-5% conversion

5.2.5. Oxidation of α-pinene

Selective oxidation of α-pinene is a considerable challenge, because the α-pinene is usually converted into a number of products because both C=C double bond and allylic –C-H bonds oxidation occur together with intramolecular rearrangement resulting from highly stressed C_4 ring present in the molecule [88]. We focused on epoxidation to form α-pinene oxide only. The observed results are listed in Table 11. Expectedly, the TS-1 was unable oxidise α-pinene. No epoxide or any other oxidation product was observed. The Ti-**CFI** (60) provided the highest conversion of all tested catalysts (24% after 4 h); however, only trace amount of the α-pinene oxide was observed. TS-1-PISi (a) gave similar yield of the epoxide. The highest epoxide yield (1.9% after 4 h) was obtained using the Ti-MCM-36 catalyst with the selectivity of 20%. Other observed oxidation products were mainly hydroxyl and carbonyl compounds whose precise identification was complex. We conclude that none of the tested catalysts performed significantly better than the catalysts reported earlier [88, 156].

Table 11: Oxidation of α-pinene over titanosilicate catalysts in acetonitrile at 60°C; conversion and yield after 4 h of the reaction

Catalyst	Conversion (%)	Epoxide yield (%)	$S_{10\%}$ (%)[a]
TS-1	0	no epoxide	--
Ti-**CFI**(60)	24	0.5	2.2
TS-1-PISi(a)	8.8	0.6	7
TS-1-PITi(20a)	12.3	1.0	8
Ti-MCM-36	9.6	1.9	20

[a] Selectivity at 10% conversion defined as [yield of epoxide]/[consumed alkene].

5.2.6. Oxidation of verbenol

Last but not least, verbenol was used as a substrate because it is one of the products of α-pinene oxidation. Rapid selective oxidation of verbenol to verbenone was observed using the various TS-1 based catalysts instead of the epoxidation. Unexpectedly, conventional TS-1(600) and layered TS-1 (a) provided higher conversion (30.6 % resp. 46.2% after 4 h) than the TS-1-PITi (20a) (10.4%). Similarly, desilicated TS-1 (0.05) gave lower conversion than TS-1(600) although the TS-1(600) is expected to suffer from higher diffusion limitations. No epoxy-verbenol was observed in any of the runs.

Van der Waal et al. observed oxidation of hydroxyl group in oxidation of allylic alcohols over Ti-**BEA**; however, the main product was always the epoxide [54]. Tatsumi et al. showed that gaining the right position to the active site may be difficult for the substrates with tri-substituted double bond (e.g. 3-methyl-2-buten-1-ol). Selectivity of parallel oxidation of C=C double bond and hydroxyl group depends on the relative position and steric hindrance of both

groups. Epoxide and aldehyde or ketone may be formed concurrently in such case [157]. Verbenol, thus, represents an extreme case when epoxidation is suppressed and only hydroxyl group is oxidised with selectivity up to 99% (using desil-TS-1 (0.05) catalyst).

Table 12: Oxidation of verbenol to verbenone over titanosilicate catalysts at 60°C; conversion and yield after 4 h

Catalyst	Conversion (%)	Verbenone yield (%)	$S_{10\%}$ (%)[a]
TS-1(600)	30.6	24.7	71
Desil-TS-1(0.05)	19.0	18.9	99
Layered TS-1(a)	46.2	44.8	97
TS-1-PITi(20a)	10.4	10.2	98
Ti-MCM-36	30.2	14.2	32

[a] Selectivity at 10% conversion defined as [yield of verbenone]/[consumed verbenol]

5.3.Oxidation of bulky organic sulphides

Selected TS-1 based materials and the Ti-**UTL** derived materials were used in oxidation of bulky organic sulphides in acetonitrile using H_2O_2 aqueous solution as the oxidant. Namely, methylphenyl sulphide (MPS), diphenyl sulphide and dibenzothiophene were oxidised to corresponding sulphoxides and sulphones. Influence of other parameters such as temperature, substrate/catalyst ratio and dosing of the oxidant was analysed. Detailed discussion is provided in the attached article [45].

5.3.1. Oxidation of methylphenyl sulphide

Methylphenyl sulphide (MPS) was oxidised at 30°C. The conversion curves using selected TS-1-based catalysts, Ti-**UTL** and Ti-IPC-1PISi are given in Figure 36. The product distribution, selectivity and TON for all tested catalysts are presented in Table 13. A blank experiment revealed that the reaction without a catalyst occurs with a low reaction rate (conversion of 2.5% after 120 min) under the experimental conditions employed. Therefore, the contribution of the non-catalytic oxidation to the observed kinetic profiles is insignificant. 0.5 molar equivalent of the oxidant was used in the experiments. Therefore, maximum theoretical conversion was 50% under the used conditions. In all cases, the reaction started rapidly and slowed down as the hydrogen peroxide was running out until it stops at the 100% conversion of H_2O_2. When fresh H_2O_2 was added, the reaction was restored.

The Ti-IPC-2 catalyst (conversion curve presented in [45]) gave the lowest conversion (5% after 30 min), most probably due to diffusion limitations in the two-dimensional system of 12x10 channels. TS-1(600) provided conversion 11% after 30 min. The use of the catalyst with smaller crystals (TS-1(200) [45]) resulted in an increase in the conversion (21% after 30 min) due to shorter diffusion paths. The use of lamellar catalysts led to another strong increase in the

conversion: TS-1-PISi(b) 26% < layered TS-1(b) 36% < TS-1-PITi(60b) 41% after 30 min. Among the lamellar TS-1 catalysts, it appears that the conversion is more dependent on the titanium content than on the textural properties. In contrast, the extra-large pore Ti-**UTL** provided conversion of 17% after 30 min standing between TS-1(600) and TS-1(200) in term of conversion. Note that the titanium content in the Ti-UTL is almost 3 times lower in comparison with the TS-1 (Si/Ti=139 vs. Si/Ti=39).

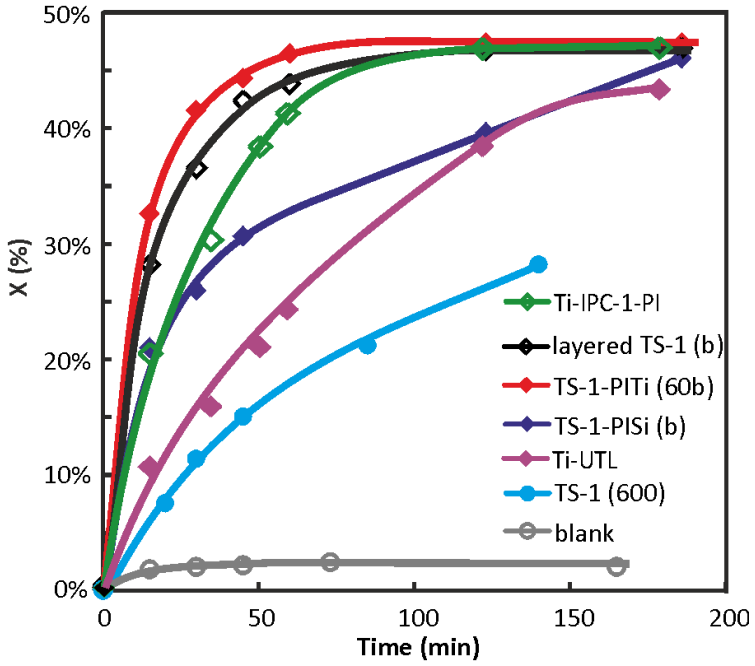

Figure 36: Conversion curves of the MPS oxidation at 30°C

The Ti-IPC-1PISi provided conversion of 29% after 30 min although its Si/Ti molar ratio is as high as 480. This is an outstanding result, which clearly shows that enhancement of the active sites accessibility may provide much higher conversion than sole increasing of the number of active sites. The TON_{tot} (including both oxidation of MPS to methylphenyl sulphoxide (MPSO) and consecutive oxidation of MPSO to methylphenyl sulphone ($MPSO_2$)) after 30 was 1418 for the Ti-IPC-1PISi, what is an order of magnitude more than TS-1-PISi(b) (TON_{tot} = 151 after 30 min), which is also silica pillared. Note, that the similar conversion was gained using the Ti-IPC-1PISi and TS-1-PISi(b) (29% vs. 26%). Detailed discussion of the intrinsic activity of the catalysts is provided in the enclosed article [45].

The Ti-**UTL** was the most selective of the discussed catalysts (98% at 40% conversion) and the Ti-IPC-1PISi is most efficiently using the H_2O_2 (E = 100%) together with the selectivity of 95% (5% of H_2O_2 is spent in consecutive oxidation of MPSO to $MPSO_2$). In contrast, the TS-1(600) provided the lowest selectivity (61 %) of the tested catalysts. The order of the catalyst selectivity to sulphoxide (at 40% conversion) is the following: TS-1(600) 61% < Ti-IPC-2 69% <

TS-1(200) 78% < layered TS-1(b) 87% < TS-1-PISi(b) 91% < Ti-IPC-1PISi 95% < Ti-**UTL** 98%. The selectivity of the reaction to the sulphoxide is mostly dependent on the diffusion restrictions in the catalyst and partially on the titanium content. The larger pores, the higher sulphoxide selectivity was observed. The theory of the diffusion driven selectivity is also in accordance with the data reported by Corma et al. [133] and Kon et al. [136] on MPS oxidation. The TS-1-PITi(60b) stands out of the trend (S = 85%) because it has an increased amount of easily accessible active sites in comparison with TS-1-PISi(b), which were formed post-synthetically during the silica-titania pillaring and thus the TS-1-PITi(60b) is less selective than it should be according to its textural properties.

Table 13: Catalytic oxidation of methylphenyl sulphide (MPS) over the TS-1 based catalysts and Ti-IPC-1PISi at 30°C. Reaction conditions: 8 mmol of MPS, 4 mmol of H_2O_2 (35 wt. %), 50 mg of catalyst, 250 µl of internal standard, 10 ml acetonitrile, 900 rpm.

	Product composition (120 min)[a]		$S_{(40\%)}$ [b]	$E_{(100\%)}$ [c]	TON_{prim} [d]	TON_{tot} [e]
Catalyst	**MPSO (%)**	**$MPSO_2$ (%)**	**(%)**	**(%)**	**(30 min)**	**(30 min)**
TS-1(600)	60	40	61 $_{(25\%)}$	n.a.	43	60
TS-1(200)	74	26	78	94	74	87
layered TS-1 (b)	94	6	87	94	127	136
TS-1-PISi (b)	91	9	91	95	137	151
TS-1-PITi (60b)	93	7	85	91	124	132
Ti-**UTL**	96	4	98	95	200	208
Ti-IPC-1PISi	94	6	95	100	1338	1418
Ti-IPC-2	84	16	69 $_{(8\%)}$	n.a.	101	115

[a] Ratio between methylphenyl sulphoxide (MPSO) and methylphenyl sulphone ($MPSO_2$) after 120 min of the reaction.

[b] Methylphenyl sulphoxide selectivity at 40 % conversion; calculated as S = [yield of MPSO]/[conversion of MPS]. Where the conversion of 40 % was not reached during the experiment, the selectivity is given at maximum conversion.

[c] Hydrogen peroxide efficiency at 100% conversion of the H_2O_2; calculated as E = ([yield of MPSO]+ 2 . [yield of $MPSO_2$])/[initial amount of H_2O_2]).

[d] TON of the primary oxidation of MPS; calculated as TON_{prim}=[n(MPS) converted]/[n(Ti)].

[e] Overall TON (including the oxidation of MPSO to $MPSO_2$); calculated as TON_{tot} = ([n(MPS) converted]+[n($MPSO_2$) formed])/[n(Ti)].

The influence of the substrate/catalyst ratio (S/C) and the influence of H_2O_2 concentration in the reaction mixture were examined as well. The influence of the S/C ratio was investigated using the layered TS-1(b) catalyst at S/C=20, 40 and 100. Based on the high selectivity obtained using the Ti-**UTL** and Ti-IPC-1PISi catalysts, which have low concentration of the active sites, we expected that the decrease in the amount of the catalyst might influence the selectivity.

However, it was found that neither the selectivity (86% at 25% conversion in all cases) nor the intrinsic activity [45] was influenced.

The concentration of hydrogen peroxide is another parameter, which can be expected to influence the selectivity in a system of two consecutive oxidation reactions. To investigate this influence, we have chosen two catalysts i.e. TS-1(600) and layered TS-1(b). We conducted the catalytic experiment with 0.5 molar equivalent of H_2O_2 based on the MPS (a standard experiment), with 1 molar equivalent of H_2O_2 and with 5 doses of 0.1 equivalent of H_2O_2 during 5 h. The obtained conversion curves resp. curves showing the development of conversion in the case of the dosing experiment are presented and discussed in the attached article [45].

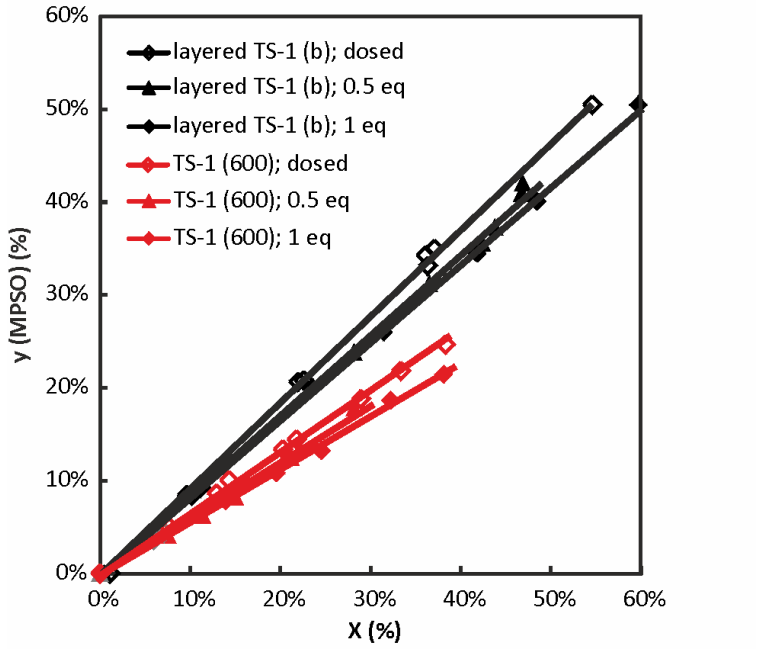

Figure 37: Selectivity curves of the experiments using different amount of H_2O_2 and dosing of the oxidant over TS-1(600) (red) and layered TS-1 (b) (black)

The selectivity curves are presented in Figure 37. An increased MPSO yield at a certain conversion in the case of 0.1 eq dosing experiment is clearly visible for both examined catalysts. The selectivity using the layered TS-1(b) (calculated at 40% conversion) increased upon dosing of hydrogen peroxide from 87% (standard experiment) to 91%. Regarding the rapid conversion of each H_2O_2 dose [45], we believe that the dosing of the oxidant can be tuned in such way that the selectivity is increased without any decrease in the reaction rate. When introducing 1 eq of H_2O_2 at the beginning of the reaction, the selectivity decreased to 85%. For the TS-1(600) similar effect was observed. When the oxidant was dosed, the selectivity increased from 61 % (standard experiment) to 65%. When the 1 eq of H_2O_2 was used, it decreased to 56%. The selectivity was compared at 25% conversion.

5.3.2. Oxidation of diphenylsulphide and dibenzothiophene

Diphenyl sulphide and dibenzothiophene were oxidised at 40°C using molar 1 eq of the oxidant. All catalysts investigated were able to oxidise the diphenyl sulphide (Ph_2S), (Table 14). Even the TS-1(600) (expected to suffer from diffusion limitations) provided conversion of 22% after 4 h. The layered TS-1(b) provided conversion of 34% and TS-1-PITi(60b) gave 59% conversion after 4 h. The Ti-**UTL** provided conversion similar to the TS-1(600). The Ti-IPC-1PISi gave conversion of 39% exhibiting (similarly to the MPS oxidation) an outstanding intrinsic activity (TON_{prim} = 1818 in 4 h) in comparison with the other catalysts (TON_{prim} from 81 (TS-1(600)) to 287 (Ti-**UTL**)).

Table 14: Oxidation of diphenyl sulphide at 40°C; results displayed after 4 h.

Catalyst	Conversion (%)	Yield (Ph_2SO)[b] (%)	TON_{prim} [a]
TS-1(600)	22	20	81
layered TS-1 (b)	34	30	117
TS-1-PITi (60b)	59	46	175
Ti-**UTL**	23	19	287
Ti-IPC-1PISi	39	31	1818
Ti-IPC-2	6.3	4.2	127

[a] TON of the primary oxidation of Ph_2S; calculated as TON_{prim}=[n(Ph_2S) converted]/[n(Ti)].

Contrary to the MPS oxidation, TS-1(600) was the most selective catalyst (selectivity 93% at 25% conversion). The Ti-**UTL** provided 87% selectivity, the selectivity over TS-1-PITi(60b) was 85% and the selectivity over Ti-IPC-1PISi was 79%. It appears that the Ph_2S is flexible enough to enter even the TS-1 micropores but the diffusion of diphenylsulphoxide (Ph_2SO) is much slower and therefore increased selectivity is gained over the catalysts with smaller pores. Influence of the temperature on the Ph_2S oxidation is discussed in the attached article [45].

In the dibenzothiophene (DBTH) oxidation, dibenzothiophene sulphone ($DBTHSO_2$) was the major product (Table 15). The highest conversion (28% after 4 h) and yield of the $DBTHSO_2$ (24 %) were obtained using the TS-1-PITi(60b) thanks to its well accessible titanium sites formed during the silica-titania pillaring. The layered TS-1(b) provided conversion of 20% because the DBTH cannot access the micropores in the layers (evidenced by the zero conversion over the TS-1(600) catalyst) and therefore only a part of the titanium sites located on the outer surface of the layers can catalyse the reaction. The Ti-IPC-1PISi catalyst provided conversion of 9.5 % and yield of 7.9 % after 4 h. Among the conventional zeolites, the Ti-**UTL** (containing the extra-large pores) was the only catalyst, which provided some conversion (3.3 % after 240 min). The

TS-1(600) and Ti-IPC-2 gave zero conversion after 4 h because their channels are not wide enough for the DBTH molecule. We conclude, that especially the silica-titania pillared catalysts like TS-1-PITi have the potential to oxidise bulky and rigid molecules like DBTF in the oxidative desulphurisation processes.

Table 15: Oxidation of dibenzothiophene at 40°C; results displayed after 4 h.

Catalyst	**Conversion (%)**	**Yield ($DBTHSO_2$) (%)**	**TON_{prim} [a]**
TS-1(600)	0	0	0
layered TS-1 (b)	20	18	69
TS-1-PITi (60b)	28	24	83
Ti-**UTL**	3.3	2.6	44
Ti-IPC-1PISi	9.5	7.9	438
Ti-IPC-2	0	0	0

[a] TON of DBTH oxidation is calculated as TON_{prim} =[n(DBTH) converted]/[n(Ti)].

6. Conclusions and perspectives

This thesis was focused on design, synthesis and characterisation of novel large pore, extra-large pore and lamellar titanosilicate materials with the ability to catalyse epoxidation of sterically demanding olefins and terpenes and with the ability to catalyse selective oxidation of bulky organic thiotehers with hydrogen peroxide as the oxidant.

Two novel extra-large pore titanosilicates were prepared by means of hydrothermal synthesis (Ti-**CFI**, Ti-**UTL**) and three large-pore titanosilicates (Ti-**CON**, Ti-**AFI**, Ti-**IFR**) together with Ti-**CFI** were prepared using two step deboronation – liquid phase titanium impregnation procedure. Extra-large pore zeolite **CFI** in a form of titanosilicate (Ti-**CFI**) was synthetized and characterised. The lowest Si/Ti ratio achieved in product was 23; however not all the titanium was found to occupy the framework positions. Duration of the hydrothermal synthesis was found to be dependent on the initial Si/Ti in the synthesis mixture. The higher titanium content, the longer crystallisation time is necessary. Seeding of the synthesis shortens the crystallisation time significantly.

The Ti-**UTL** was prepared with Si/Ti ratio 139 and majority of the titanium atoms located in the framework positions. The presence of germanium-rich D4R units in its structure allows disassembly into Ti-IPC-1P lamellar precursor and subsequent reassembly into new titanosilicates Ti-IPC-2 (**OKO** structure) and Ti-IPC-4 (**PCR** structure) by means of ADOR transformation. This is the first example of an ADOR transformation of a titanosilicate material.

Post-synthesis titanium incorporation is an alternative to direct hydrothermal synthesis of a titanosilicate. Titanium containing materials Ti-**CON**, Ti-**AFI**, Ti-**IFR** and Ti-**CFI** were prepared from corresponding borosilicate zeolites using a simple two step procedure. The materials were deboronated with HCl solution and subsequently impregnated by a titanium source solution. The structure of the zeolites was not influenced by the post-synthesis treatment. The DR-UV/Vis analysis showed that samples impregnated with TBOTi contained mainly tetrahedrally coordinated titanium species contrary to the $TiCl_4$ impregnated samples, where also extra-framework and anatase-like species were present. However, there was no significant difference in the conversion of the catalysts prepared in the two ways and the $TiCl_4$ impregnated Ti-**CON** exhibited even higher selectivity over TBOTi impregnated samples.

Silica-titania pillaring was developed and applied in preparation of lamellar titanosilicate materials. Pillared TS-1 catalysts were prepared from TS-1 nanosheets, using TEOS as a pillaring medium. The pillaring treatment helps to preserve the mesoporosity of the material

and to keep the active centres accessible even for bulky molecules. TBOTi addition into the pillaring medium helps to compensate the dilution of the active crystalline phase and thus boosts the Ti content in the material. We assume that an *in-situ* impregnation of the titanosilicate layers with additional titanium centres occurs. Based on the catalytic testing of materials with different Ti content, we conclude that an optimum composition of the pillaring medium is close to TEOS/TBOTi ratio 20 for the pillaring of layered TS-1 materials.

The Ti-IPC-1P lamellar precursor, obtained by hydrolysis of Ti-**UTL** was swollen with cetyltrimethylammonium hydroxide and subjected to silica and silica-titania pillaring. The prepared materials Ti-IPC-1PISi and Ti-IPC-1PITi (30) are purely mesoporous with well accessible titanium sites located on the surface of the layers. In fact they combine the advantages of both crystalline titanosilicate zeolites and mesoporous molecular sieves: (i) well defined and stable active centres on the surface crystalline layers and (ii) excellent accessibility of the active centres via mesopores.

The prepared materials were used as epoxidation catalysts for sterically demanding substrates and in selective oxidation of bulky organic sulphides to corresponding sulphoxides and sulphones. Namely cyclooctene, cyclodecene, norbornene, linalool, verbenol, α-pinene, methylphenyl sulphide, diphenyl sulphide and dibenzothiophene were oxidised with hydrogen peroxide at mild conditions. Oxidising cyclooctene, it was found, there is no difference in the yield of cyclooctene oxide between Ti-**CON** impregnated with $TiCl_4$ and TBOTi solution. The Ti-**CON**($TiCl_4$ sol) provided slightly higher selectivity (90% vs. 77% at 20% conversion) although is contains extra-framework titanium species and some share of anatase phase. Silica-titania pillared TS-1 materials provided increased conversion (18.6 – 21% vs. 6.5% after 4 h) as well as selectivity (76-80% vs. 58% at 20% conversion) in comparison with silica pillared TS-1. The Ti-IPC-1PITi (30) catalyst provided cyclooctene conversion 26% and cyclooctene oxide yield 19.5% after 1 h of the reaction being the most active of all the prepared materials and one of the most active catalysts reported for epoxidation of bulky olefins with hydrogen peroxide.

Cyclodecene oxide proved to be resistant toward epoxide ring opening under the testing reaction conditions and thus high selectivity (95-97% at 10% conversion) and high yield (TS-1-PITi 15%, Ti-IPC-1PITi 23% at 60°C after 4 h) were achieved in epoxidation of cyclodecene. Conventional TS-1(600) provided yield below 1%.

Ti-**CON**($TiCl_4$ sol) and TS-1-PITi (20b) were found to be the most selective catalysts for epoxidation of norbornene providing 2,3-epoxynorbornane yield of 15.4% resp. 14.8% after 4 h and selectivity of 76% resp. 56% at 10% conversion.

Oxidising linalool, an exclusive oxidation of C6=C7 double bond, which is more electron rich, was observed together with an acid catalysed intramolecular reaction of the hydroxyl group with epoxide ring forming linalool oxide. Ti-IPC-1PITi catalysts were the most active and selective in this reaction providing conversion up to 46.6% after 4 h and selectivity to the final linalool oxide between 50 and 58% at 20% conversion.

In oxidation of verbenol, the only product was verbenone. Epoxide selectivity in the oxidation α-pinene did not exceed 20% using any of the catalysts and a complex mixture of different products was obtained in all experiments.

We conclude the catalysts with most open structures and therefore the lowest diffusion limitations and sufficient amount of the titanium centres (Ti-IPC-1PITi (30), Ti-IPC-1PITi (100), TS-1-PITi (20b) and TS-1-PITi (60b)) provided the highest yields as well as the selectivity. Simple silica-titania pillaring treatment improves the catalyst performance dramatically. Based on the observed catalytic results and DR-UV/Vis spectra (*vide supra*), we support the points of Sasaki et al. [41] and Guo et al. [102] that also titanium species other that the single tetrahedrally coordinated one are active in oxidation catalysis.

Selectivity of the MPS oxidation to MPSO was driven by the diffusion rate in the catalyst. The lower were the diffusion restrictions the higher was the selectivity. It was demonstrated that the selectivity might be further increased by dosing of hydrogen peroxide to keep its concentration low during all the reaction. The Ti-IPC-1PISi catalyst exhibited an outstanding activity in both MPS and Ph_2S oxidations. TON_{tot} = 1418 was observed after 30 min and MPS conversion was 48% after 2 h what is similar to other lamellar titanosilicates (e.g. layered TS-1 46% after 2 h). We can, therefore, draw a conclusion that in oxidation of bulky sulphides, the accessibility of the active centres is more important than their amount.

Silica-titania pillared TS-1-PITi (60b) catalyst showed the highest potential of the tested catalysts to act as an oxo-desulphuration catalyst, easilly oxidising the DBTH to $DBTHSO_2$ (DBTH conversion 28% after 4 h). Conventional zeolites TS-1 and Ti-IPC-2 catalysts did not provide any conversion of DBTH.

The lamellar titanosilicate materials proved to be very effective in selective oxidation of bulky substrates. Therefore potential ways how to simplify their syntheses should be investigated. In

the case of layered TS-1 surfactant template, a synthesis using a mixture of templates with different chain lengths of the hydrophobic part (e.g. C_{14} – C_{22}) could be the first step. Such a mixed template is expected to be cheaper and thus decrease the cost of the synthesis.

Future work in the area of top-down prepared and ADORactive titanosilicates should be focused on (i) increasing the titanium content in the parent Ti-**UTL**, (ii) investigation if there are any preferred crystallographic sites for titanium incorporation and (iii) tuning the silica-titania pillaring of Ti-IPC-1PITi in order to suppress the anatase formation and increase the hydrogen peroxide efficiency.

Extension of the silica-titania pillaring concept to a silica-metal oxide pillaring concept (incorporation of metals other than titanium) could represent a way how to prepare e.g. lamellar tinosilicates or zirconosilicates, which might be used in catalysts of other reactions e.g. Baeyer-Villiger oxidation, Meerwein-Ponndorf-Verley reactions etc.

The layered titanosilicates contain high amount of silanol groups on the surface of the layers. Therefore, a study on the influence of their hydrophilicity/hydrophobicity on the catalytic reactions and possibilities of the hydrophobicity driving is an important milestone on the way towards industrial application.

References

[1] K.P. de Jong, in: K.P. de Jong, (Ed.), Synthesis of Solid Catalysts, Wiley-VCH, Weinheim, 2009, pp. 3-12.

[2] J. Čejka, A. Corma, S.I. Zones (Eds.), Zeolites and Catalysis: Synthesis, Reactions and Applications, Wiley-VCH, Weinheim, 2010.

[3] J. Čejka, G. Centi, J. Perez-Pariente, W.J. Roth, Catalysis Today 179 (2012) 2-15.

[4] C. Baerlocher, L.B. McCusker, Database of Zeolite Structures: http://www.iza-structure.org/databases/.

[5] S.T. Oyama, in: S.T. Oyama, (Ed.), Mechanisms in homogeneous and heterogeneous epoxidation catalysis, Elsevier, Amsterdam, 2008, pp. 5-12.

[6] L.B. McCusker, C. Baerlocher, in: J. Čejka, H. Van Bekkum, (Eds.), Zeolites and Ordered Mesoporous Materials: Progress and Prospects, 2005, pp. 41-64.

[7] S.M. Csicsery, Zeolites 4 (1984) 202-213.

[8] J. Hagen, in, Industrial Catalysts: a practical approach, Wiley-VCH, Weinheim, 1999, pp. 225-245.

[9] J. Perez-Ramírez, Design of hierarchical zeolite catalysts: where pore and active site quality meet, 6th International FEZA Conference, Leipzig, 2014.

[10] J.C. Groen, L.A.A. Peffer, J.A. Moulijn, J. Pérez-Ramírez, Chemistry – A European Journal 11 (2005) 4983-4994.

[11] A.H. Janssen, I. Schmidt, C.J.H. Jacobsen, A.J. Koster, K.P. de Jong, Microporous and Mesoporous Materials 65 (2003) 59-75.

[12] W.J. Roth, P. Nachtigall, R.E. Morris, J. Čejka, Chemical Reviews 114 (2014) 4807-4837.

[13] W.J. Roth, Studies in Surface Science and Catalysis 158A and B (2005) 19-26.

[14] L. Schreyeck, P. Caullet, J.-C. Mougenel, J.-L. Guth, B. Marler, Journal of the Chemical Society, Chemical Communications (1995) 2187-2188.

[15] M. Choi, K. Na, J. Kim, Y. Sakamoto, O. Terasaki, R. Ryoo, Nature 461 (2009) 828-828.

[16] W.J. Roth, O.V. Shvets, M. Shamzhy, P. Chlubná, M. Kubů, P. Nachtigall, J. Čejka, The Journal of American Chemical Society 133 (2011) 6130-6133.

[17] W.J. Roth, P. Nachtigall, R.E. Morris, P.S. Wheatley, V.R. Seymour, S.E. Ashbrook, P. Chlubná, L. Grajciar, M. Položij, A. Zukal, O. Shvets, J. Čejka, Nature Chemistry 5 (2013) 628-633.

[18] Y. Wang, Y. Liu, L. Wang, H. Wu, X. Li, M. He, P. Wu, The Journal of Physical Chemistry C 113 (2009) 18753-18760.

[19] W.J. Roth, B. Gil, B. Marszalek, Catalysis Today 227 (2014) 9-14.

[20] P. Wu, J.F. Ruan, L.L. Wang, L.L. Wu, Y. Wang, Y.M. Liu, W.B. Fan, M.Y. He, O. Terasaki, T. Tatsumi, Journal of the American Chemical Society 130 (2008) 8178-8187.

[21] M.E. Landis, B.A. Aufdembrink, P. Chu, I.D. Johnson, G.W. Kirker, M.K. Rubin, Journal of the American Chemical Society 113 (1991) 3189-3190.

[22] W.J. Roth, C.T. Kresge, J.C. Vartuli, M.E. Leonowicz, A.S. Fung, S.B. McCullen, Studies in Surface Science and Catalysis 94 (1995) 301-308.

[23] M. Kubů, W.J. Roth, H.F. Greer, W. Zhou, R.E. Morris, J. Přech, J. Čejka, Chemistry – A European Journal 19 (2013) 13937-13945.

[24] M. Opanasenko, W.O.N. Parker, M. Shamzhy, E. Montanari, M. Bellettato, M. Mazur, R. Millini, J. Čejka, Journal of the American Chemical Society 136 (2014) 2511-2519.

[25] H. Gies, M. Feyen, T. De Baerdemaeker, D.E. De Vos, B. Yilmaz, U. Müller, X. Meng, F.-S. Xiao, W. Zhang, T. Yokoi, T. Tatsumi, X. Bao, Microporous and Mesoporous Materials 222 (2016) 235-240.

[26] A. Corma, V. Fornes, S.B. Pergher, T.L.M. Maesen, J.G. Buglass, Nature 396 (1998) 353-356.

[27] J. Přech, 2015 (Unpublished results).

[28] T. Maluangnont, Y. Yamauchi, T. Sasaki, W.J. Roth, J. Čejka, M. Kubů, Chemical Communications 50 (2014) 7378-7381.
[29] K. Varoon, X. Zhang, B. Elyassi, D.D. Brewer, M. Gettel, S. Kumar, J.A. Lee, S. Maheshwari, A. Mittal, C.-Y. Sung, M. Cococcioni, L.F. Francis, A.V. McCormick, K.A. Mkhoyan, M. Tsapatsis, Science 334 (2011) 72-75.
[30] T. Tatsumi, in: N. Mizuno, (Ed.), Modern Heterogenous Oxidation Catalysis, Wiley-VCH, Weinheim, 2009, pp. 125-153.
[31] M. Taramasso, G. Perego, B. Notari, US Pat. 4410501 (1983).
[32] R. Millini, E. Previde Massara, G. Perego, G. Bellussi, Journal of Catalysis 137 (1992) 497-503.
[33] H.P. Wulff, GB Pat. 1249079 (1971).
[34] R.A. Sheldon, M. Wallau, I.W.C.E. Arends, U. Schuchardt, Accounts of Chemical Research 31 (1998) 485-493.
[35] C. Perego, A. Carati, P. Ingallina, M.A. Mantegazza, G. Bellussi, Applied Catalysis A: General 221 (2001) 63-72.
[36] A. Corma, P. Esteve, A. Martinez, S. Valencia, Journal of Catalysis 152 (1995) 18-24.
[37] J. Přech, M. Kubů, J. Čejka, Catalysis Today 227 (2014) 80-86.
[38] J. Přech, D. Vitvarová, L. Lupínková, M. Kubů, J. Čejka, Microporous and Mesoporous Materials 212 (2015) 28-34.
[39] T. Tatsumi, M. Nakamura, S. Negishi, H.-o. Tominaga, Journal of the Chemical Society, Chemical Communications (1990) 476-477.
[40] G. Peregot, G. Bellussi, C. Corno, M. Taramasso, F. Buonomot, A. Esposito, in: A.I. Y. Murakami, J.W. Ward, (Eds.), Studies in Surface Science and Catalysis, Elsevier, 1986, pp. 129-136.
[41] M. Sasaki, Y. Sato, Y. Tsuboi, S. Inagaki, Y. Kubota, ACS Catalysis 4 (2014) 2653-2657.
[42] P. Birke, P. Kraak, R. Schödel, F. Vogt, in: H. Tadashi, Y. Tatsuaki, (Eds.), Studies in Surface Science and Catalysis, Elsevier, 1994, pp. 425-432.
[43] J.S. Reddy, P.A. Jacobs, Catalysis Letters 37 (1996) 213-216.
[44] V. Hulea, F. Fajula, J. Bousquet, Journal of Catalysis 198 (2001) 179-186.
[45] J. Přech, R.E. Morris, J. Čejka, Catalysis Science & Technology 6 (2016) 2775-2786.
[46] http://www.eni.com/en_IT/attachments/azienda/attivita-strategie/petrolchimica/licensing/TS1-flyer-lug09.pdf (29.4.2016).
[47] P. Wu, T. Tatsumi, T. Komatsu, T. Yashima, Journal of Catalysis 202 (2001) 245-255.
[48] B. Tang, W. Dai, X. Sun, N. Guan, L. Li, M. Hunger, Green Chemistry 16 (2014) 2281-2291.
[49] M.A. Camblor, A. Corma, J. Pérez-Pariente, Zeolites 13 (1993) 82-87.
[50] M.A. Camblor, M. Costantini, A. Corma, L. Gilbert, P. Esteve, A. Martinez, S. Valencia, Chemical Communications (1996) 1339-1340.
[51] J.C. van der Waal, P. Lin, M.S. Rigutto, H. van Bekkum, in: S.-K.I. Hakze Chon, U. Young Sun, (Eds.), Studies in Surface Science and Catalysis, Elsevier, 1997, pp. 1093-1100.
[52] T. Blasco, M.A. Camblor, A. Corma, P. Esteve, J.M. Guil, A. Martínez, J.A. Perdigón-Melón, S. Valencia, The Journal of Physical Chemistry B 102 (1998) 75-88.
[53] T. Tatsumi, N. Jappar, The Journal of Physical Chemistry B 102 (1998) 7126-7131.
[54] J.C. van der Waal, M.S. Rigutto, H. van Bekkum, Applied Catalysis A: General 167 (1998) 331-342.
[55] P. Wu, T. Tatsumi, T. Komatsu, T. Yashima, Chemistry Letters 29 (2000) 774-775.
[56] P. Wu, T. Tatsumi, T. Komatsu, T. Yashima, Journal of Physical Chemistry B 105 (2001) 2897-2905.
[57] P. Wu, T. Komatsu, T. Yashima, The Journal of Physical Chemistry 100 (1996) 10316-10322.
[58] D. Levin, A.D. Chang, S. Luo, US Pat. 6114551 (2000).

[59] P. Wu, T. Tatsumi, Chemical Communications (2002) 1026-1027.
[60] J.S. Reddy, R. Kumar, P. Ratnasamy, Applied Catalysis 58 (1990) L1-L4.
[61] A. Tuel, Zeolites 15 (1995) 236-242.
[62] A. Corma, U. Diaz, M.E. Domine, V. Fornes, Chemical Communications (2000) 137-138.
[63] M.-J. Diaz-Cabanas, L.A. Villaescusa, M.A. Camblor, Chemical Communications (2000) 761-762.
[64] K.J. Balkus Jr, A.G. Gabrielov, S.I. Zones, in: B. Laurent, K. Serge, (Eds.), Studies in Surface Science and Catalysis, Elsevier, 1995, pp. 519-525.
[65] J. Přech, J. Čejka, Catalysis Today (ahead of print) (2015).
[66] M.S. Rigutto, R. de Ruiter, J.P.M. Niederer, H. van Bekkum, in: H.G.K.H.P. J. Weitkamp, W. Hölderich, (Eds.), Studies in Surface Science and Catalysis, Elsevier, 1994, pp. 2245-2252.
[67] P. Wu, T. Komatsu, T. Yashima, Journal of Catalysis 168 (1997) 400-411.
[68] P. Wu, T. Komatsu, T. Yashima, The Journal of Physical Chemistry B 102 (1998) 9297-9303.
[69] Y. Kubota, Y. Koyama, T. Yamada, S. Inagaki, T. Tatsumi, Chemical Communications (2008) 6224-6226.
[70] C.B. Dartt, M.E. Davis, Applied Catalysis A: General 143 (1996) 53-73.
[71] A. Corma, U. Diaz, V. Fornes, J.L. Jorda, M. Domine, F. Rey, Chemical Communications (1999) 779-780.
[72] J. Kim, J. Chun, R. Ryoo, Chemical Communications 51 (2015) 13102-13105.
[73] A. Corma, U. Diaz, M.E. Domine, V. Fornes, Journal of the American Chemical Society 122 (2000) 2804-2809.
[74] W.B. Fan, P. Wu, S. Namba, T. Tatsumi, Angewandte Chemie-International Edition 43 (2004) 236-240.
[75] J. Ruan, P. Wu, B. Slater, O. Terasaki, Angewandte Chemie International Edition 44 (2005) 6719-6723.
[76] M. Moliner, A. Corma, Chemistry of Materials 24 (2012) 4371-4375.
[77] P. Wu, D. Nuntasri, J.F. Ruan, Y.M. Liu, M.Y. He, W.B. Fan, O. Terasaki, T. Tatsumi, Journal of Physical Chemistry B 108 (2004) 19126-19131.
[78] A. Corma, V. Fornes, J.M. Guil, S. Pergher, T.L.M. Maesen, J.G. Buglass, Microporous and Mesoporous Materials 38 (2000) 301-309.
[79] X. Ouyang, Y.-J. Wanglee, S.-J. Hwang, D. Xie, T. Rea, S.I. Zones, A. Katz, Dalton Transactions 43 (2014) 10417-10429.
[80] K. Na, C. Jo, J. Kun, W.S. Ahn, R. Ryoo, ACS Catalysis 1 (2011) 901-907.
[81] M. Taramasso, G. Perego, B. Notari, in: H. Robson, (Ed.), Verified Syntheses of Zeolitic Materials, Elsevier, Amsterdam, 2001, pp. 207.
[82] J. Přech, P. Eliášová, D. Aldhayan, M. Kubů, Catalysis Today 243 (2015) 134-140.
[83] I. Schmidt, A. Krogh, K. Wienberg, A. Carlsson, M. Brorson, C.J.H. Jacobsen, Chemical Communications (2000) 2157-2158.
[84] H. Xin, J. Zhao, S. Xu, J. Li, W. Zhang, X. Guo, E.J.M. Hensen, Q. Yang, C. Li, The Journal of Physical Chemistry C 114 (2010) 6553-6559.
[85] D.-Y. Ok, N. Jiang, E.A. Prasetyanto, H. Jin, S.-E. Park, Microporous and Mesoporous Materials 141 (2011) 2-7.
[86] Z. Kang, G. Fang, Q. Ke, J. Hu, T. Tang, ChemCatChem 5 (2013) 2191-2194.
[87] X. Ke, L. Xu, C. Zeng, L. Zhang, N. Xu, Microporous and Mesoporous Materials 106 (2007) 68-75.
[88] G.A. Eimer, I. Díaz, E. Sastre, S.G. Casuscelli, M.E. Crivello, E.R. Herrero, J. Perez-Pariente, Applied Catalysis A: General 343 (2008) 77-86.
[89] Y. Cheneviere, F. Chieux, V. Caps, A. Tuel, Journal of Catalysis 269 (2010) 161-168.

[90] Z. Zhao, Y. Liu, H. Wu, X. Li, M. He, P. Wu, Journal of Porous Materials 17 (2009) 399-408.
[91] C. Pei-Yu, T. Shang-Tien, T. Tseng-Chang, M. Jingbo, G. Xin-Wen, Topics in Catalysis 52 (2009) 185-192.
[92] A. Silvestre-Albero, A. Grau-Atienza, E. Serrano, J. García-Martínez, J. Silvestre-Albero, Catalysis Communications 44 (2014) 35-39.
[93] C.-G. Li, Y. Lu, H. Wu, P. Wu, M. He, Chemical Communications 51 (2015) 14905-14908.
[94] C.T. Kresge, M.E. Leonowicz, W.J. Roth, J.C. Vartuli, J.S. Beck, Nature 359 (1992) 710-712.
[95] A. Corma, M.T. Navarro, J.P. Pariente, Journal of the Chemical Society, Chemical Communications (1994) 147-148.
[96] P.T. Tanev, M. Chibwe, T.J. Pinnavaia, Nature 368 (1994) 321-323.
[97] K.A. Koyano, T. Tatsumi, Chemical Communications (1996) 145-146.
[98] P. Wu, T. Tatsumi, T. Komatsu, T. Yashima, Chemistry of Materials 14 (2002) 1657-1664.
[99] T. Tatsumi, K. A. Koyano, N. Igarashi, Chemical Communications (1998) 325-326.
[100] B. Notari, in: W.O.H. D.D. Eley, G. Bruce, (Eds.), Advances in Catalysis, Academic Press, 1996, pp. 253-334.
[101] F. Bonino, A. Damin, G. Ricchiardi, M. Ricci, G. Spanò, R. D'Aloisio, A. Zecchina, C. Lamberti, C. Prestipino, S. Bordiga, The Journal of Physical Chemistry B 108 (2004) 3573-3583.
[102] Q. Guo, K. Sun, Z. Feng, G. Li, M. Guo, F. Fan, C. Li, Chemistry – A European Journal 18 (2012) 13854-13860.
[103] K.G. Ione, L.A. Vostrikova, V.M. Mastikhin, Journal of Molecular Catalysis 31 (1985) 355-370.
[104] A. Zecchina, G. Spoto, S. Bordiga, A. Ferrero, G. Petrini, G. Leofanti, M. Padovan, in: P.A. Jacobs, N.I. Jaeger, L. Kubelková, B. Wichterlová, (Eds.), Studies in Surface Science and Catalysis, Elsevier, 1991, pp. 251-258.
[105] P. Ratnasamy, D. Srinivas, H. Knözinger, in, Advances in Catalysis, Academic Press, 2004, pp. 1-169.
[106] W. Fan, P. Wu, T. Tatsumi, Journal of Catalysis 256 (2008) 62-73.
[107] Z. Deng, Y. Yang, X. Lu, J. Ding, M. He, P. Wu, Catalysis Science & Technology 6 (2016) 2605-2615.
[108] T. Tatsumi, M. Nakamura, K. Yuasa, H.-o. Tominaga, Chemistry Letters 19 (1990) 297-298.
[109] M.G. Clerici, P. Ingallina, Journal of Catalysis 140 (1993) 71-83.
[110] A. Corma, M.A. Camblor, P. Esteve, A. Martinez, J. Perezpariente, Journal of Catalysis 145 (1994) 151-158.
[111] J.C. van der Waal, H. van Bekkum, Journal of Molecular Catalysis A: Chemical 124 (1997) 137-146.
[112] S.-Y. Kim, H.-J. Ban, W.-S. Ahn, Catalysis Letters 113 (2007) 160-164.
[113] F.S. Xiao, B. Xie, H.Y. Zhang, L. Wang, X.J. Meng, W.P. Zhang, X.H. Bao, B. Yilmaz, U. Muller, H. Gies, H. Imai, T. Tatsumi, D. De Vos, ChemCatChem 3 (2011) 1442-1446.
[114] J.G. Wang, L. Xu, K. Zhang, H.G. Peng, H.H. Wu, J.G. Jiang, Y.M. Liu, P. Wu, Journal of Catalysis 288 (2012) 16-23.
[115] V. Hulea, E. Dumitriu, F. Patcas, R. Ropot, P. Graffin, P. Moreau, Applied Catalysis A: General 170 (1998) 169-175.
[116] M. Sasidharan, A. Bhaumik, Physical Chemistry Chemical Physics 13 (2011) 16282-16294.
[117] X.H. Shen, W.B. Fan, Y. He, P. Wu, J.G. Wang, T. Tatsumi, Applied Catalysis a-General 401 (2011) 37-45.

[118] L.L. Wang, Y. Wang, Y.M. Liu, H.H. Wu, X.H. Li, M.Y. He, P. Wu, Journal of Materials Chemistry 19 (2009) 8594-8602.
[119] I. Bombarda, L. Cezanne, E.M. Gaydou, Flavour and Fragrance Journal 19 (2004) 275-280.
[120] M. Sasidharan, A. Bhaumik, Journal of Molecular Catalysis A: Chemical 328 (2010) 60-67.
[121] T. Kamegawa, N. Suzuki, M. Che, H. Yamashita, Langmuir 27 (2011) 2873-2879.
[122] N. Wilde, C. Worch, W. Suprun, R. Gläser, Microporous and Mesoporous Materials 164 (2012) 182-189.
[123] B.M. Trost, Bulletin of the Chemical Society of Japan 61 (1988) 107-124.
[124] H. Satoh, in: T. Chiba, p. Malfertheiner, H. Satoh, (Eds.), Proton Pump Inhibitors: A Balanced View, Karger, Basel, 2013, pp. 1.
[125] T. Roberts, D. Hutson, (Eds.), Metabolic Pathways of Agrochemicals: Insecticides and fungicides, The Royal Society of Chemistry, Cambridge, 1999, pp. 535.
[126] J.M. Fraile, C. Gil, J.A. Mayoral, B. Muel, L. Roldán, E. Vispe, S. Calderón, F. Puente, Applied Catalysis B: Environmental 180 (2016) 680-686.
[127] M.B. Smith, J. March (Eds.), March's Advanced Organic Chemistry, Wiley, New York, 2007.
[128] S. Vayssié, H. Elias, Angewandte Chemie International Edition 37 (1998) 2088-2090.
[129] M. De Rosa, M. Lamberti, C. Pellecchia, A. Scettri, R. Villano, A. Soriente, Tetrahedron Letters 47 (2006) 7233-7235.
[130] C. Bolm, F. Bienewald, Angewandte Chemie International Edition in English 34 (1996) 2640-2642.
[131] R. Noyori, M. Aoki, K. Sato, Chemical Communications (2003) 1977-1986.
[132] X.-F. Wu, Tetrahedron Letters 53 (2012) 4328-4331.
[133] A. Corma, M. Iglesias, F. Sánchez, Catalysis Letters 39 (1996) 153-156.
[134] V. Hulea, P. Moreau, F. Di Renzo, Journal of Molecular Catalysis A: Chemical 111 (1996) 325-332.
[135] P. Moreau, V. Hulea, S. Gomez, D. Brunel, F. Di Renzo, Applied Catalysis A: General 155 (1997) 253-263.
[136] Y. Kon, T. Yokoi, M. Yoshioka, S. Tanaka, Y. Uesaka, T. Mochizuki, K. Sato, T. Tatsumi, Tetrahedron 70 (2014) 7584-7592.
[137] L.P. Hammett, Journal of the American Chemical Society 59 (1937) 96-103.
[138] S. Du, F. Li, Q. Sun, N. Wang, M. Jia, J. Yu, Chemical Communications 52 (2016) 3368-3371.
[139] N. Wilde, J. Přech, M. Pelz, M. Kubů, J. Čejka, R. Gläser, 2016 (Unpublished results).
[140] M.V. Shamzhy, O.V. Shvets, M.V. Opanasenko, P.S. Yaremov, L.G. Sarkisyan, P. Chlubná, A. Zukal, V.R. Marthala, M. Hartmann, J. Čejka, Journal of Material Chemistry 22 (2012) 15793-15803.
[141] O.V. Shvets, N. Kasian, A. Zukal, J. Pinkas, J. Čejka, Chemistry of Materials 22 (2010) 3482-3495.
[142] Y. Kubota, S. Tawada, K. Nakagawa, C. Naitoh, N. Sugimoto, Y. Fukushima, T.-a. Hanaoka, Y. Imada, Y. Sugi, Microporous and Mesoporous Materials 37 (2000) 291-301.
[143] R.F. Lobo, M.E. Davis, Microporous Materials 3 (1994) 61-69.
[144] M. Yoshikawa, P. Wagner, M. Lovallo, K. Tsuji, T. Takewaki, C.-Y. Chen, L.W. Beck, C. Jones, M. Tsapatsis, S.I. Zones, M.E. Davis, The Journal of Physical Chemistry B 102 (1998) 7139-7147.
[145] S.I. Zones, US Pat. 4,963,337 (1990).
[146] S.I. Zones, US Pat. 5,770,175A (1998).
[147] B.C. Lippens, J.H. de Boer, Journal of Catalysis 4 (1965) 319-323.

[148] E.P. Barrett, L.G. Joyner, P.P. Halenda, Journal of the American Chemical Society 73 (1951) 373-380.
[149] P. Wagner, M. Yoshikawa, K. Tsuji, M. E. Davis, P. Wagner, M. Lovallo, M. Taspatsis, Chemical Communications (1997) 2179-2180.
[150] B.M. Lok, M.B. Kristoffersen, E.M. Flanigen, EP 121232 (1984).
[151] K. Na, M. Choi, W. Park, Y. Sakamoto, O. Terasaki, R. Ryoo, Journal of the American Chemical Society 132 (2010) 4169-4177.
[152] A. Thangaraj, S. Sivasanker, Journal of the Chemical Society, Chemical Communications (1992) 123-124.
[153] C. Pirovano, M. Guidotti, V. Dal Santo, R. Psaro, O.A. Kholdeeva, I.D. Ivanchikova, Catalysis Today 197 (2012) 170-177.
[154] A. Corma, M. Iglesias, F. Sanchez, Journal of the Chemical Society, Chemical Communications (1995) 1635-1636.
[155] A. Bhaumik, T. Tatsumi, Journal of Catalysis 182 (1999) 349-356.
[156] A.L. Cánepa, E.R. Herrero, M.E. Crivello, G.A. Eimer, S.G. Casuscelli, Journal of Molecular Catalysis A: Chemical 347 (2011) 1-7.
[157] T. Tatsumi, M. Yako, M. Nakamura, Y. Yuhara, H. Tominaga, Journal of Molecular Catalysis 78 (1993) L41-L45.

Enclosures

1) **J. Přech,** M. Kubů, J. Čejka; Synthesis and catalytic properties of titanium containing extra-large pore zeolite CIT-5, Catal. Today 227 (2014) 80–86.

2) **J. Přech,** P. Eliášová, D. Aldhayan, M. Kubů, Epoxidation of bulky organic molecules over pillared titanosilicates, Catal. Today 243 (2015) 134-140.

3) **J. Přech,** D. Vitvarová, L. Lupínková, M. Kubů, J. Čejka, Titanium impregnated borosilicate zeolites for epoxidation catalysis, Microporous Mesoporous Mater. 212 **2015**, 28-34.

4) **J. Přech,** J. Čejka, UTL titanosilicate: An extra-large pore epoxidation catalyst with tunable textural properties, Catal. Today (2016), DOI: 10.1016/j.cattod.2015.09.036

5) **J. Přech,** R.E. Morris, J. Čejka, Selective oxidation of bulky organic sulphides over layered titanosilicate catalysts, Catal. Sci. Technol. 6 (2016) 2775-2786.